5-2018

Discovery and Development of Potassium-Based Metal Halide Scintillators for Radiation Detection Applications

Luis Manuel Stand Stracuzzi
University of Tennessee

To the Graduate Council:

I am submitting herewith a dissertation written by Luis Manuel Stand Stracuzzi entitled "Discovery and Development of Potassium-Based Metal Halide Scintillators for Radiation Detection Applications." I have examined the final electronic copy of this dissertation for form and content and recommend that it be accepted in partial fulfillment of the requirements for the degree of Doctor of Philosophy, with a major in Energy Science and Engineering.

Charles L. Melcher, Major Professor

We have read this dissertation and recommend its acceptance:

Jason P. Hayward, Eric. D. Lukosi, Mariya Zhuravleva

Accepted for the Council:

Dixie L. Thompson

Vice Provost and Dean of the Graduate School

(Original signatures are on file with official student records.)

Discovery and Development of Potassium-Based Metal Halide Scintillators for Radiation Detection Applications

A Dissertation Presented for the

Doctor of Philosophy

Degree

The University of Tennessee, Knoxville

Luis Manuel Stand Stracuzzi

May 2018

DEDICATION

I dedicate my work to my Nonno.

ACKNOWLEDGEMENTS

Firstly, I would like to express my sincere gratitude to my advisors Dr. Charles Melcher, Dr. Mariya Zhuravleva and Mrs. Merry Koschan for their patience, motivation, and for sharing their immense knowledge, without their continuous support I would not be in this stage in my life. Besides my advisors, I would like to thank the rest of my thesis committee Dr. Eric Lukosi, and Dr. Jason Hayward, for their insightful comments, and for sharing their valuable time with me. Also, I would like to express my sincere gratitude to Dr. Riedinger and Bredesen Center staff for their support.

I would like to acknowledge our funding sources for their support. This work was supported by the Siemens Medicals solution, and US Department of Homeland Security, Domestic Nuclear Detection Office, under grant # 2014-DN-077-ARI088-01 and grant # 2012-DN-077-ARI067-04. This support does not constitute an express or implied endorsement on the part of the Government.

I would like to thank my fellow lab mates: Dr. Tyagi, Dr. Wu, Dr. Rothfuss, Dr. Donnald, Dr. Lindsey, Dr. Wei, Bonnie Blalock, Pancho McAlexander, Matthew Loyd, Camera Foster, Jesse Johnson, Victoria Martin, Eleanor Comer, Josh Smith, Delzer Cordell and Daniel Rutstrom, at the Scintillation Materials Research Center for the stimulating discussions, and for all the fun we have had over the years. Also, I wish to acknowledge the staff at UT that made my research possible: Bo Bishop, Larry Smith, Danny Hackworth, Doug Fielden, Frank Holiway, Randy Stooksbury.

Also, I would like to thank to our collaborators for sharing their valuable time and knowledge: Dr. Brian Chakoumakos and Dr. Lynne Boatner from Oak Ridge National Lab, Dr. Giuseppe Camarda from Brookhaven National Laboratory, Dr. Kanai Shah from Radiation Monitoring devices, and Dr. Nerine Cherepy and Dr. Steve Payne from Lawrence Livermore National Laboratory.

Last but not the least, I would like to thank my family for their support during this journey.

ABSTRACT

Scintillators are important materials for radiation detection applications such as homeland security, geological exploration, and medical imaging. Scintillators for nuclear nonproliferation applications must have excellent energy resolution to distinguish the gamma-ray signatures of potentially dangerous radioactive sources from non-threat radioactive sources. There is an established need for scintillators with energy resolution in the 1-2 % (percent) range at 662 kiloelectron volts. However, there are challenges surrounding the development of this new generation of high light yield/high resolution scintillators; for example, the high cost of production due to low crystal yield and slow growth process, and crystal inhomogeneity. In this work we present the crystal growth, the physical and scintillation properties of four newly discovered europium doped scintillators; potassium strontium iodide (KSr_2I_5:Eu), potassium strontium bromide (KSr_2Br_5:Eu), potassium barium iodide (KBa_2I_5:Eu), potassium barium iodide (K_2BaI_4:Eu). These scintillators materials had excellent properties with light yields well above 50,000 photons per megaelectron volt and energy resolution between 2.4 – 2.9% (Percent) at 662 kiloelectron volts.

Due to its ease of growth, Europium doped potassium strontium iodide was selected for further development. We focused our efforts optimizing the growth parameters required to grow one-inch diameter crystals at pulling rates up to 7 millimeters per hour. High performing, nearly crack free single crystals measuring up to one-inch diameter by six-inch in length were grown via the vertical Bridgman technique. The scintillation properties were evaluated using specimen that ranged ranging from 0.012 to 54 cubic centimeters.

To further enhance the light yield and energy resolution in europium doped potassium strontium iodide, anion and cation substitution were investigated. We found that replacing 2% (percent) of the matrix iodine atoms with bromine increased the light yield from 84,000 to 97,900 ph/MeV (Photon per megaelectron volt), while maintaining it excellent energy resolution of 3.0% (percent) at 662 keV

(Kiloelectron volts). We also found that by replacing 35% of strontium for barium not only increased the light yield increased from 84,000 to 120,000 ph/MeV (Photon per megaelectron volt) and but also improved the energy resolution from 3.0 to 2.3% (percent) at 662 keV (Kiloelectron volts) for 1 cm^3 (cubic centimeter) crystals.

TABLE OF CONTENTS

LIST OF TABLES

LIST OF FIGURES

Chapter 1
Introduction

1.1. Scintillators

Scintillator materials are used as radiation sensors for many gamma-ray and X-ray applications, and the physical and luminescent properties are often tailored to satisfy the specific requirements for each application. Scintillators used for nuclear nonproliferation applications are required to have excellent energy resolution to minimize false alarms by providing unambiguous identification and discrimination between the gamma-ray signatures of highly enriched uranium and plutonium from other non-threat radioactive sources. For national security application, the scintillator must have:

- A high density and effective Z number to provide good stopping power. This allows the material to interact with high energy X-ray and gamma-ray radiation (Interaction with matter).
- A high light yield and low energy resolution to identify the signature of the radionuclide sources (Scintillation process).
- Ease of production to provide large volumes of material for various detector configurations (Crystal growth).

The gamma interactions and their dependency on the gamma ray energy, and Z of the absorber is shown in Figure 1.

During the ionization process the electrons and *γ* quanta lose energy when traversing the scintillator material, such process is dictated by the three fundamental mechanisms of electromagnetic interactions: Photoelectric effect, Compton scatting and pair production. In the photoelectric (photon-electron) interaction, a photon transfers all its energy to an electron located in one of the atomic shells. The electron is ejected from the atom by this energy and begins to pass through the surrounding matter. The electron rapidly loses its energy and moves only a relatively short distance from its original location. The photon's energy is, therefore, deposited in the matter close to the site of the photoelectric interaction. The energy transfer is a two-step process. The photoelectric interaction in which the photon transfers its energy to the electron is the first step.

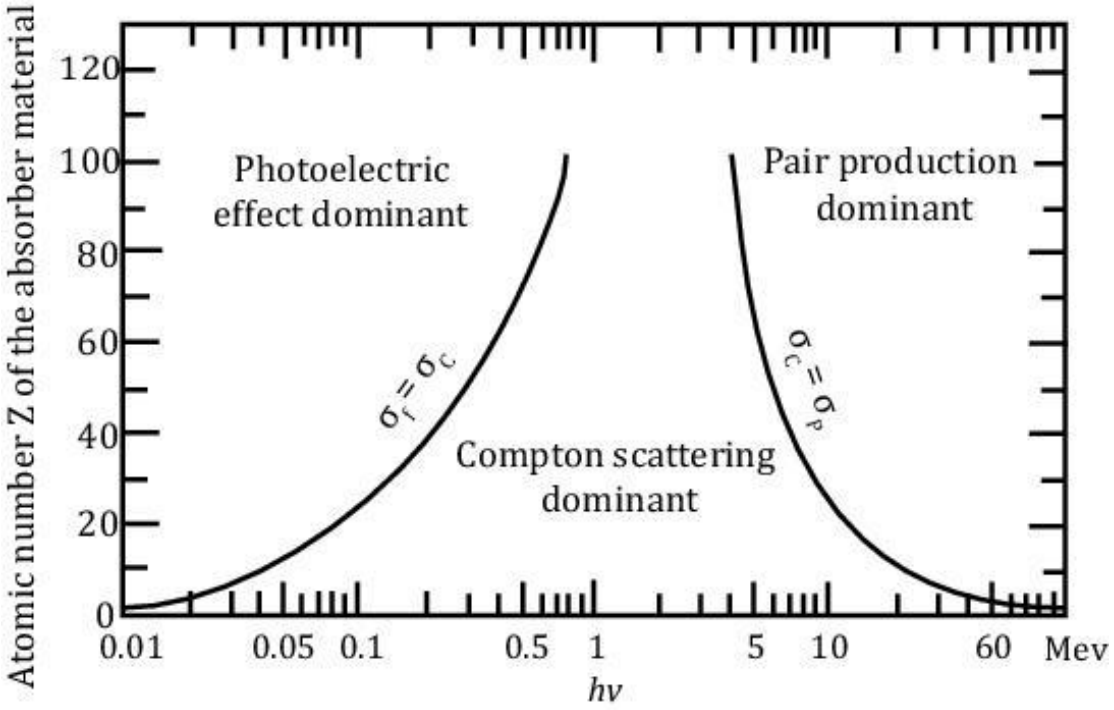

Figure 1. Plot shows the three main gamma interactions and their dependency on the gamma ray energy, and Z of the absorber [1].

The depositing of the energy in the surrounding matter by the electron is the second step. Photoelectric interactions usually occur with electrons that are firmly bound to the atom, that is, those with a relatively high binding energy. Photoelectric interactions are most probable when the electron binding energy is only slightly less than the energy of the photon. If the binding energy is more than the energy of the photon, a photoelectric interaction cannot occur. This interaction is possible only when the photon has sufficient energy to overcome the binding energy and remove the electron from the atom. The photon's energy is divided into two parts by the interaction. A portion of the energy is used to overcome the electron's binding energy and to remove it from the atom. The remaining energy is transferred to the electron as kinetic energy and is deposited near the interaction site. Since the interaction creates a vacancy in one of the electron shells, typically the K or L, an electron moves down to fill in. The drop-in energy of the filling electron often produces a characteristic x-ray photon. The energy of the characteristic radiation depends on the binding energy of the electrons involved. This process sometimes converts x-rays into light photons. In the Compton scattering process, the incident gamma ray energy is partially transferred to the electron and the incoming gamma-ray photon is deflected through an angle with respect to its original direction. In the pair production process, the gamma ray with energies above 1.02 MeV are subjected to strong field effects from the nucleus and may disappear and reappear as electron-positron pair identical energy (511 keV), but travel in opposite directions.

A scintillator can be simply defined as a wavelength shifter because it converts the energy (or wavelength) of energetic photons into a number of photons of much lower energy (or longer wavelength) in the near visible or visible range, which can to be detected by photomultiplier tubes or any other photodetectors. For a material to be considered a scintillator it must have a luminescence center, such centers could be due to lattice defects or core to valence transition for intrinsic scintillators, or by intentional addition of impurities (extrinsic). In both cases, there

is a radiative transition between an excited and a lower energy state. Such levels must be contained within the forbidden energy band (bandgap) of the scintillator material. Typical energy losses during the scintillation process are caused by nonradiative defects, deep electron traps and electron-hole pairs deexciting through coupling with lattice phonons during the thermalization process. The elementary scintillation process in an inorganic scintillator following the absorption of incident radiation is described by vector diagram shown the Figure 2.

As a general idea the scintillation process can be simply described as the conversion of incident gamma-rays or particles into low energy photons. The scintillation process can be divided into 4 basic stages [2]:

1. Energy conversion: electron hole pair creation by absorption of ionizing radiation.
2. Relaxation and thermalization of electron hole pairs with an energy roughly equal to the band gap energy.
3. Transfer of electron hole pair to the luminescence centers and their excitation
4. Light emission from the luminescence center

Steps 3 and 4 of the scintillation process in an energy – band scheme for single crystalline inorganic scintillators are shown in Figure 3.

Ce^{3+} and Eu^{2+} are commonly used as luminescence centers in scintillator materials. These rare earth ions have parity allowed electronic transitions between the electron configurations $4f^{n-1}5d$ and $4f^{n}$, which provides the fast-decaying luminescence required for radiation detection applications. The luminescence transition in Ce^{3+} is 5d (^{2}D) → 4f (^{2}F), and the transition in Eu^{2+} is described as $4f^6$ (^{7}F) 5d -> $4f^6$ (^{7}F) 4f, which is $4f^7$ (^{8}S) [3]. In Eu^{2+} probability of 5d → 4f of Eu^{2+} is reduced by a factor of 1/49, since the initial state $4f^6$-core has forty-nine alternatives of ^{7}F as the final state, thus the luminescence lifetime of Eu^{2+} is several tens longer than Ce^{3+} [3]. In this work the investigated scintillators activated with Eu^{2+}.

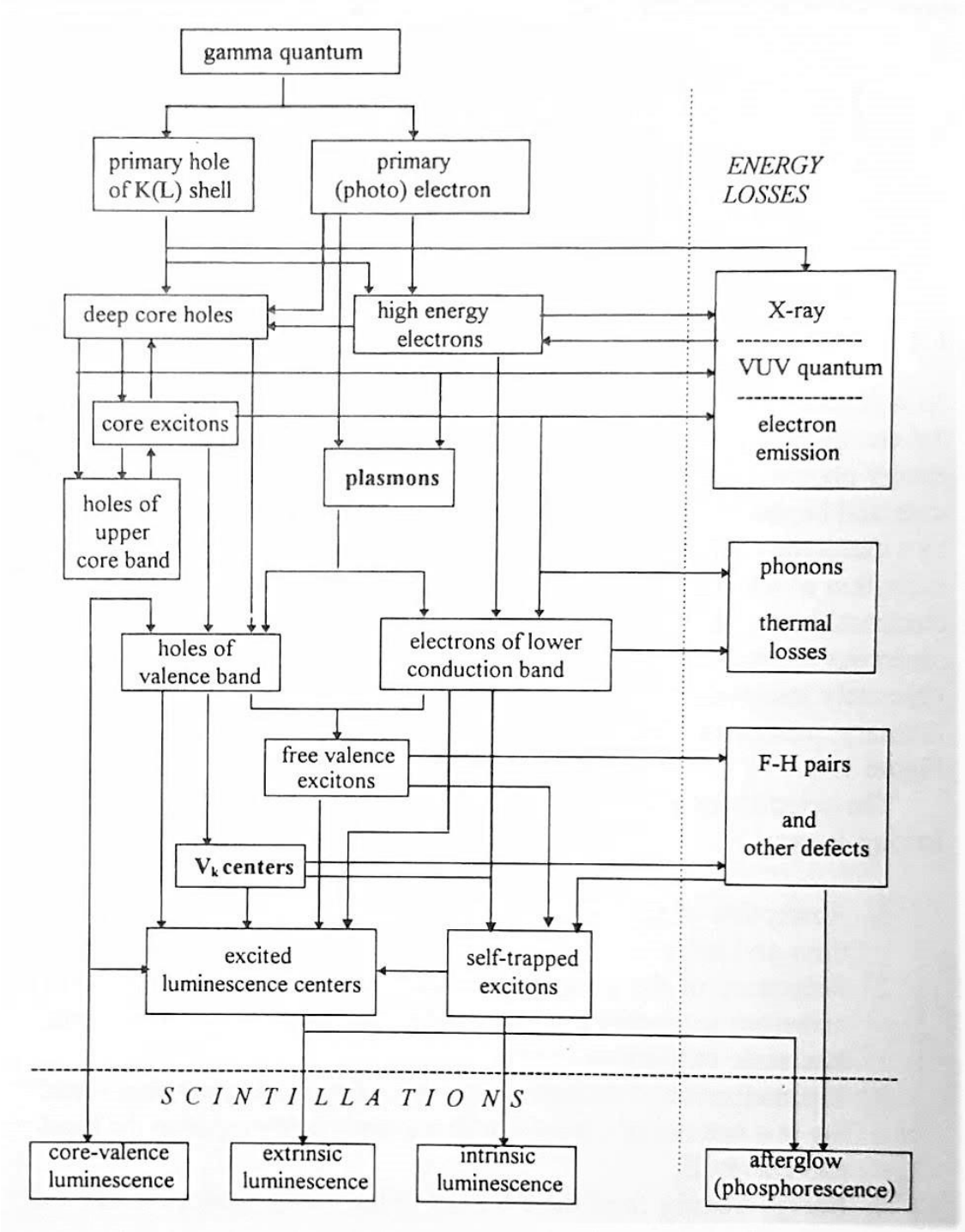

Figure 2. Vector diagram of the scintillation processes in inorganic scintillators [2].

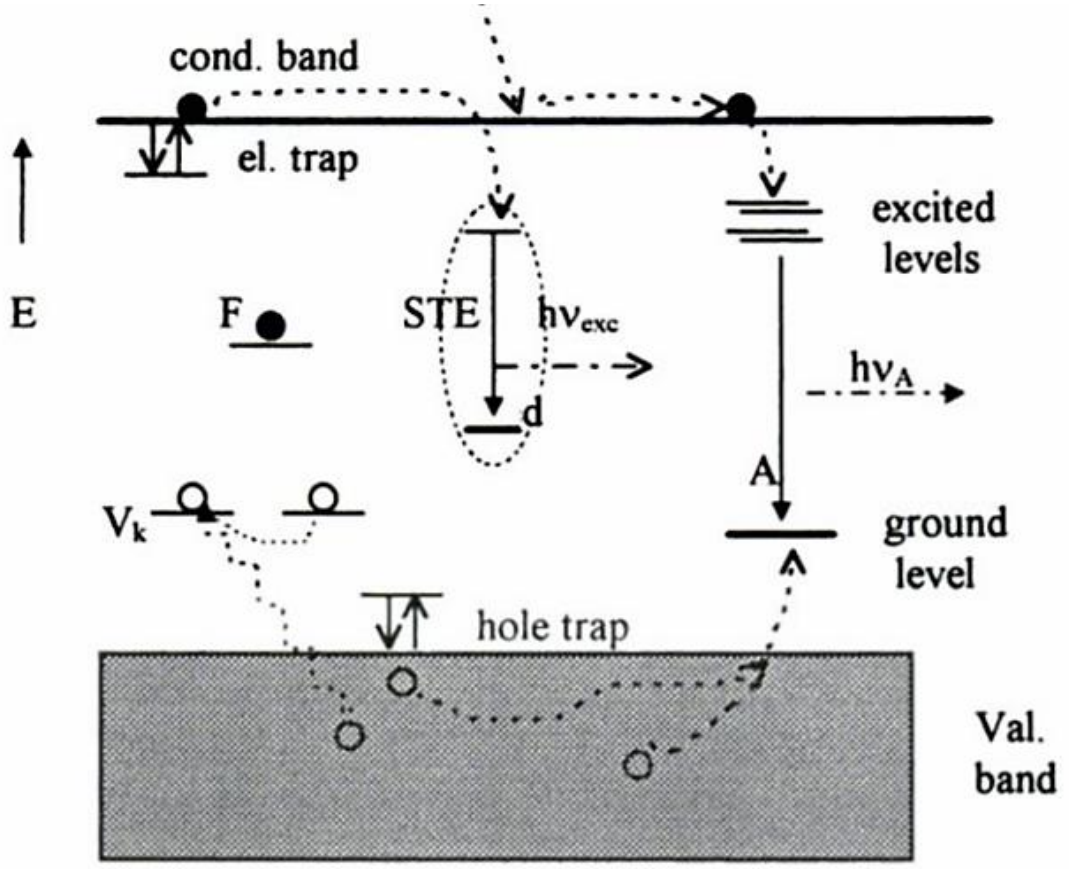

Figure 3. Energy band scheme of the final stages of the scintillation process in single crystals [2].

1.2. Crystal Growth

Bridgman-Stockbarger technique was name after Percy Williams Bridgman and Donald C. Stockbarger. The scintillators investigated for this work were grown using this technique. In this process, a top zone which temperature is set above the melting point of your material, and a bottom zone with a temperature lower than your melting point. The growth process is started by slowly moving the ampoule through the thermal gradient and enters the cold zone. A schematic diagram of a typical two zone furnace Figure 4. For this work a three zone, an electrodynamic gradient (EDG) and a two-zone transparence furnace were used to produce single crystal scintillators.

1.3. History of Scintillators

The discovery and use of scintillators can be traced back to the 1900's with Calcium tungstate ($CaWO_4$) which was used in the year following Rontgen's discovery of X-rays; uranyl salts, used by Becquerel to discover radioactivity; and zinc sulfide (ZnS) used by Crookes to detect and count radioactivity and by Rutherford to study alpha particle scattering [4]. After the discovery of photomultiplier tubes (PMT) in 1940s, the discovery of scintillators has been steady. One of the major discoveries in the scintillator community was done in the late 1940s by Hofstadter, with the discovery of sodium iodide doped thallium (NaI:Tl) and cesium iodide doped with thallium (CsI:Tl) [5]. Up to date these activated alkali halide crystals are widely used for many gamma detection applications. Figure 5 shows a timeline of the most important scintillators discovered in the last century [6].

Scintillators are common radiation detectors with a variety of applications, many of which have specialized requirements; as a result, scintillators are often developed with properties suitable for specific applications and devices in mind. Utilization for nuclear nonproliferation requires excellent energy resolution for spectroscopic differentiation of radioisotopes in order to minimize false alarms [7].

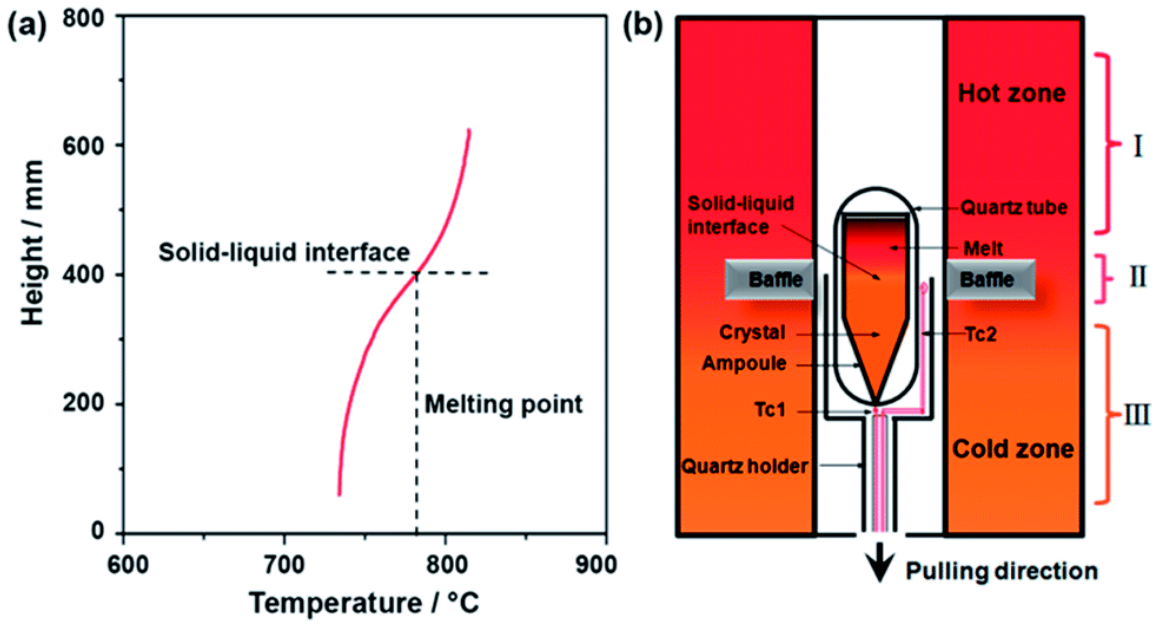

Figure 4a. Generic thermal profile and (b) shows the typical configuration of a three-zone vertical Bridgman furnace.

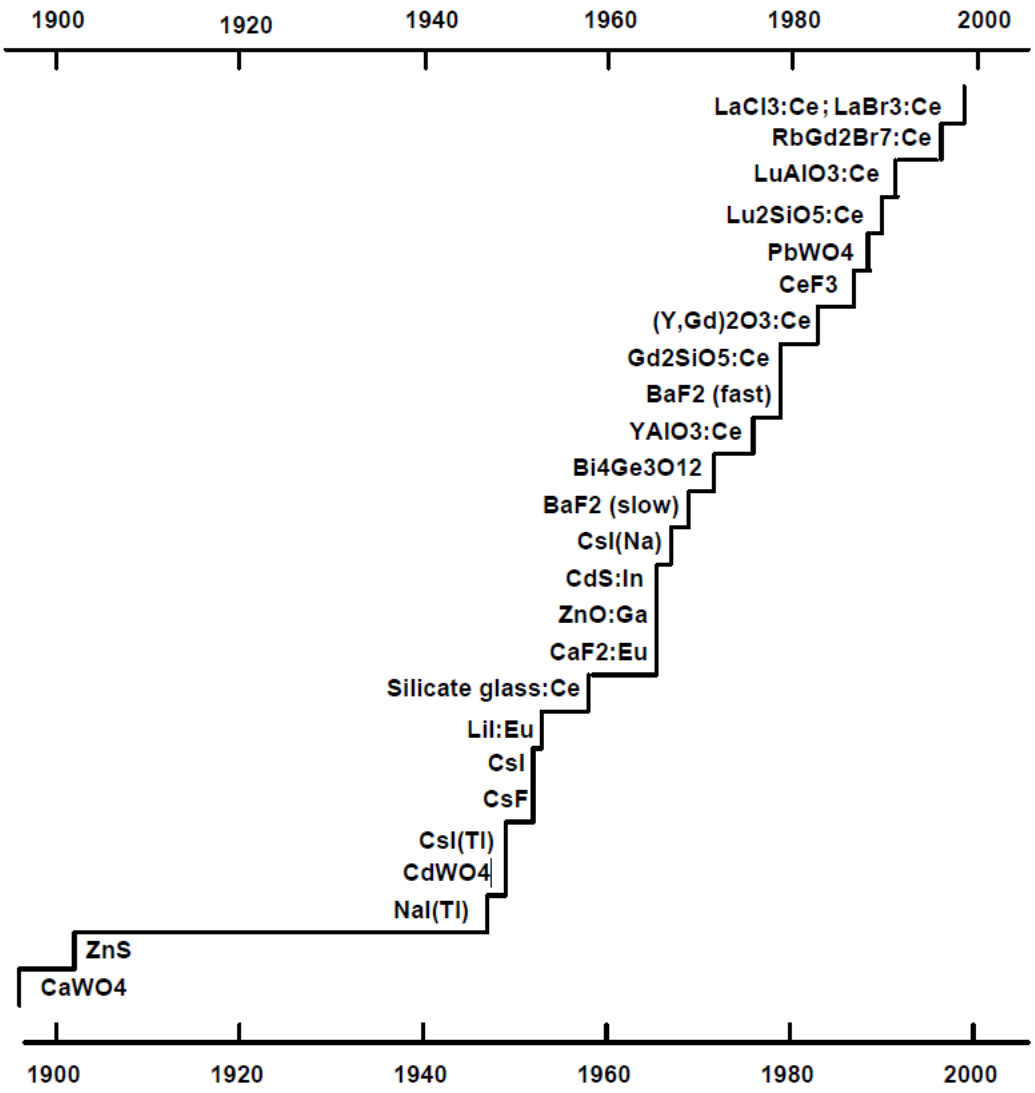

Figure 5. History of the discovery of important inorganic scintillator materials [6].

Medical imaging applications favor scintillators with high light output for improved spatial resolution of pixel arrays. Such arrays can then be used to produce high quality images to aid medical professionals in the early diagnosis of disease. Regardless of the application, cost is a major consideration for the widespread implementation of a detector [8].

The new generation of metal halide scintillator materials offers higher sensitivity and improved radioisotope identification. Crystals such as Lanthanum bromide doped with cerium ($LaBr_3$:Ce) and strontium iodide doped with europium (SrI_2:Eu), with light yields above 70,000 photons per megaelectron volts (ph/MeV) and energy resolutions well below 3% at 662 kiloelectron volts (keV), have shown the potential to replace NaI:Tl in applications where excellent energy resolution and high light yield are required. But their higher cost and lower production yield compared to NaI(Tl) have prevented their wide spread utilization in many gamma ray applications [6, 9-12]

1.4. Research Overview

The purpose of this project is to address the need for cost effective high-performance scintillator material that could be used for radiation detection application for national security applications. The current state-of-the-art for isotope identification via gamma ray spectroscopy includes: (1) High Purity Germanium detectors (HPGe) offer an unparalleled energy resolution but are expensive and require cryogenic cooling which is cumbersome to maintain, (2) Cadmiun Zinc Telluride (CZT) semiconductors are also expensive and the growth technology has not advanced enough to produce crystals large enough for some applications, (3) Na:Tl scintillators are much less expensive than semiconductors but their poor energy resolution limits its usability in next generation instruments, and (4) Plastic scintillators with low cost but almost no spectroscopic capability [10]. Figure 6 shows natural background spectra collected using various detectors. Table 1 summarizes the most important parameters of these materials. HPGe and

CZT have far superior isotope identification capability compared NaI:Tl, but their high initial cost limits their wide spread utilization [9]. Thus, there is a clear need for large size, low cost detectors with energy resolution below 3% at 662 keV.

The compositional space that we have been investigating is shown in Figure 7. Specifically, we have been exploring ternary metal halide compounds on the left side of the triangle with the general formulas ABX_3, AB_2X_5, and A_2BX_4, where A is an alkali metal, B is an alkaline earth metal, and X is a halogen. In all cases the compounds are activated with divalent europium to provide scintillation emission via 5d to 4f radiative transitions. Europium occupies the alkali earth site in these compounds. Note that our research differs from the more traditional approach in that we did not exclude potassium compounds from consideration.

Thus, we discovered three new scintillators from the AB_2X_5 compositional family; potassium strontium iodide doped europium (KSr_2I_5:Eu), potassium strontium bromide doped europium (KSr_2Br_5:Eu), potassium barium iodide doped europium (KBa_2I_5:Eu) and one belonging to the A_2BX_4 compositional family: potassium barium iodide doped europium (K_2BaI_4:Eu). From our initial screening process these scintillators showed promising properties with light yields well above 50,000 ph/MeV and energy resolution 2.4 – 2.9% at 662 keV in small sizes. Equally important is that fact that these new scintillators have the potential to be inexpensive due to the combination of low cost raw materials, high yield and production rates up to 10 times faster, compared to SrI_2:Eu and $LaBr_3$:Ce. The materials have about the same level of hygroscopicity as NaI:Tl, and effective packaging is available. The newly discovered scintillator materials and their properties are listed in Table 2. Note that these results represent only the very first samples ever grown of these compounds, and it reasonable to expect significant improvement during this work.

The only obvious disadvantage of these new compounds is their potassium content which produces a gamma-ray background of six disintegrations per second per cube centimeter of scintillator volume from the potassium 40 (^{40}K).

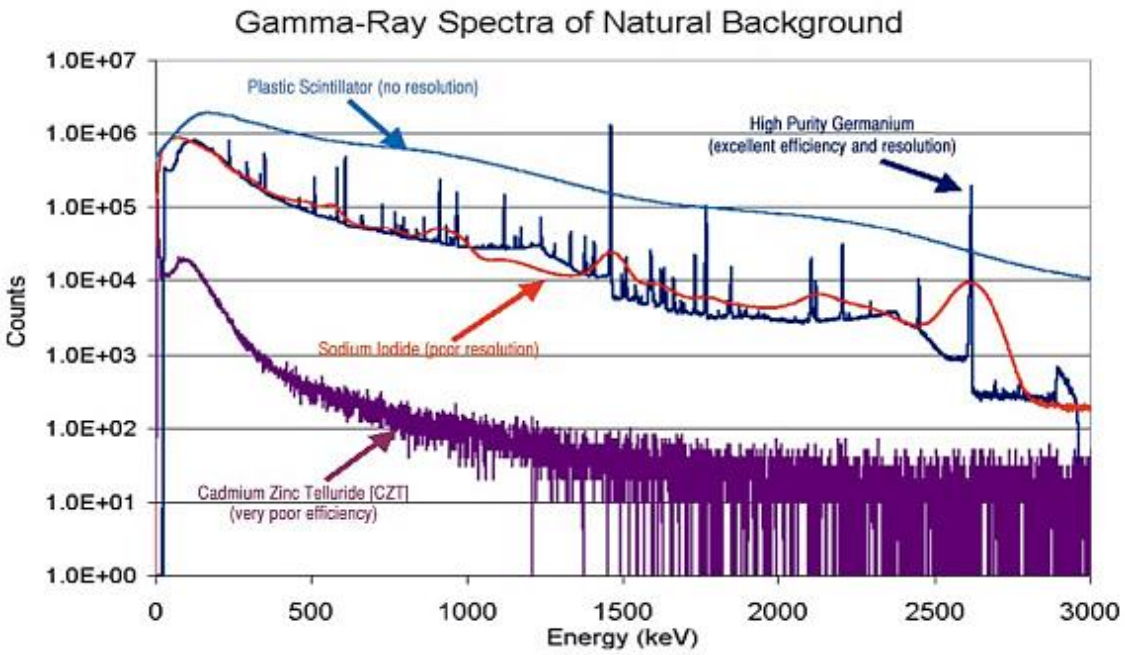

Figure 6. Comparison of natural background spectra measured with various detectors [13].

Table 1. Parameters of various radiation detectors.

	Adequate resolution?	*Availability (size)?*	*Low cost?*
PVT	***No***	Yes	$
NaI:Tl	***No***	Yes	$$
CZT	Yes	***No***	***$$$$***
HPGe	Yes	Yes	***$$$$$$***

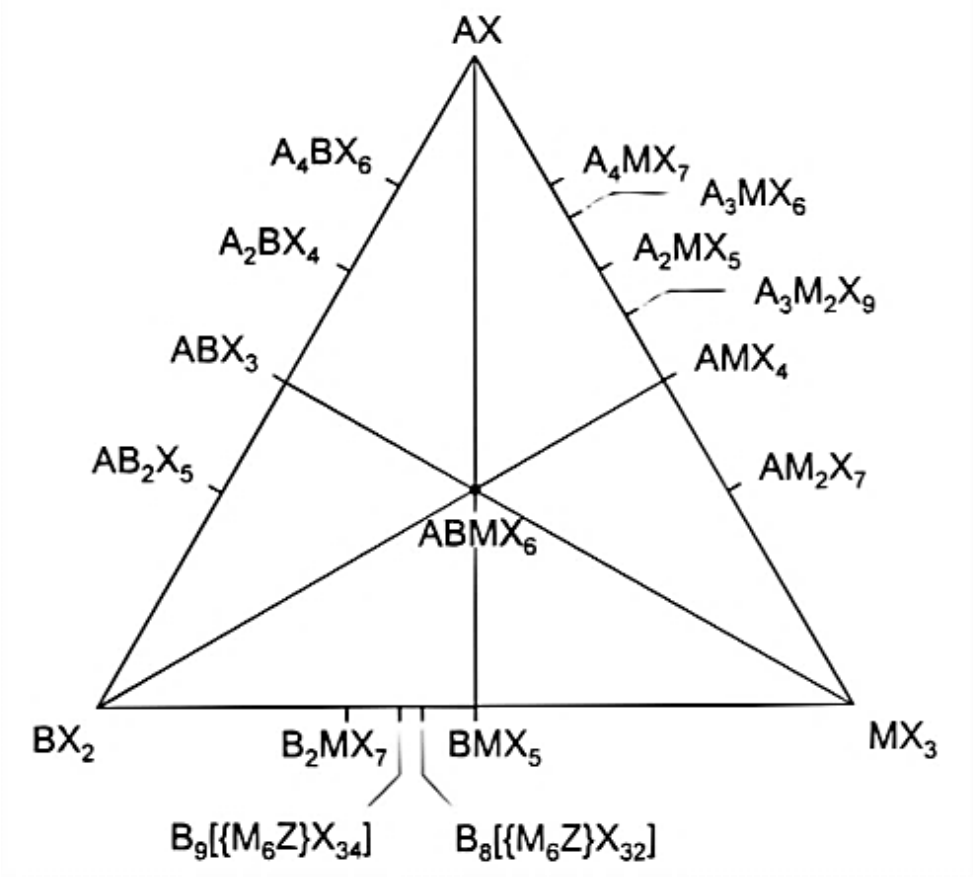

Figure 7. Ternary metal halide compositional space [14].

Table 2. Newly discovered scintillators.

	LY (Ph/MeV)	*E.R (662 keV)*	*Decay time (ns)*
KSr_2I_5:*Eu*	94,000	2.4%	990
K_2BaI_4:*Eu*	57,000	2.7%	720
KSr_2Br_5:*Eu*	75,000	3.5%	1080
KBa_2I_5:*Eu*	87,000	2.6%	910

^{40}K is a long-lived radioisotope that is naturally occurring. It is 0.0117% abundant in natural potassium with a half-life of $1.248*10^9$ years. Its decay has three different paths, as outlined in Figure 8. ^{40}K decays via electron capture 10.72% and negatron emission 89.28% of the time. When decaying through electron capture there is a small, but measurable, probability of decaying through positron emission with the maximum number of counts at 483 keV and a maximum energy of 1.31 MeV. Further, 99.5% of electron capture decays to an excited state of calcium 40, resulting in the emission of a 1.46 MeV gamma-ray 10.67% of the time. However, we feel that the actual effect of the background radiation on detector sensitivity and specificity has not yet been adequately characterized, and the performance and cost of these scintillators is so promising that we should devote considerable effort to this issue.

One simple calculation can be done to crudely compare the relative background intensities of ^{40}K in KSr_2I_5:Eu and lanthanum 138 (^{138}La-138) in $LaBr_3$:Ce. As seen in Table 3, the background intensity per cm^3 of scintillator crystal is about four times higher in the potassium compound compared to $LaBr_3$:Ce. However, note that La also can contain actinium 227 (^{227}Ac) contamination that decays by alpha particle emission. Due to their short range, the alpha particles are efficiently detected even by very small crystals.

The purpose of this work is to produce single crystals of these newly discovered scintillators KSr_2I_5:Eu, KSr_2Br_5:Eu, KBa_2I_5:Eu and K_2BaI_4:Eu, to investigate their physical and scintillation properties, and to select the most promising candidate for further development for national security applications. Note that for this work effect of ^{40}K background on the detection efficiency and time of detection in national security application is not discussed.

1.4.1. Preview of Dissertation Structure

This work can be divided into three major parts:

1. Discovery and characterization of ternary Eu^{2+} doped K-based scintillators.

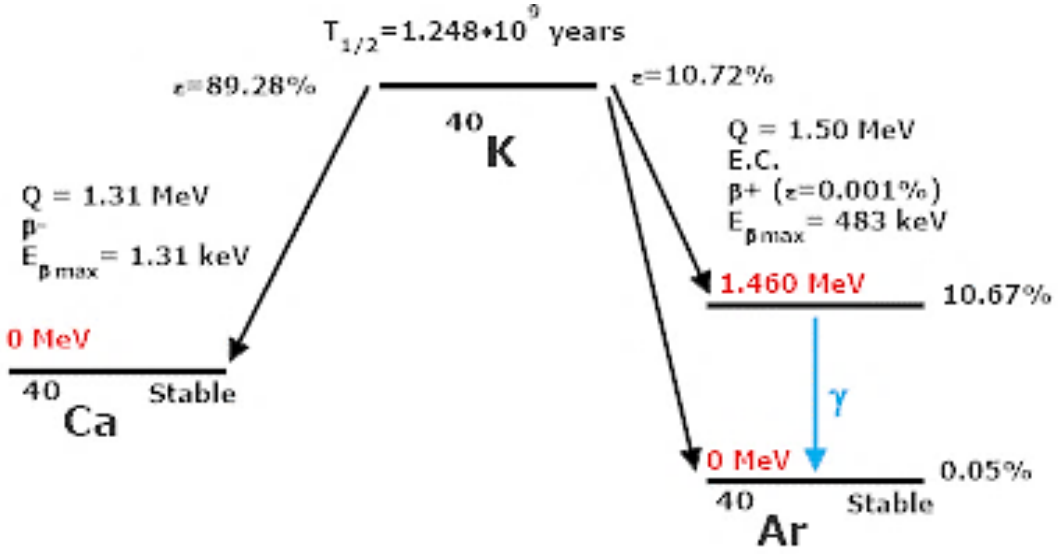

Figure 8. Decay scheme of potassium-40.

Table 3. Comparison of natural activity in $LaBr_3$:Ce and KSr_2I_5:Eu scintillators per crystal volume. Assumes 5% Ce in $LaBr_3$:Ce. Note that $LaBr_3$:Ce can also exhibit background due to alpha decay from ^{227}Ac contamination.

	Isotope	*Natural Abundance(%)*	*Half-life (yr)*	*Gamma-ray energy (MeV)*	*Activity (Bq/cm^3)*
$LaBr_3$:Ce	^{138}La	0.090	1.05×10^{11}	1.44	1.5
KSr_2I_5:Eu	^{40}K	0.012	1.25×10^{9}	1.46	6.5

- Chapter 2 Growth and characterization of potassium strontium iodide: A new high light yield scintillator with 2.4% energy resolution
- Chapter 3 Crystal growth and Scintillation Properties of Potassium Strontium Bromide.
- Chapter 4 Scintillation properties of Eu^{2+}-doped KBa_2I_5 and K_2BaI_4

2. Development of Eu^{2+} doped of KSr_2I_5
   - Chapter 5 Exploring Growth Conditions and Eu^{2+} Concentration Effects for KSr_2I_5:Eu Scintillator Crystals.
   - Chapter 6 Exploring Growth Conditions and Eu^{2+} Concentration Effects for KSr_2I_5:Eu Scintillator Crystals II: Ø 25 mm Crystals.
   - Chapter 7 Characterization of Large-Volume KSr_2I_5:Eu^{2+} Scintillators.
3. Compositional and defect engineering in KSr_2I_5 scintillators.
   - Chapter 8 Crystal Growth and Scintillation Characterization of High Performing $KSr_2Br_xI_{5-x}$:Eu^{2+} and $KSr_{1.3}Ba_{0.7}I_5$:Eu^{2+} Solid Solutions.

Chapter 2
Growth and Characterization of Potassium Strontium Iodide: A New High Light Yield Scintillator With 2.4% Energy Resolution

A version of this chapter was originally published in peer-reviewed journal by Luis Stand. No additional changes were made other than formatting to conform to the dissertation format.

The full citation is as follows: L. Stand, M. Zhuravleva, A. Lindsey, C.L. Melcher, Growth and characterization of potassium strontium iodide: A new high light yield scintillator with 2.4% energy resolution, Nuclear Instruments and Methods in Physics Research Section A: Accelerators, Spectrometers, Detectors and Associated Equipment, 780 (2015) 40-44 [15].

The co-authors provided valuable research advice during this research.

Abstract

A new ternary metal halide scintillator, potassium strontium iodide, activated with divalent europium (KSr_2I_5: Eu) has been discovered. This material has a monoclinic crystal structure with a density of 4.39 g/cm^3. Differential scanning calorimetry indicates a congruent melting point of 470 °C (degree Celsius) and suggests that this compound has no solid–solid phase transitions. As is the case with most metal halides, the material is hygroscopic, and it has some internal radioactivity due to the presence of ^{40}K. Single crystals of KSr_2I_5 doped with 4% Eu were grown in evacuated quartz ampoules via the Bridgman technique. The X-ray excited emission spectrum consisted of a single peak at 445 nm due to the 5d–4f transition in Eu^{2+}. The measured light yield is 94,000 photons/MeV with an energy resolution of 2.4% at 662 keV. The crystal has an excellent proportionality response over a wide range of energies from 14 keV to 1275 keV.

2.1. Introduction

Scintillators are common radiation detectors with a variety of applications, many of which have specialized requirements; as a result, scintillators are often developed with properties suitable for specific applications and devices in mind. Utilization for nuclear nonproliferation requires excellent energy resolution for

spectroscopic differentiation of radioisotopes to minimize false alarms [16]. Medical imaging applications favor scintillators with high light output for improved spatial resolution of pixel arrays. Such arrays can then be used to produce high quality images to aid medical professionals in the early diagnosis of disease. Regardless of application, cost is a major consideration for widespread implementation of a detector [7]. Current radiation detectors fail to satisfy these requirements to some extent. High purity germanium detectors offer an unparalleled energy resolution, but are expensive and require cryogenic cooling which is cumbersome to maintain. Another promising semiconductor radiation detector, CZT, is also expensive and growth technology has not advanced enough to produce crystals large enough for some applications. One of the most common scintillators on the market, NaI:Tl, has become very cheap to manufacture in large quantities though its energy resolution limits its usability in next generation instruments [11]. Plastic scintillators are attractive for some applications because they can be made in a variety of shapes and sizes, but their very poor energy resolution limits their applicability. Metal halide compositions have been used as scintillators since NaI:Tl was first discovered in 1948. More recently, $LaBr_3$:Ce [17] and SrI_2:Eu [18] have emerged as materials with potential to supersede NaI:Tl due to their excellent scintillation properties.

Recently, KSr_2I_5:Eu was discovered at the Scintillation Materials Research Center. KSr_2I_5:Eu 4% has a measured light yield of 94,000 ph/MeV and an excellent energy resolution of 2.4% at 662 keV [19]. The crystal structure of KSr_2I_5 was first reported by Schilling et al. It has a monoclinic structure with space group $P121/c_1$ and a density of 4.39 g/cm^3 [20]. The effect of the ^{40}K background radiation on isotope identification sensitivity remains to be quantitatively analyzed, but these properties suggest that it may be well suited for uses in both homeland security and medical imaging where this high light output and excellent energy resolution are crucial for next generation applications.

2.2. Experimental Techniques

2.2.1. Crystal Growth and Characterization

The 99.99% pure KI, SrI_2 and EuI_2 raw materials from Sigma-Aldrich were mixed and loaded into quartz ampoules in a dry box with <0.1 ppm moisture and oxygen. All ampoules were cleaned with deionized water and baked at 200°C before use. The loaded ampoules were dried at 200°C and sealed under a vacuum of 10^{-6} torr. Single crystals of 13 and 22 mm in diameter were grown by the Bridgman technique. A two-zone transparent furnace was used to allow the observation of melting, nucleation, and evolution of the solid-liquid interface shape. Crystal growth was initiated on a 2-mm diameter grain selector connected to the bottom of the ampoule. A relatively fast solidification rate of 5 mm/h and cooling rate of 10°C/h were used for the ø 13 mm crystal. For the ø 25 mm crystal a pulling rate of 1 mm/h and cooling rate of 5°C/h were used.

The melting and crystallization temperatures were determined through differential scanning calorimetry-thermogravimetric analysis (DSC-TGA) using a Setaram Labsys Evo TG-DSC. The measurement was carried out on a ~50 mg specimen at 5 K/min, under a flow of ultra-high purity argon gas. Moisture sorption profiles were recorded using a Dynamic Vapor Sorption technique with a DVS Intrinsic instrument by Particulate Systems. Spherical samples with a surface area of ~28±2 mm^2 were prepared. The measurements were carried out at 25°C for 60 minutes at a relative humidity of 40%. Steady state photoluminescence spectra were collected at room temperature using a Horiba Fluorolog-3 Spectrofluorometer equipped with a Xe lamp and dual scanning monochromators.

The scintillation light yield was measured by coupling a sample to a Hamamatsu 3177-50 PMT and recording the response to 662 keV gamma rays from a ^{137}Cs source. The specimens were placed in a quartz container filled with mineral oil to protect them from moisture during the measurement. The mineral oil also served as optical coupling between the quartz container and PMT. A

hemispherical dome of Spectralon was used to diffusely reflect the scintillation light into the PMT, and a shaping time of 10 μs was used to ensure the complete integration of the light pulse. The number of photoelectrons was calculated from the position of the 662 keV photopeak and the peak from single photoelectrons. The conversion from the number of measured photoelectrons to the number of photons/MeV emitted by the scintillator was accomplished by convolving the quantum efficiency of the PMT as a function of wavelength (measured by the manufacturer of our specific PMT) with the X-ray excited emission spectrum of the sample. We assumed 100% collection of photons by the PMT which likely gives a somewhat pessimistic estimate of the crystal's actual light output. Measurements of energy resolution for ^{137}Cs, ^{57}Co and ^{241}Am gamma rays were recorded by coupling the samples to a Hamamatsu R6231-100 PMT. Radioluminescence spectra were measured at room temperature under continuous 30 keV X-ray irradiation. The emission spectra were recorded with a 150-mm focal length monochromator over a wavelength range of 200 to 800 nm. The scintillation decay time was measured under irradiation from a ^{137}Cs sealed source with the time-correlated single photon counting technique.

2.3. Result and Discussion

2.3.1. Crystal Growth

Large single crystals were obtained from both growth attempts. The ø 13 mm boule was grown at a remarkably fast rate (5 mm/hr) and fast cooling rate (10°C/hr), and the result was the highly transparent, virtually crack free, colorless single crystal shown in Figure 9. The ø 22 mm boule was growth rate at 1 mm/h and cooled to room temperature at 5 °C/h. The result was a highly transparent crystal, shown in Figure 10. The growth parameters used for KSr_2I_5:Eu are at least 5 times faster when compared SrI_2:Eu.

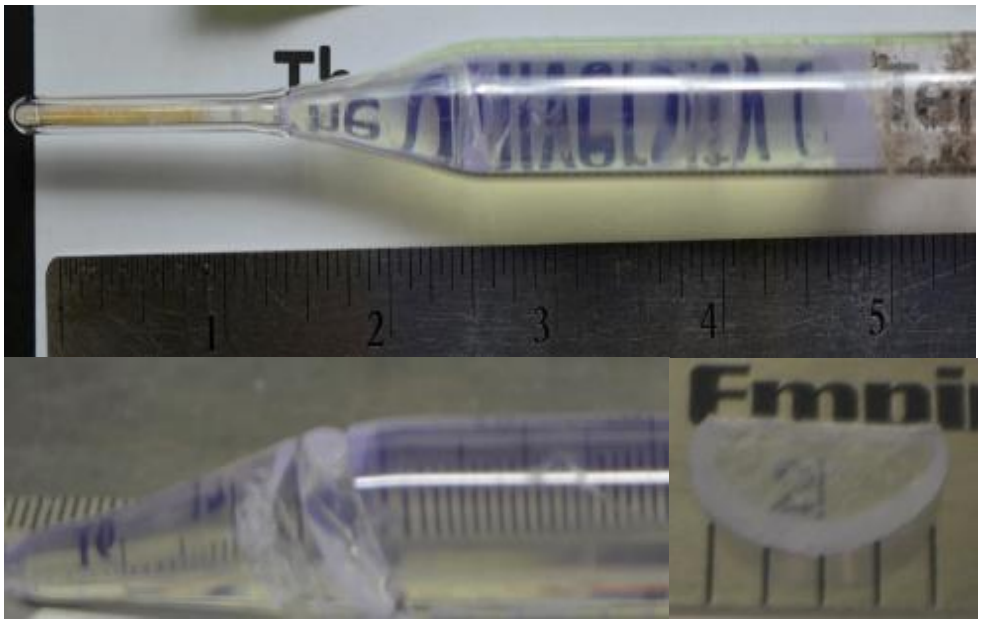

Figure 9. Appearance of a 13 mm diameter single crystal of KSr_2I_5:Eu 4%: top – in the ampoule.

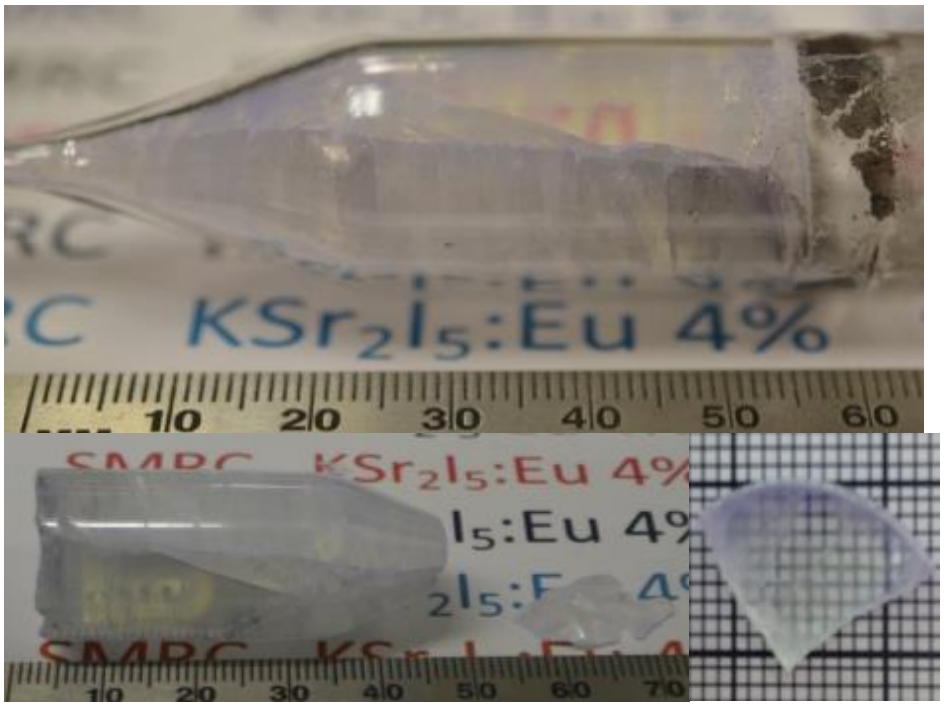

Figure 10. Appearance of a 22 mm diameter single crystal of KSr_2I_5:Eu 4%: top – in the ampoule, bottom – bare crystal.

2.3.2. Melting Point Determination and Hygroscopicity Evaluation

Differential scanning calorimetry was performed on KSr_2I_5:Eu 4% to determine its melting point. The scan shown in Figure 11 indicates that the melting point is 470°C, and its crystallization point is 466°C. A small feature at 410°C needs further investigation.

The Dynamic Vapor Sorption technique was used to compare the moisture absorption rate of KSr_2I_5:Eu 4% to other scintillators. The moisture absorption rate of $LaBr_3$:Ce 5%, SrI_2:Eu 1% and NaI:Tl were measured under identical conditions. Attempting to reproduce typical operational conditions of detectors, a temperature of 25 °C and relative humidity of 40% were selected. The initial degradation effects from moisture can be seen almost instantaneously, and further moisture absorption continues during the 60-minute acquisition time used for this measurement. The moisture absorption rate of KSr_2I_5:Eu is ~2.5 times higher than the one of NaI:Tl, but when compared to SrI_2:Eu and $LaBr_3$:Ce, a ~20% reduction of the rate is observed, as shown in Figure 12. This could represent a significant advantage for handling and packaging for various applications.

2.3.3. Luminescence Properties

The xray emission peak is at ~445 nm and is ascribed to the Eu^{2+} 5d-4f transitions [21, 22]. Also the presence of a~560 nm band was seen which is associated with oxygen related impurities. The X-ray excited radioluminescence spectrum of KSr_2I_5 with Eu^{2+} concentration 4 mol% is shown in Figure 13.

Photoluminescence excitation and emission spectra of KSr_2I_5:Eu 4% are shown in Figure 14. The emission spectrum consists of a single peak at 445 nm, where the excitation used was 430 nm. The excitation spectrum was measured using 445 nm as the emission. It consists of multiple unresolved bands from ~375 nm to ~433 nm, which is characteristic of Eu-doped scintillators. No evidence of emission from perturbed Eu was observed.

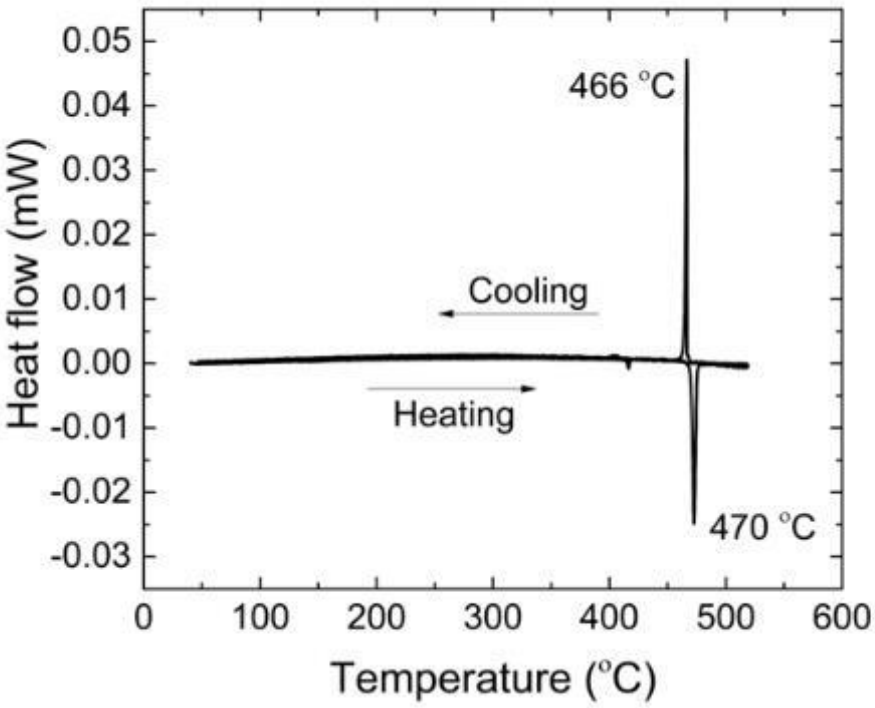

Figure 11. Differential scanning calorimetry indicates a melting point of 470°C and crystallization point of 466°C.

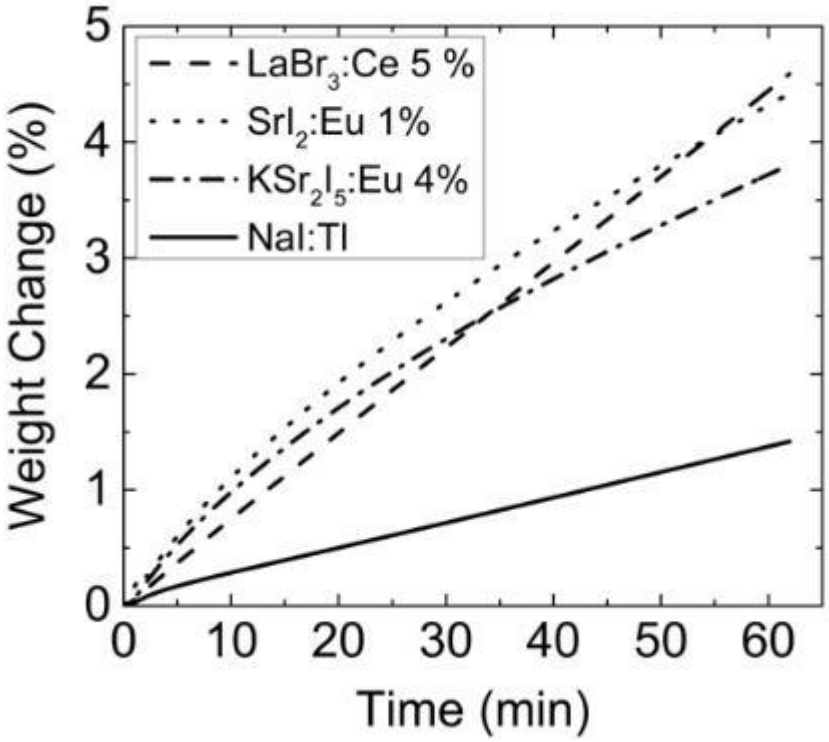

Figure 12. DVS curves of $LaBr_3$:Ce (most hygroscopic), SrI_2:Eu 1%, KSr_2I_5:Eu 4% and NaI:Tl (least hygroscopic).

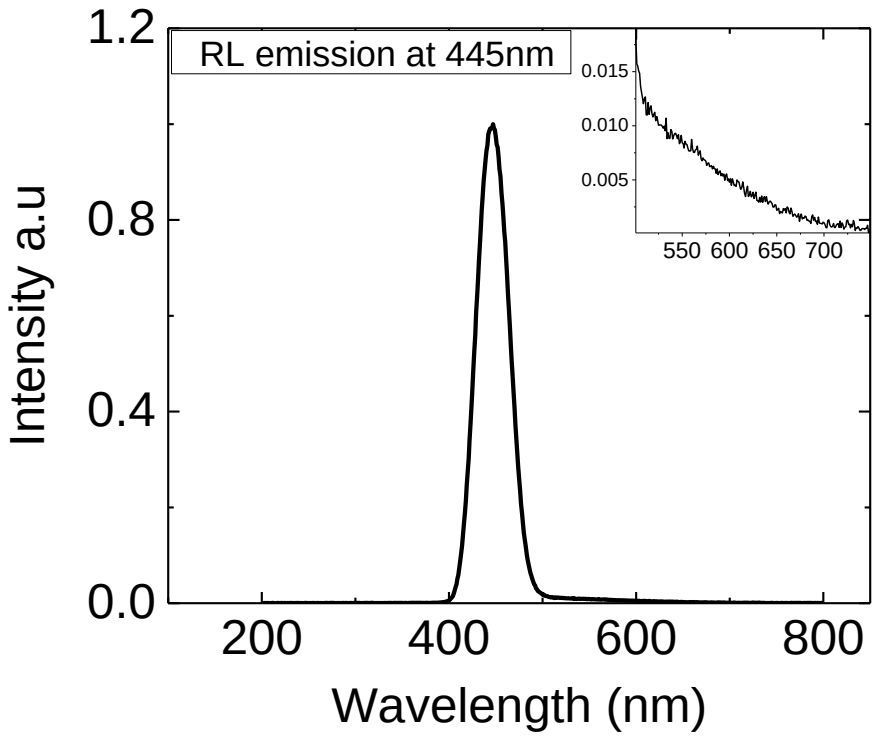

Figure 13. RL emission spectrum excited with 30 keV X-rays of KSr_2I_5:Eu 4%.

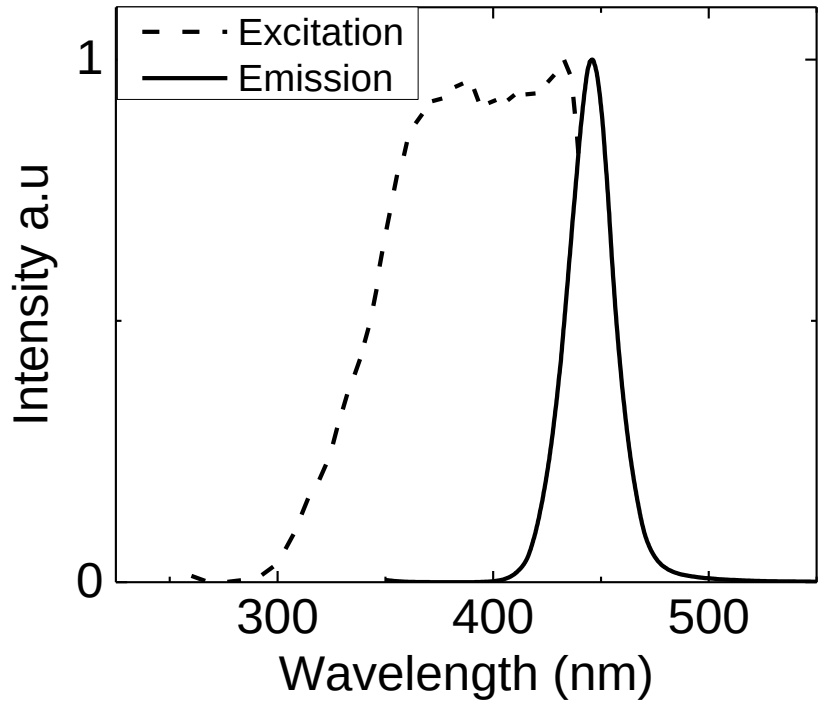

Figure 14. Photoluminescence excitation and emission spectra of KSr_2I_5:Eu 4%.

2.3.4. Scintillation Properties

The scintillation light yield and energy resolution of KSr_2I_5:Eu 4% at 662 keV showed a slight variation according to the size of the measured sample. With a specimen measuring ~2 × 1 × 1 mm^3, we measured a yield of 94,000 ph/MeV with an energy resolution of 2.4% at 662 keV, as shown in Figure 15a. The energy resolution at 122 keV (^{57}Co) was measured to be 5.7% as shown in Figure 15b and 7.2% at 59.6 keV (^{241}Am) shown in Figure 15c. These energy resolutions, obtained on samples from early growth runs, are comparable to the best achieved by more mature high performance scintillators, such as $LaBr_3$:Ce,Sr, SrI_2:Eu and $CsBa_2I_5$:Eu [18, 23-30]. Table 4 shows a summary of scintillation properties of KSr_2I_5:Eu, compared to other known scintillators. For γ-ray non-proportionality measurements, a set of γ-ray sources was used to obtain excitation energies ranging from 14 to 1275 keV. The scintillation light yield per unit energy as a function of deposited γ-ray energies is shown in Figure 15d. The relative light yield varies by less than 3% over the entire measured energy range. A slight increase is observed between 31 and 88 keV, and a slight decrease is observed below 22 keV. The scintillation decay profile of a single crystal of KSr_2I_5:Eu 4% is shown in Figure 15e. The scintillation decay time was fitted with a two-component exponential function. The primary decay component was found to be 0.99 μs and consisted of ~89% of the total emitted light. The secondary decay component of 5 μs accounts for the remaining light. These time profiles are typical for Eu^{2+} doped scintillators.

2.4. Conclusion

Potassium strontium iodide doped with divalent europium is a very promising candidate for many gamma-ray and X-ray detection applications. While the effect of the ^{40}K background on isotope identification sensitivity remains to be quantitatively analyzed, it is worth noting that potassium is sometimes incorporated into radiation detectors for energy calibration.

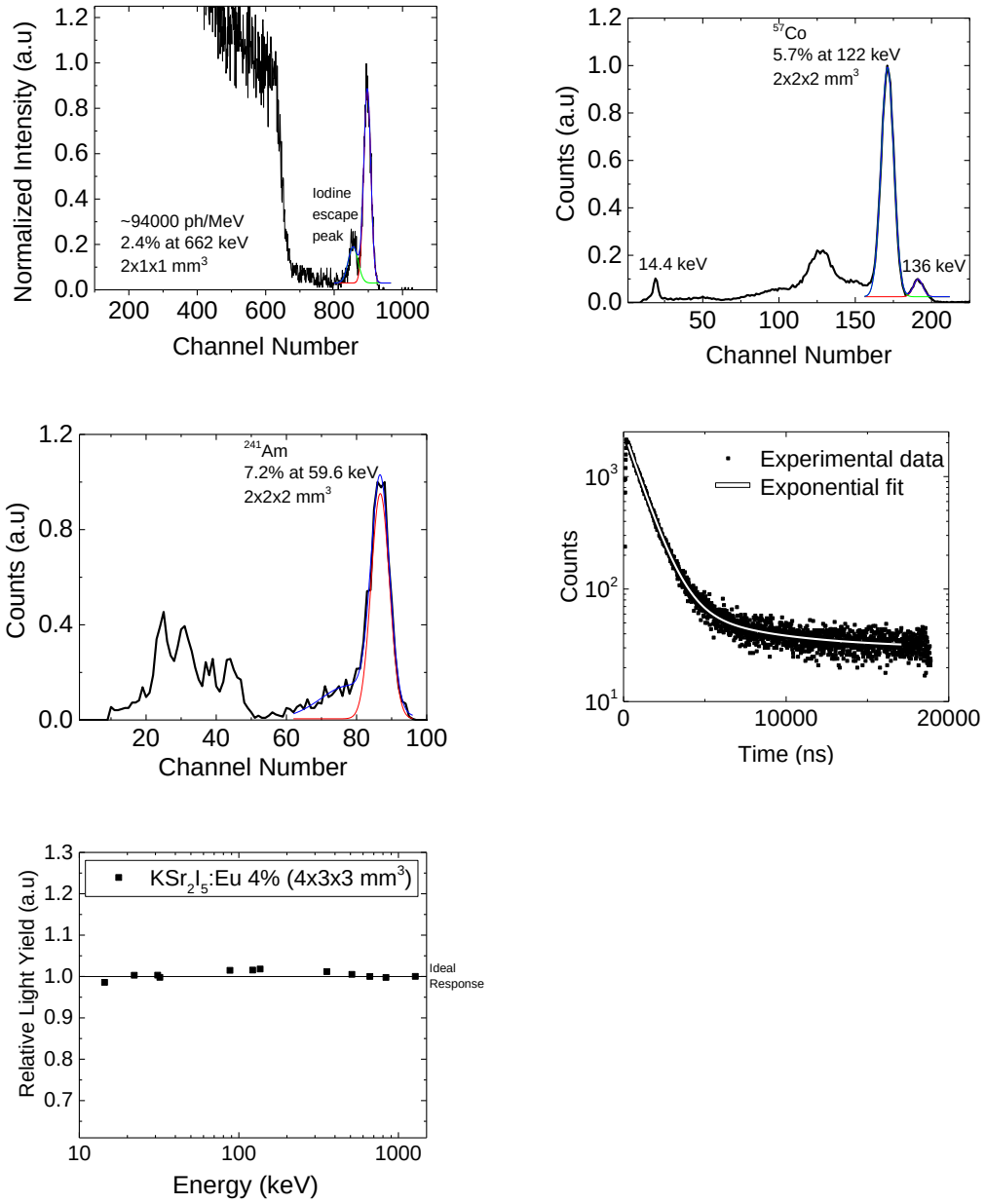

Figure 15a-c. Pulse height spectrum of KSr_2I_5:Eu 4% under ^{137}Cs , ^{57}Co and ^{241}Am excitation and (5d-e) Scintillation decay time and non-proportionality measurement of KSr_2I_5:Eu 4%.

Table 4. Comparison of scintillation properties

	KSr_2I_5:Eu 4%	*NaI:Tl*	*$CsBa_2I_5$:Eu*	*SrI_2:Eu*	*$LaBr_3$:Ce*
RL (nm)	445	415	432	435	380
Decay (ns)	990	230	1000	1000	16
LY (ph/MeV)	94,000	38,000	80,000	100,000	67,000
E.R @ 662 keV	2.4%	7.1%	2.3%	2.6%	3.2%

A summary of the physical and scintillation performance properties of KSr_2I_5:Eu 4% is shown in Table 5. Its high light yield of 94,000 ph/MeV and excellent energy resolution of 2.4% at 662 keV are comparable to the best known scintillators such as $LaBr_3$:Ce, SrI_2:Eu and $CsBa_2I_5$:Eu. Its excellent proportionality response to γ-rays suggests that further improvement in energy resolution may be possible. The ease of crystal growth and the ability to grow high quality crystals at rates at least 5 times faster than SrI_2:Eu, is promising and expect to have a significant impact on the production cost.

Future investigations will focus on optimizing the crystal growth conditions, purification of the raw materials and codoping to improve response and performance.

Table 5. Summary of properties of KSr_2I_5:Eu 4%

Tm (°C)	*Density (g/cm^3)*	*Crystal structure*	*Light Yield (ph/MeV)*	*Energy Resolution (at 662 keV)*	*Primary Decay (ns)*
471	4.39	Monoclinic	94,000	2.4%	990

Chapter 3
Crystal Growth and Scintillation Properties of Potassium Strontium Bromide

A version of this chapter was originally published in peer-reviewed journal by Luis Stand. No additional changes were made other than formatting to conform to the dissertation format.

The full citation is as follows: L. Stand, M. Zhuravleva, H. Wei, C.L. Melcher, Crystal growth and scintillation properties of potassium strontium bromide, Optical Materials, 46 (2015) 59-63 [31].

The co-authors provided valuable research advice during this research.

Abstract

In this work, potassium strontium bromide activated with divalent europium, (KSr_2Br_5:Eu) has been studied. It has a monoclinic crystal structure and a density of 3.98 g/cm^3. Two single crystals of KSr_2Br_5 doped with 5% Eu^{2+}, with diameters of 13 mm and 22 mm, were grown in a two zone transparent furnace via the Bridgman technique. The X-ray excited emission spectrum consisted of a single peak at ~427 nm due to the 5d-4f transition in Eu^{2+}. The measured light yield and energy resolution at 662 keV was 75,000 ph/MeV and 3.5%. At low energies KSr_2Br_5:Eu 5% also displays good energy resolution, 6.7% at 122 keV and 7.9% at 59.5 keV.

3.1. Introduction

Scintillators are used for many gamma-ray and X-ray applications, each of which may require specific and differing properties. Gamma-ray spectrometers used for nuclear nonproliferation will aid in the search for nuclear weapons by identifying the X-ray and gamma-ray signatures of highly enriched uranium and plutonium. Therefore, a detector with excellent energy resolution is essential in order to correctly identify radioisotopes and to minimize false alarms [32]. Medical imaging applications favor scintillators with high light output for improved spatial resolution of pixel arrays that are used to produce high quality images for the early diagnosis of disease [8]. In both cases the cost is a key factor when considering a

scintillator for widespread implementation. For this reason alone, NaI:Tl^+, is one of the most commonly used scintillators, despite its modest light yield and energy resolution [11], which will limit its usability in next generation instruments [33].

In recent years substantial efforts have been made to discover and develop new metal halide scintillators, mainly due to their high light yield and excellent energy resolution. Scintillators such as SrI_2:Eu^{2+}[34], $LaBr_3$:Ce^{3+}[9] , LuI_3:Ce^{3+}[35], $CsSrI_3$:Eu^{2+} [36], $CsBa_2I_5$:Eu^{2+} [30] and KSr_2I_5:Eu^{2+} [15] have shown exceptional properties, approaching the fundamental limits [6].

KSr_2Br_5, the bromide analog to KSr_2I_5, it also has a monoclinic crystal structure with space group $P12_1/c1$ and a density of 3.98 g/$cm^{3,}$ as first reported by Schilling et al. [19]. In this work we present the crystal growth and scintillation properties of Eu^{2+}-doped KSr_2Br_5:Eu 5%.

3.2. Experimental

3.2.1. Crystal Growth

The 99.99% pure, anhydrous KBr, $SrBr_2$ and $EuBr_2$ raw materials from Sigma-Aldrich were mixed and loaded into a quartz ampoule in a dry box with <0.1 ppm concentration of water and oxygen. All ampoules were cleaned with deionized water and baked at 200˚C before use. The loaded ampoules were dried at 200˚C and sealed under a vacuum of 10^{-6} torr.

Single crystal boules, 13 and 22 mm in diameter (ø), of KSr_2Br_5:Eu 5% were grown using a two zone transparent furnace. A diaphragm was used to achieve thermal separation between the heating zones; gradients ranging from 14°C/cm to 55°C/cm were used. Both crystal growth experiments were initiated by a ø 2 mm grain selector connected to the bottom of the ampoule. A solidification rate of 2 mm/h and a cooling rate of 7°C/h were used for the ø 13 mm crystal while for the ø 22 mm crystal a slower growth rate of 1 mm/h and a slower cooling rate of 5°C/h were used. Table 6 shows a summary of the growth conditions used.

Table 6. Summary of growth conditions

Crystal Diameter (mm)	*Growth Rate (mm/h)*	*Gradient at interface (°C/cm)*	*Cooling rate (°C/h)*	*Grain selector*
13	2	14	7	Yes
22	1	55	5	Yes

3.2.2. Characterization

The melting and crystallization points of an approximately 50 mg specimen were determined using a Setaram Labsys Evo TG-DSC [37]. In order to avoid sample degradation, the measurement was carried out under flowing ultra-high purity argon gas. Moisture sorption profiles were recorded using a Dynamic Vapor Sorption technique with a DVS Intrinsic instrument by Particulate Systems [38, 39]. These measurements were carried out at 25°C for 60 minutes at a relative humidity of 40%.

A Hamamatsu 3177-50 photomultiplier tube (PMT) and a Hamamatsu R6231-100 PMT were used to measure the absolute light yield and energy resolution (ER), respectively. The samples were placed in a quartz container filled with mineral oil to protect them from moisture during data acquisition. A hemispherical dome of Spectralon was used to diffusely reflect the scintillation light into the PMT, and a shaping time of 10 μs was used to ensure the complete integration of the light pulse.

Radioluminescence (RL) spectra were acquired at room temperature under continuous 30 kV X-ray irradiation. The emission spectra were recorded with a 150-mm focal length monochromator over a wavelength range of 200 to 800 nm. Steady state photoluminescence (PL) spectra were measured at room temperature with a Horiba Jobin Yvon Fluorolog 3 Spectrofluorometer equipped with a Xe lamp and dual scanning monochromators.

The scintillation decay time was measured under irradiation from a ^{137}Cs sealed source with the time-correlated single photon counting technique [40].

3.3. Results and Discussion

3.3.1. Melting Point Determination and Hygroscopicity Evaluation

The KBr-$SrBr_2$ phase diagram proposed by R. Riccardi *et al*. suggests that KSr_2Br_5 can be grown from the melt at a melting point of 572°C, with no low-temperature phase transition, and these results were confirmed by our differential

scanning calorimetry measurements [41]. The scan shows an endothermic peak at 575 °C and an exothermic peak at 557 °C corresponding to the melting and crystallization points, respectively. Therefore, KSr_2Br_5:Eu exhibits a characteristic supercooling of ~18 °C, shown in Figure 16. Small endothermic features are seen during the heating cycle at around 520 °C which could be related to impurities introduced during the measurement. No corresponding features were found upon cooling, which implies that the crystallization process is not affected. The melting and crystallization temperatures obtained from DSC measurements were used to design a thermal profile that produces a stable solid-liquid interface during crystal growth.

Since most metal halide scintillators are hygroscopic, it is imperative to understand how their physical integrity is affected by the absorption of moisture. The Dynamic Vapor Sorption (DVS) technique was used to measure the moisture absorption rate of KSr_2Br_5:Eu 5%. The DVS curve shows the change in weight due to the moisture absorption by the specimen as a function of time. In an effort to simulate the typical operational environment of gamma-ray detectors, the moisture absorption was measured at room temperature and a relative humidity of 40%. For comparison purposes several benchmark scintillators were measured under identical conditions. The weight change (%) over 60 min is shown in Figure 17. The weight gained by KSr_2Br_5:Eu 4% (2%) is comparable to NaI:Tl (1.6%), which is significantly lower than that of KSr_2I_5:Eu 4% (3.8%) and $LaBr_3$:Ce (8.9%). It is important to mention that scintillation properties of bromide-based crystals are not affected by the degradation products created by moisture absorption [42].

3.3.2. Crystal Growth of KSr_2Br_5:Eu 5%

Two single crystal boules of KSr_2Br_5:Eu 5% with 13 mm and 22 mm diameters were grown using a two-zone transparent furnace. For the 13 mm ø boule a thermal gradient of 14 °C/cm and a growth rate of 2 mm/h was used. To improve the optical quality of KSr_2Br_5:Eu the solidification rate was reduced from

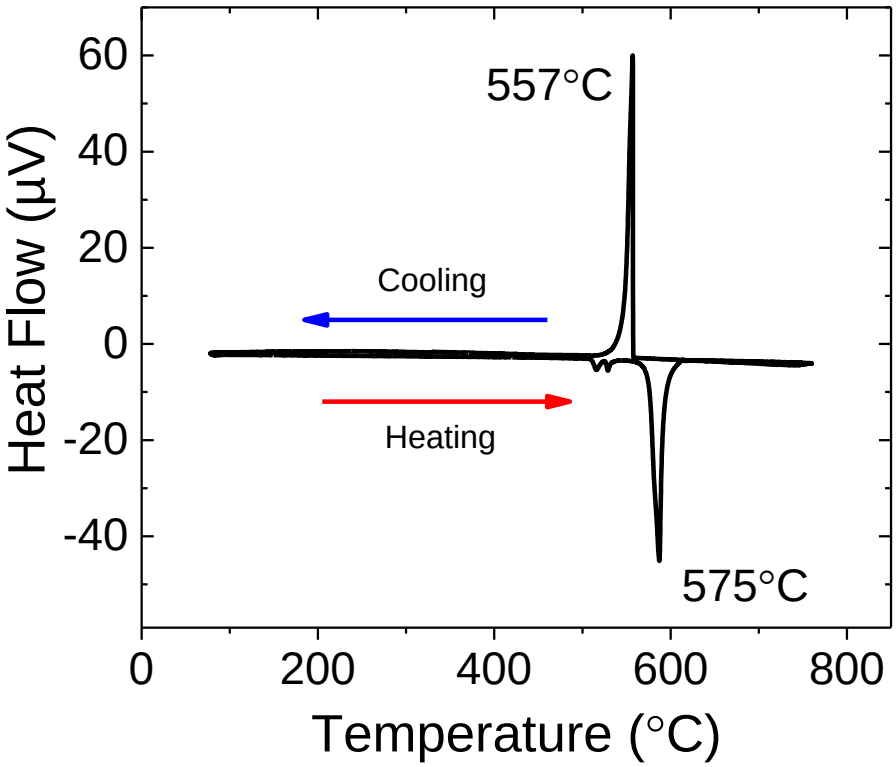

Figure 16. Differential scanning calorimetry of $KSr_2Br_5:Eu^{2+}$.

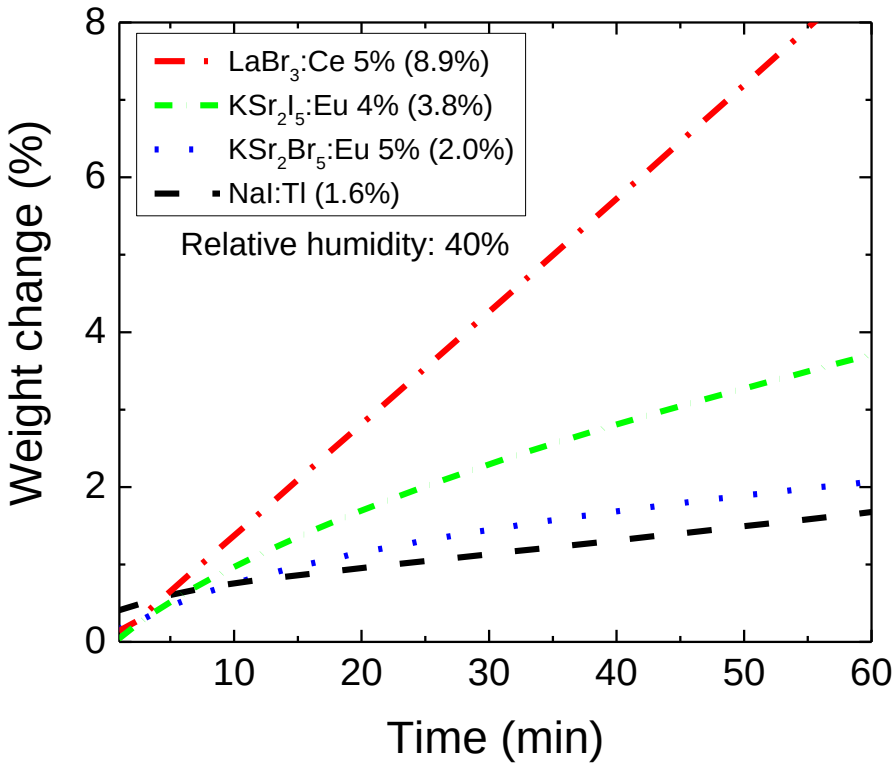

Figure 17. DVS curves of $LaBr_3$:Ce (most hygroscopic), KSr_2I_5:Eu 4%, KSr_2Br_5:Eu 2.5% and NaI:Tl (least hygroscopic).

2 mm/h to 1 mm/h for the 22 mm ø boule, under a thermal gradient of 55 °C/cm. The results of both experiments were nearly crack free, colorless single crystals as shown in Figure 18, and Figure 19 with even better optical clarity due to the improved growth parameters. It should be noted that the growth rates used for these KSr_2Br_5:Eu boules are very favorable to those reported for SrI_2:Eu (0.2 to 0.8 mm/h) [25, 43] and $La(Br/Cl)_3$:Ce (0.2 to 1.3 mm/h) [28].

3.3.3. Optical and Scintillation Properties

Photoluminescence (PL) excitation and emission spectra of KSr_2Br_5:Eu 5% are shown in Figure 20. The PL excitation spectrum comprises multiple unresolved overlapping bands from 300 nm to 410 nm. It was measured following 428 nm emission. KSr_2Br_5:Eu 5% exhibit a sharp PL emission band with peak maximum around 427 nm, when using any excitation wavelength in the range of 300–410 nm. These spectral features are attributed to the 5d-4f radiative transitions in Eu^{2+} [21, 22]. X-ray excited radioluminescence (RL) spectrum of KSr_2Br_5:Eu^{2+} 5 % is shown in Figure 21. The RL emission peak is centered at 427 nm [9]. The observed single emission peak can be solely attributed to the characteristic emission of divalent Eu 5d–4f transitions, which points to the fact that the Eu ions enter the crystal lattice in divalent form and easily substitute for Sr due to the similar ionic radius and valence [21].

The scintillation light yield and energy resolution of KSr_2Br_5:Eu 5% were acquired using a specimen measuring ~4 × 3 × 2 mm^3. We were able to achieve ~75,000 ph/MeV and an energy resolution of 3.5 % at 662 keV (^{137}Cs) as shown in Figure 22a. The energy resolution at 122 keV (^{57}Co) was 6.7% as shown in Figure 22b and 7.9% at 59.5 keV (^{241}Am) as shown in Figure 22c. At its optimal Eu^{2+} concentration of 5%, KSr_2Br_5 is one of the brightest single crystal bromide scintillators ever reported. The scintillation decay and nPR of a single crystal of KSr_2Br_5:Eu 5% is shown in Figure 22d and Figure 22e. The specimen measured was roughly 4 × 3 × 2 mm^3. The scintillation decay time was fitted with a two-

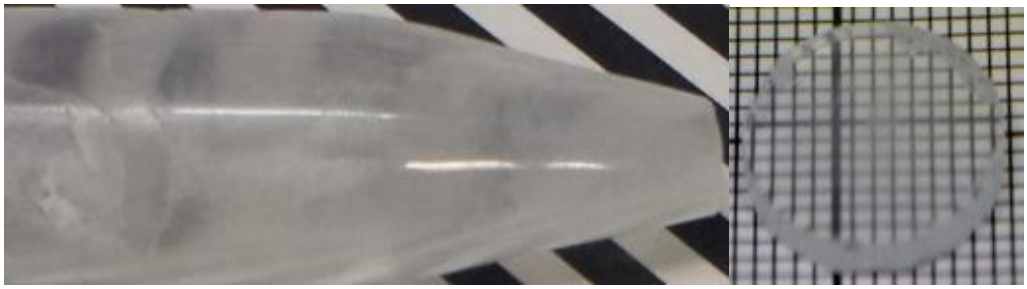

Figure 18. A 13 mm diameter single crystal boule of KSr_2Br_5:Eu 5% (left); a 2 mm thick polished disk (right).

Figure 19 . A 22 mm diameter single crystal boule of KSr_2Br_5:Eu 5% still within the quartz ampoule (left); a 10 mm tall truncated cone, ø 22 mm bottom × ø 15 mm top (right). Note that despite the significantly larger size, this sample is much more transparent.

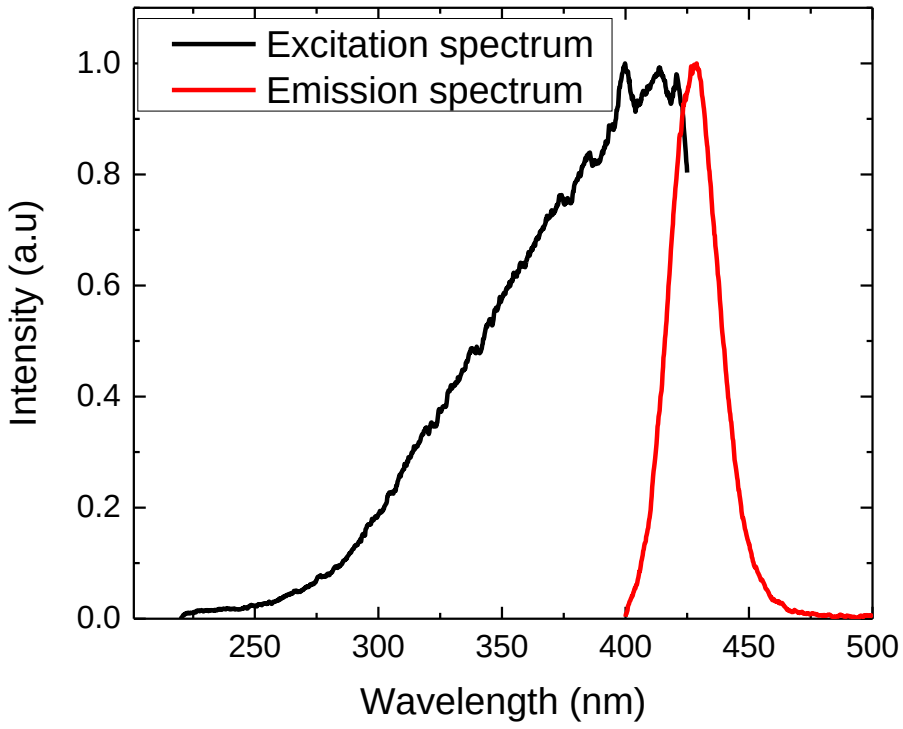

Figure 20. Photoluminescence excitation and emission spectra of KSr_2Br_5:Eu 5%.

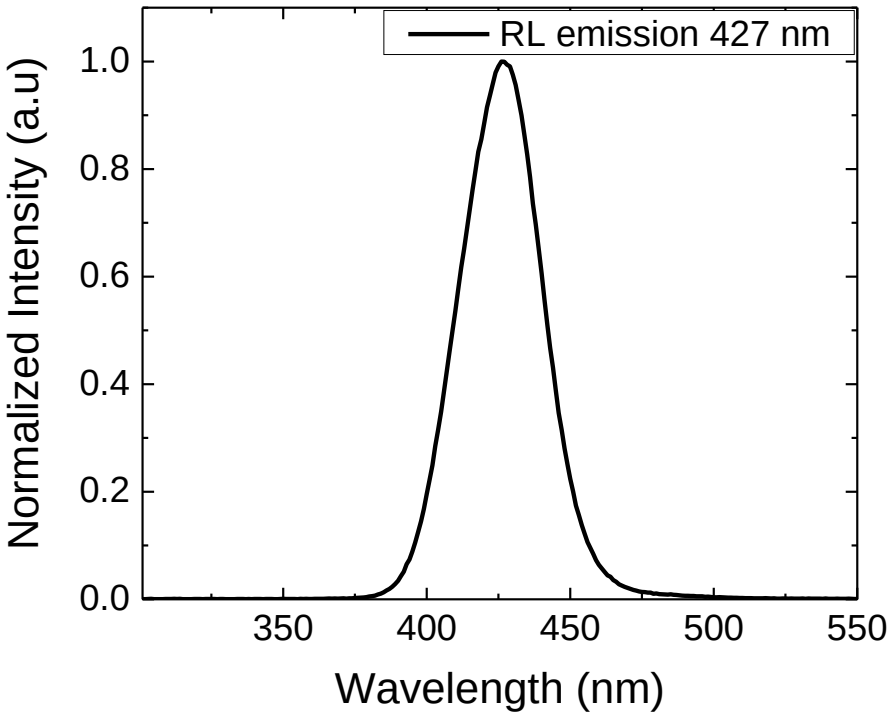

Figure 21. X-ray excited emission spectra of KSr_2Br_5:Eu 5%.

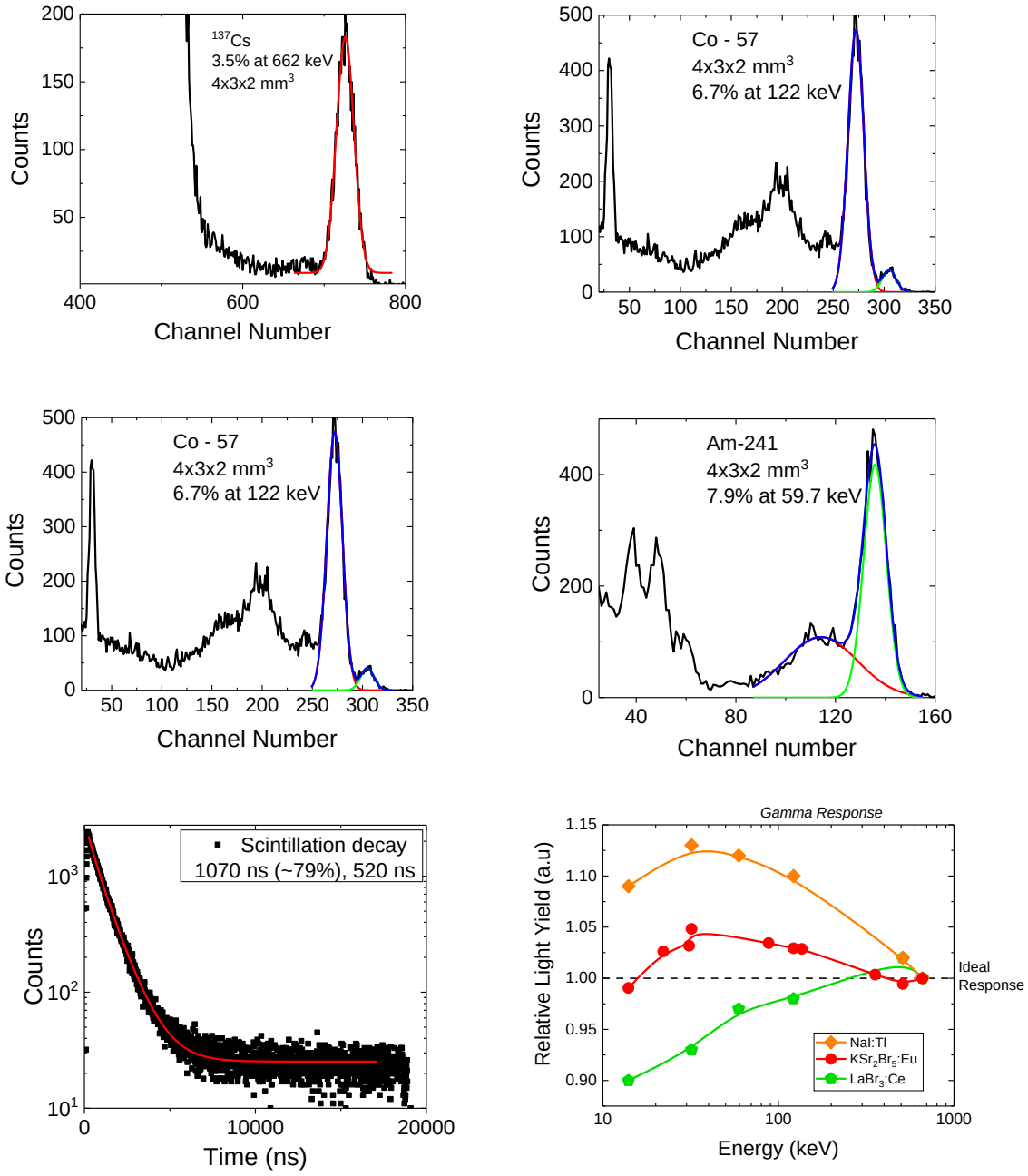

Figure 22a-c. Pulse height spectrum of KSr_2Br_5:Eu 5% under ^{137}Cs , ^{57}Co and ^{241}Am excitation. (5d). Scintillation decay time of KSr_2Br_5:Eu 5% and (5e) Non-proportionality response of KSr_2Br_5:Eu 5% compared to benchmark scintillators, NaI:Tl and $LaBr_3$:Ce.

component exponential function. The stronger decay component was found to be 1076 ns accounting for 79% of the light. A second decay component of 520 ns accounts for the rest of the light. Since the sample measured was relatively small, the scintillation decay time is expected to increase for larger detector sizes. This is a common behavior on Eu^{2+} doped scintillators. The scintillation decay time heavily depends on the europium concentration and the size of the measured sample, primarily due to radiation trapping; self-absorption effects. These effects have previously been investigated in SrI_2:Eu [44] and $CsBa_2I_5$:Eu [30]. For scintillation light yield non-proportionality measurements, a set of γ-ray sources was used to obtain various γ-ray excitation energies. Scintillation light yield was measured as a function of deposited γ-ray energy, which is shown in Figure 22e. The γ-ray response of $KSr_2Br_5:Eu^{2+}$ is closer to the ideal response than NaI:Tl and $LaBr_3:Ce^{3+}$. The light yield per unit energy deviates by approximately +/- 4 % over the measured gamma-ray energy range of 14 – 662 keV.

3.4. Summary

In this work we present a new Eu^{2+}-doped scintillator, KSr_2Br_5. We were able to grow a crack free 13 mm diameter single crystal. The transparency of the crystal was improved by slowing the solidification rate from 2 mm/h to 1 mm/h. This material has a high light yield of 75,000 ph/MeV and energy resolution of 3.5% at 662 keV.

Our initial results are very promising and future research will focus on the optimization of crystal growth parameters for larger diameter boules, along with zone refining of the raw material to improve the overall performance. Table 7 shows a summary of scintillation properties of KSr_2Br_5:Eu 5% compared to NaI:Tl, $LaBr_3$:Ce and SrI_2:Eu.

The effect of the radioactive background from ^{40}K on gamma-ray detection sensitivity and radioisotope identification is currently under investigation. The

intrinsic radioactivity can potentially be used for energy calibration and the stabilization of detector gain.

Table 7. A comparison of scintillation properties.

	KSr_2Br_5:Eu 5%	*NaI:Tl*	*$LaBr_3$:Ce*	*SrI_2:Eu*
RL emission (nm)	427	415	380	435
Decay time (ηs)	1076	230	16	1000
Light yield (ph/MeV)	75,000	38,000	67,000	100,000
ER at 662 keV	3.5%	7.1%	3.2	2.6%

Chapter 4
Scintillation Properties of Eu^{2+}-doped KBa_2I_5 and K_2BaI_4

A version of this chapter was originally published in peer-reviewed journal by Luis Stand. No additional changes were made other than formatting to conform to the dissertation format.

The full citation is as follows: L. Stand, M. Zhuravleva, B. Chakoumakos, J. Johnson, A. Lindsey, C.L. Melcher, Scintillation properties of Eu2+-doped KBa_2I_5 and K_2BaI_4, Journal of Luminescence, 169, Part A (2016) 301-307 [45].

Dr. Chakoumakos (Oakridge National Laboratory) measured the single crystal x-ray diffraction shown in section 4.3.1 and J. Johnson cut and polished the specimens measured in this work. The remaining co-authors provided valuable research advice during this research.

Abstract

We report two new ternary metal halide scintillators, KBa_2I_5 and K_2BaI_4, activated with divalent europium. Single crystal X-ray diffraction measurements confirmed that KBa_2I_5 has a monoclinic structure ($P2_1/c$) and that K_2BaI_4 has a rhombohedral structure ($R3c$). Differential scanning calorimetry showed singular melting and crystallization points, making these compounds viable candidates for melt growth. We grew 13 mm diameter single crystals of $KBa_2I_5:Eu^{2+}$ and $K_2BaI_4:Eu^{2+}$ in evacuated quartz ampoules via the vertical Bridgman technique. The optimal Eu^{2+} concentration was 4% for KBa_2I_5 and 7% for K_2BaI_4. The X-ray excited emissions at 444 nm for KBa_2I_5:Eu 4% and 448 nm for K_2BaI_4:Eu 7% arise from the 5d-4f radiative transition in Eu^{2+}. KBa_2I_5:Eu 4% has a light yield of 90,000 photons/MeV, with an energy resolution of 2.4% and K_2BaI_4:Eu 7% has a light yield of 63,000 ph/MeV, with an energy resolution of 2.9% at 662 keV. Both crystals have an excellent proportional response to a wide range of gamma-ray energies.

4.1. Introduction

Scintillators are used in a wide variety of applications as radiation sensors. As a result, such materials are developed with a specific set of properties that will

satisfy the requirement for each application. For medical imaging applications scintillators with a high light yield are preferred [16]. This will improve the spatial resolution and produce a higher quality image, thus enabling new technology for earlier diagnosis of disease. Scintillators used in gamma-ray spectroscopy for national security applications require both high light output and excellent energy resolution. This provides unambiguous identification of radioactive sources and discrimination of potential threat sources from non-threat sources, especially in the presence of background radiation [7]. Regardless of the application, cost of the radiation detector is a major factor for consideration of widespread utilization, and for this reason alone NaI:Tl^+ is the most commonly used scintillator [2]. It has a modest light yield of ~38,000 ph/MeV and a relatively poor energy resolution approaching 7% at 662 keV [11], but it is much less expensive than semiconductor radiation detectors and most other available scintillators, mainly due to precursor availability and ease of growth.

In recent years, great efforts have been made to discover and develop new metal halide scintillators, mainly due to their potentially high scintillation light yield of 80,000+ ph/MeV and energy resolution approaching the ideal ~2% at 662 keV. Crystals such as SrI_2:Eu [18], $CsBa_2I_5$:Eu [46], BaBrI:Eu [47] and $LaBr_3$:Ce,Sr [17] have the potential to replace NaI:Tl in some applications [48]. We have recently reported a promising scintillator, Eu^{2+}-doped KSr_2I_5, with exceptional scintillation properties including a light yield of 94,000 ph/MeV with an energy resolution of 2.4% at 662 keV [15]. The objective of the present work is to demonstrate scintillation performance of two new Eu^{2+}-doped scintillators, K_2BaI_4 and KBa_2I_5, grown via the vertical Bridgman method. Compared to the Sr-containing counterpart, these Ba-containing compounds are expected to have higher density, which is advantageous for efficient detection of gamma-ray radiation. In addition, Ba-containing scintillators are known to be less deliquescent [42, 49, 50], which makes them a more practical choice for detector device integration. Similar to KSr_2I_5, both K_2BaI_4 and KBa_2I_5 can be activated with the Eu^{2+} luminescence

centers via partial replacement of Ba atoms in the crystal lattice. KBa_2I_5 has a monoclinic crystal structure, with a density of 4.52 g/cm^3 [19]. Although neither the KI-BaI_2 phase diagram nor the crystallographic information for K_2BaI_4 are available in the literature, our initial growth experiments suggest that both compounds melt congruently. In this work we present the structural analysis and scintillation properties of Eu^{2+} - doped KBa_2I_5 and K_2BaI_4.

4.2. Experimental

4.2.1. Crystal Growth

The optimum europium concentration was investigated by synthesizing 4 g polycrystalline samples of $K_2Ba_{1-x}Eu_xI_4$ and $KBa_{2(1-y)}Eu_{2y}I_5$ with $5 \leq x \leq 10$ and $2.5 \leq y \leq 6$ in a single-zone clamshell furnace. The 99.99% pure anhydrous KI, BaI_2 and EuI_2 raw materials from Sigma-Aldrich were mixed and loaded into quartz ampoules in a glove box with an atmosphere containing < 0.1 ppm of water and oxygen. The loaded ampoules were dried at 200 °C and sealed under a vacuum of 10^{-6} torr. The temperature was slowly raised to 740 °C, which is 29 °C above the melting point of BaI_2, the component with the highest melting point. This temperature was held for 7 h and then slowly decreased to room temperature over a period of 7 h. The ampoule was then inverted and the procedure above was repeated to encourage complete mixing of all constituents. The resulting solidified material was polycrystalline, but 4 mm^3 to 8 mm^3 single crystal specimens could be identified and were selected for evaluation. These specimens, with Eu concentrations ranging from 2.5 to 10 %, allowed us to estimate the optimal Eu concentration for maximum light yield. Once this was done, 13 mm diameter crystals of KBa_2I_5:Eu^{2+} and K_2BaI_4:Eu^{2+} were grown using a two-zone transparent vertical Bridgman furnace, using a solidification rate of 1 mm/h and cooling a rate of 10 ^oC/h. It should be recognized that additional factors such self-absorption and a segregation coefficient different from unity could slightly shift the optimal Eu concentration for larger crystals grown under different conditions.

4.2.2. Characterization

Crystallographic studies utilized ~ 0.001 mm^3 crystal fragments isolated from boules grown in this study and suspended in paratone oil and each mounted on a plastic loop attached to copper pin/goniometer. Single-crystal diffraction data were collected at 250K using a Rigaku XtaLAB PRO diffractometer with MoKα radiation (**λ** = 0.71073 Å) equipped with a Dectris Pilatus 200K detector and an Oxford N-HeliX cryocooler. Peak indexing and integration was done using d*trek in the CrystalClear package [51]. A numerical absorption correction was applied using ABSCOR [52]. The SIR-2011 in WinGX and SHELXL-2013 software packages were used for data processing and structure solution and refinement [53]. Crystal structure projections were made with VESTA [54]. Monoclinic structures like KBa_2I_5, where the beta angle is close to 90, can mimic orthorhombic structures, and in this case, addition of the twin model 1 0 0, 0 -1 0, 0 0 -1, with unequal fractions of the two domains lowers the R1 agreement factor by nearly one half.

The melting and crystallization temperatures were determined through differential scanning calorimetry-thermogravimetric analysis (DSC-TGA) using a Setaram Labsys Evo TG-DSC. The measurement was carried out on a ~50 mg specimen at a ramp rate 5 K/min, under a flow of ultra-high purity argon gas.
Moisture sorption profiles were recorded using a Dynamic Vapor Sorption technique on a DVS Intrinsic by Particulate Systems. The measurements were carried out under identical conditions: spherical samples with a surface area ~28 ± 2 mm^2, 25 ℃, 40 % relative humidity, 60 minutes exposure time [42].

The radioluminescence (RL) emission spectra were recorded at room temperature under continuous 30 keV X-ray irradiation. The steady state photoluminescence (PL) spectra and the PL decay time (lifetime) were measured at room temperature with a Horiba Jobin Yvon Fluorolog 3 Spectrofluorometer. The PL lifetime was measured using the time correlated single photon counting technique. A Horiba Jobin Yvon NanoLed with an emission wavelength of 370 nm

and a pulse width of ~1 ns was used as an excitation source. The emission monochromator was set to 444 nm and 448 nm for $KBa_2I_5:Eu^{2+}$ and $K_2BaI_4:Eu^{2+}$ respectively to monitor the Eu^{2+} emission intensity.

For accurate light yield and scintillation decay time measurements, the specimens were protected from moisture by immersing them in an oil-filled quartz cell. The scintillation decay time was measured with the time-correlated single photon counting technique with excitation by a ^{137}Cs gamma-ray source [40]. The cell was coupled to a Hamamatsu 3177-50 photomultiplier tube (PMT) and to a Hamamatsu R6231-100 PMT for measuring the absolute light yield and energy resolution (ER), respectively, where energy resolution is defined as R=ΔE(FWHM)/E, of a photopeak of energy E [55]. A hemispherical dome of Spectralon was used as a reflector. An amplifier shaping time of 10 μs was used to integrate the exponentially decaying scintillation pulse.

4.3. Results and Discussion

4.3.1. Crystal Structure

KBa_2I_5 is a new compound with the $TlPb_2Cl_5$ structure-type, which is known for at least 13 different compositions already reported in the Inorganic Crystal Structure Database. The $TlPb_2Cl_5$ structure-type is fairly densely packed despite having ions with large coordination numbers. All polyhedra share corners, edges and faces, with no open channels. There are two types of BX_n polyhedra, a BX_8 distorted square antiprism and a BX_7 distorted monocapped trigonal prism. The AX_8 is the largest polyhedron and is also a distorted square antiprism. In the case of KBa_2I_5 the polyhedral volumes are 60.07 ($Ba1I_7$), 83.33 ($Ba2I_8$), and 90.25 (KI_8) $Å^3$, which suggests that Eu doping would likely prefer the Ba1 site given its significantly smaller relatively ionic size of Eu to that of Ba; structure drawing in Figure 23. Given the poor fidelity to determine the Eu over Ba using x-rays, the Eu content was not refined. Table 8 and Table 9 summarize the structural parameters and refinement details.

K_2BaI_4 is a new compound with the Yb_3As_4 structure-type, which is known for two different compositions already reported in the Inorganic Crystal Structure Database. A wider compositional range for the chlorides, A_2MCl_4, A = K, Rb, Cs, M = Eu, Sr, Ba, Pb, has been reported in the thesis by Flick (1990) [20]. Crystal structures for few of these compounds have been reported in detail, and that may be related to the presence of incommensurate modulations.

Phase studies of binaries, K-I nor Ba-I, have not reported an A_3I_4 phase, so apparently K_2BaI_4 phase is stabilized by the ternary composition. The structure is rhombohedral (noncentrosymmetric), and its single $(K,Ba)I_8$ polyhedron can be described as a distorted square antiprism with a mean bond length of 3.66 Å; see structure drawing in Figure 24. The refinement strategy adopted was to preserve the K:Ba ratio of 2, but let the occupancy of the A-site vary. The resulting occupancy is slightly in excess of 1 and is close to being charge balanced. The K and Ba ions are assumed to be randomly distributed on the metal site. Table 8 and Table 10 summarize the structural parameters and refinement details.

4.3.2. Melting Point Determination and Moisture Absorption

Differential scanning calorimetry curves are shown in Figure 25 and Figure 26, respectively. KBa_2I_5:Eu 4% has a melting point of 569°C and a crystallization point of 554°C. K_2BaI_4:Eu 7% has a melting point of 579°C and a crystallization point of 550°C. The difference between the melting and the crystallization peaks indicates that K_2BaI_4:Eu 7% has a larger degree of supercooling (29°C) compared to KBa_2I_5:Eu 4% (15°C). This information is needed in order to design a thermal profile that would allow us to grow the crystals with a stable solid-liquid interface. It is also important to note that no phase transitions were found in the specimens measured.

The Dynamic Vapor Sorption technique was used to determine the moisture absorption of KBa_2I_5:Eu 4% and K_2BaI_4:Eu 7% as shown in Figure 27. For comparison purposes the moisture absorption of two well-known scintillators,

Table 8. Crystal structure data and single-crystal X-ray diffraction refinement results for KBa_2I_5 and $(K_{2.07(3)}Ba_{1.05(3)})I_4$.

Formula	*KBa_2I_5*	*$(K_{2.07(3)}Ba_{1.05(3)})I_4$*
fw (g)	948.28	4973.34
T (K)	250	250
Crystal system	monoclinic	Rhombohedral
Space group	*$P2_1/c$*	*$R3c$*
a (Å)	10.2922(11)	14.937(9)
b (Å)	9.1713(9)	14.937(9)
c (Å)	14.6853(15)	9.165(6)
α (°)	90	90
β (°)	90.025(3)	90
γ (°)	90.	120.
V (Å³)	1386.2(2)	1771(17)

Table 9. Fractional atomic coordinates and equivalent isotropic atomic displacement parameters for KBa_2I_5 (space group $P2_1/c$)*at 250K.

Atom	*x*	*y*	*Z*	U_{eq} (Å^2)
K	-0.0005(3)	0.9723(3)	-0.1789(2)	0.0118(6)
Ba1	0.24795(14)	0.57674(9)	0.00739(6)	0.0267(2)
*Ba2***	0.49980(18)	0.97050(17)	-0.17803(12)	0.0394(6)
I1	0.54283(14)	0.66696(17)	0.09578(11)	0.0368(3)
I2	-0.04304(14)	0.67043(18)	0.09647(12)	0.0415(4)
I3	0.2619(2)	0.96188(13)	0.00157(8)	0.0507(4)
I4	0.2642(2)	0.33147(13)	0.18482(9)	0.0501(4)
I5	0.25549(18)	0.69491(11)	-0.22081(7)	0.0336(3)

* All atoms are in general positions.

** Site occupancy refined to 0.851(8) Ba + 0.149(8) K, giving the formula $K_{1.15}Ba_{1.85}I_5$.

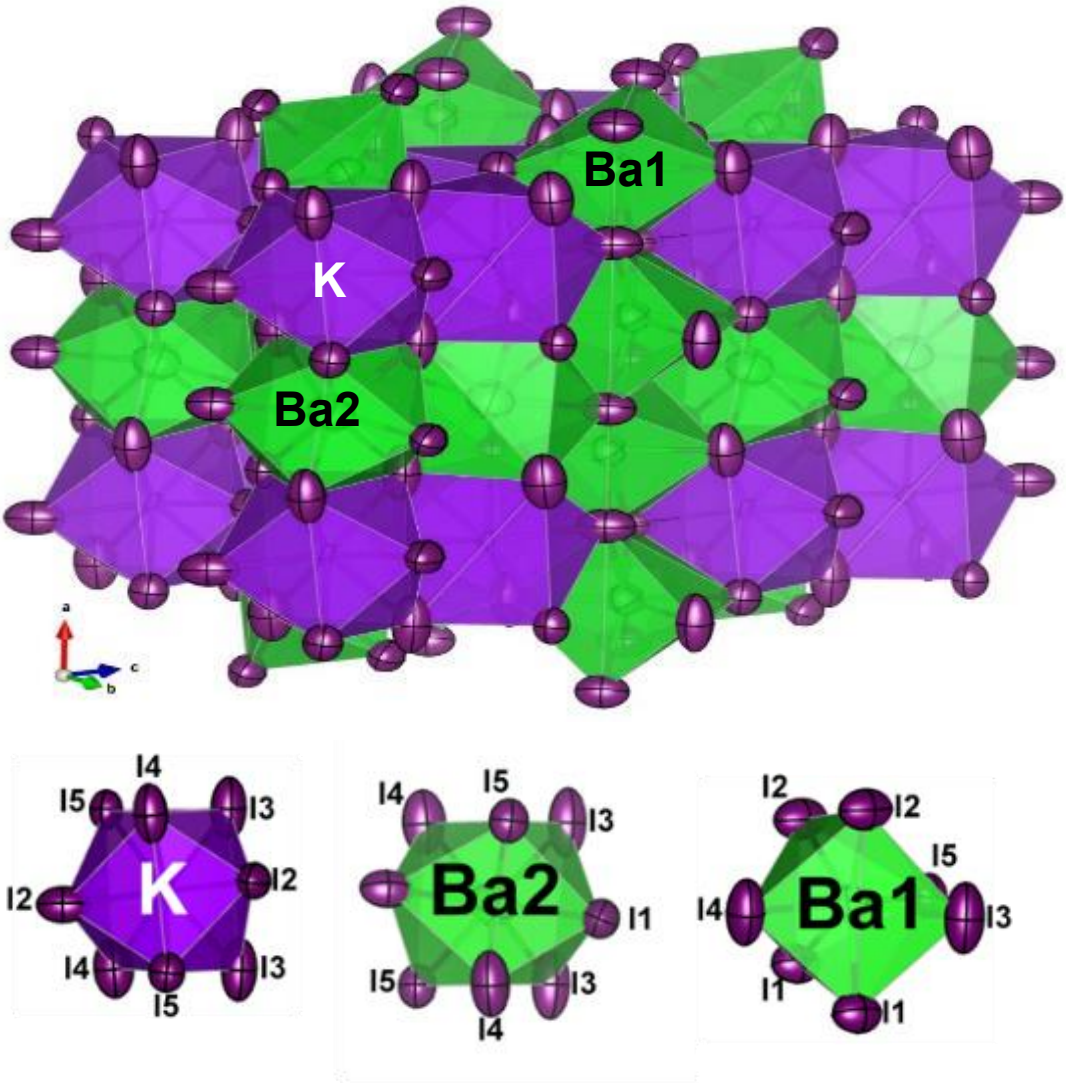

Figure 23. Crystal structure of KBa_2I_5 at 250K showing the KI_8, $Ba1I_7$ and $Ba2I_8$ polyhedra. Anisotropic atomic displacement ellipsoids are plotted at 99% probability.

Table 10. Fractional atomic coordinates and equivalent isotropic atomic displacement parameters for $(K_{2.07}Ba_{1.05})I_4$ (space group *R*3*c*) at 250K.

Atom	*Site*	*Symmetry*	*x*	*Y*	*Z*	U_{eq} (Å^2)
*A**	18*b*	1	0.6240(2)	0.1247(2)	0.0787(4)	0.0405(5)
I1	6*a*	3	0	0	0.1313(3)	0.0428(8)
I2	18*b*	1	0.2123(1)	0.2849(1)	0.1172(2)	0.040(1)

* refined occupancy = 0.69(1)K + 0.35(1)Ba

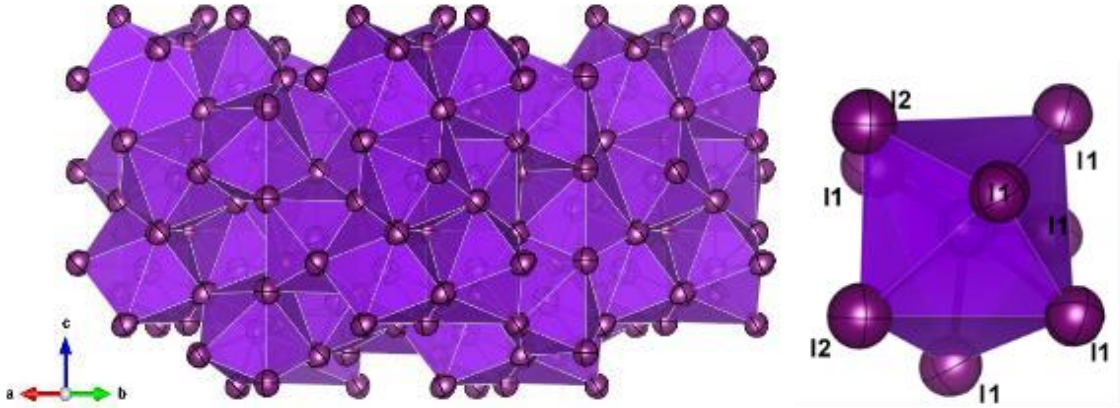

Figure 24. Crystal structure of K_2BaI_4 at 250K showing the $(K,Ba)I_8$ polyhedron. Anisotropic atomic displacement ellipsoids are plotted at 99% probability.

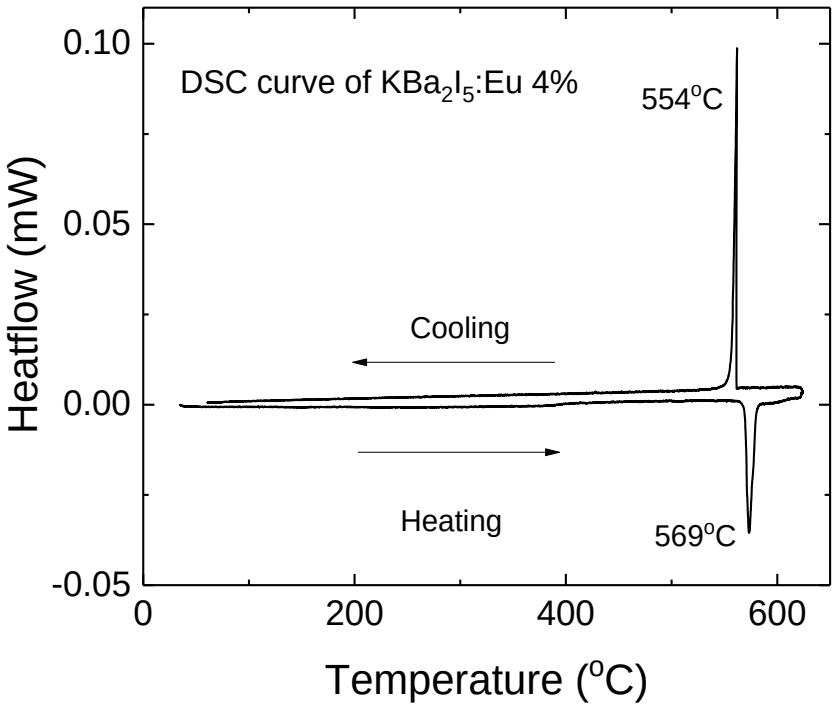

Figure 25. Differential scanning calorimetry curve, KBa_2I_5:Eu has a melting point of 569°C and a crystallization point of 554°C.

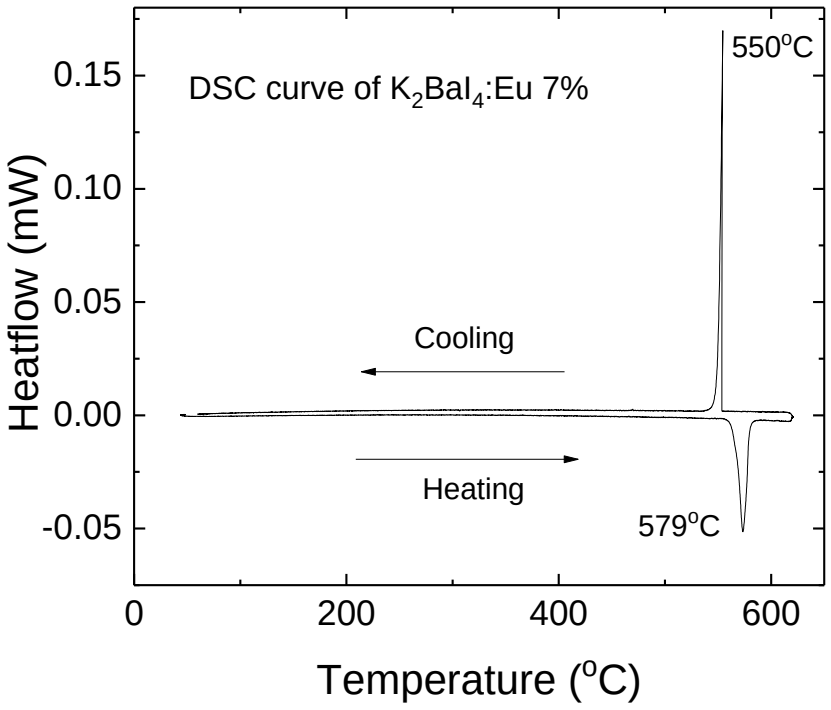

Figure 26. Differential scanning calorimetry curve, K_2BaI_4:Eu has a melting point of 579°C and a crystallization point of 550°C.

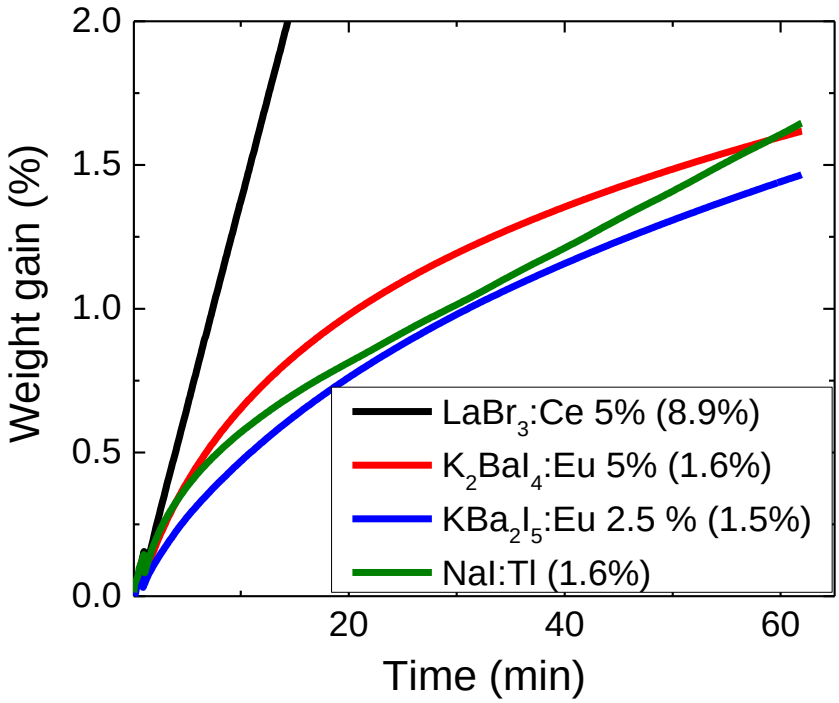

Figure 27. Moisture absorption rate of $LaBr_3$:Ce, K_2BaI_4:Eu 5%, NaI:Tl and KBa_2I_5:Eu 4%.

$LaBr_3$:Ce 5% and NaI:Tl, were measured under identical conditions. Both Ba-containing crystals have relatively low moisture uptake, comparable to the absorption rate of NaI:Tl that shows approximately 2% weight gain over 60 minutes at 40% humidity.

4.3.3. Europium Optimization and Crystal Growth

The optimum activator concentration in a scintillator often involves a tradeoff between efficient charge carrier migration to the activator sites which is aided by high activator concentration and minimization of self-absorption which is aided by low activator concentration. The measured scintillation light yield versus Eu concentration for rapidly screened samples is shown in Figure 28. The maximum light yield was found to be at 4% and 7% Eu^{2+} molar concentration for KBa_2I_5 and K_2BaI_4 respectively. It is worth noting that the optimum europium concentration that yielded the maximum light yield, may not be the concentration used for detector applications. Eu^{2+} activated crystals are known for having self-absorption effects [56, 57]. This affects the performance of the crystals as they increase in size [12]; therefore a lower concentration of europium will be considered for crystals 1 inch or larger.

Two 13 mm diameter single crystals were grown using a two-zone transparent furnace. We were able to extract a 5 × 8 × 13 mm^3 and a 5 × 5 × 7 mm^3 samples from the grown boules of KBa_2I_5:Eu 4% and K_2BaI_4:Eu 7%, shown Figure 29 and Figure 30. K_2BaI_4:Eu 7% displayed better transparency than KBa_2I_5:Eu 4%, but both crystals are far from ideal. In general, the crystal growth of Ba-containing scintillators is challenging, mainly due to cracking. This has slowed the development and widespread application of scintillation crystals such as $CsBaI_3$:Eu, $CsBa_2I_5$:Eu and BaBrI:Eu [47, 58-60].

4.3.4. Optical and Scintillation Properties

The x-ray excited radioluminescence (RL) spectrum of KBa_2I_5:Eu 4% has a single emission peak at 444 nm while K_2BaI_4:Eu 7% has an emission centered at

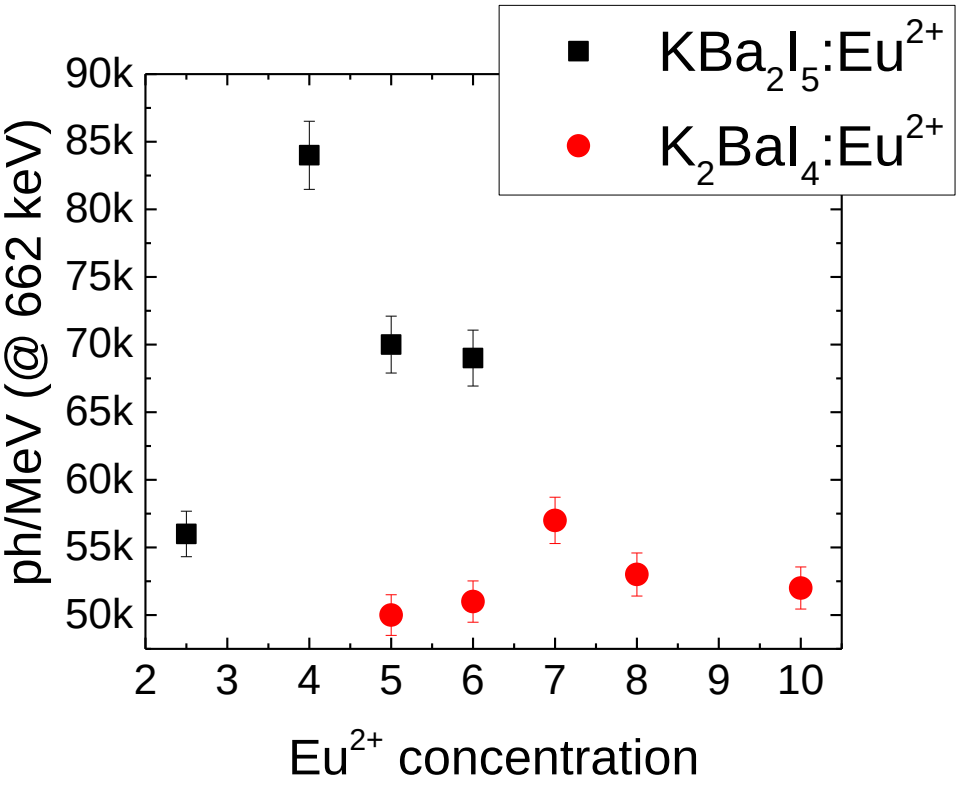

Figure 28. Light output as a function of Eu^{2+} concentration in KBa_2I_5 and K_2BaI_4.

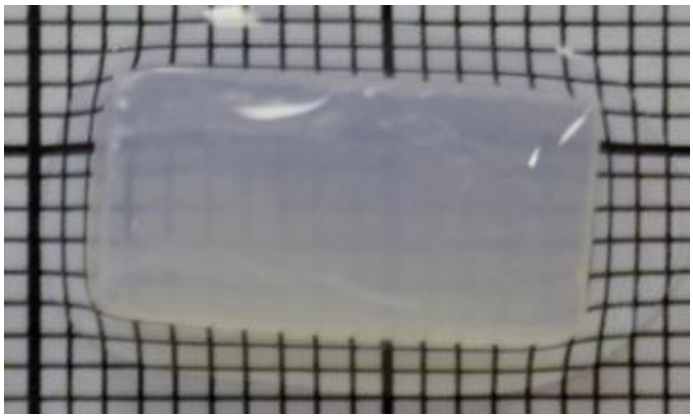

Figure 29. A 5 × 8 × 13 mm^3 crystal of KBa_2I_5:Eu 4%, under white ambient light..

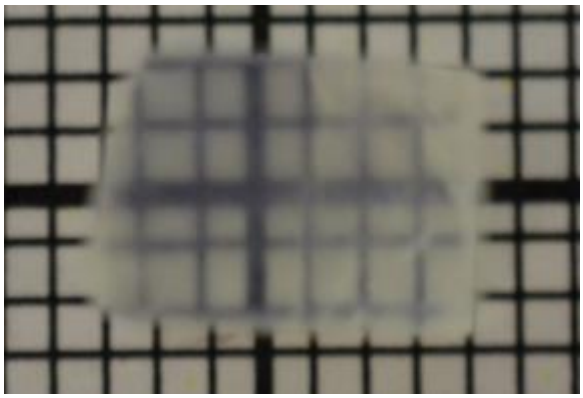

Figure 30. A 5 × 5 × 7 mm^3 crystal of K_2BaI_4:Eu 7%, under white ambient light.

448 nm, with a slight broadening on the longer wavelength side of the band. This small asymmetry in K_2BaI_4:Eu is under further investigation, but it may reflect the different ligand structure surrounding the Eu site as compared to KBa_2I_5, thus causing the emission to be slightly broader, as shown in Figure 31

Photoluminescence (PL) excitation and emission of KBa_2I_5:Eu 4% and K_2BaI_4:Eu 7% are shown in Figure 32. The PL excitation spectrum of each compound exhibits a broad region of poorly resolved bands from ~270 nm to ~420 nm resulting from the complex manifold of energy levels in Eu^{2+}. On the other hand, the PL emission spectrum of each compound consisted of a single well defined peak centered at 444 nm for KBa_2I_5:Eu 4% and 448 nm for K_2BaI_4:Eu 7%, thus confirming that the only radiative transition is from the lowest energy 5d excited state. Similar to the RL emission, the PL emission of K_2BaI_4:Eu 7% is slightly broadened, thus suggesting that the cause lies in the local environment of the Eu^{2+} site rather than defects or distortions in the matrix. For both PL emission measurements, an excitation of 400 nm was used. The photoluminescence decay time is shown in Figure 33, the Eu^{2+} center was directly excited by a 370 nm NanoLED pulser; the tracked emissions were 444 nm for KBa_2I_5:Eu 4% and 448 nm for K_2BaI_4:Eu 7%, i.e. the peak emission wavelengths. The lifetime of the Eu^{2+} $5d_1$ excited state was 840 ns and 700 ns for KBa_2I_5:Eu 4% and K_2BaI_4:Eu 7%, respectively. The baseline difference between the two samples is due to different count rates arising from different sample sizes and sample positioning in the excitation light path. The baseline is considered when fitting the data in order to extract the excited state lifetime. The observed PL decay is typical for Eu^{2+} 5d to 4f transitions, and a single exponential decay function provides a good fit to the data.

In the previous section we discussed that the KBa_2I_5 ($P2_1/c$ - monoclinic) structure has two Ba sites, Ba1 ($Ba1I_7$ - 60.07 $Å^3$) and Ba2 ($Ba2I_8$ - 83.33 $Å^3$) and these results suggested that Eu ions would prefer the Ba1 site given the smaller ionic size of Eu compared to Ba. . In addition, the narrow peaks in the PL and RL

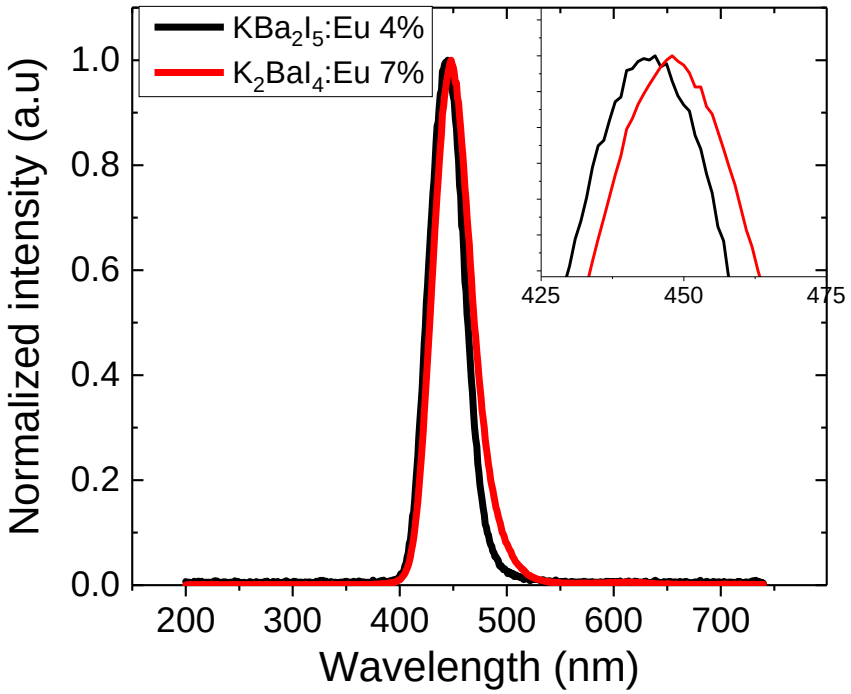

Figure 31. Radioluminescence emission spectra of KBa_2I_5:Eu 4% (peak maximum at 444 nm) and K_2BaI_4:Eu 7% (peak maximum at 448 nm

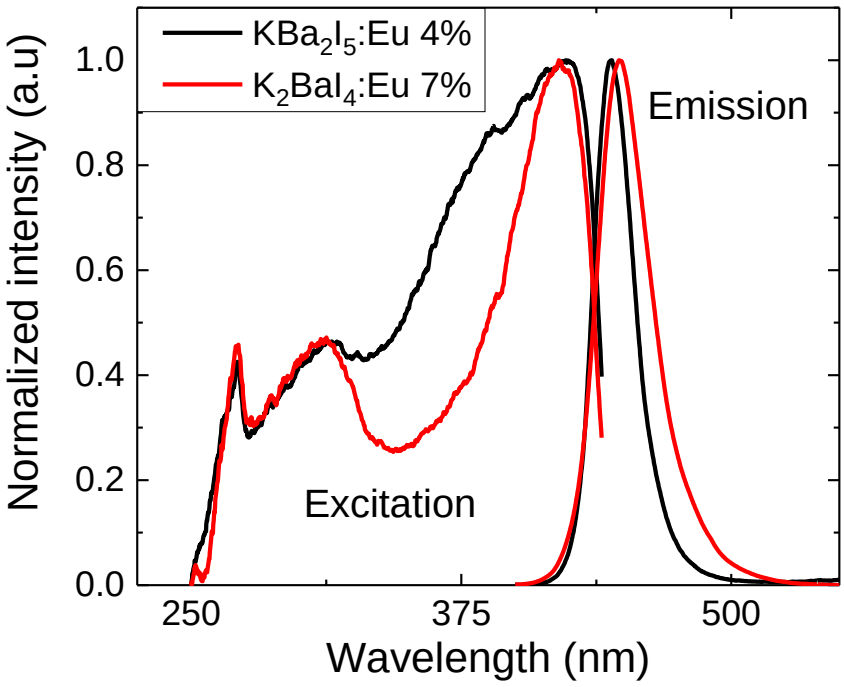

Figure 32. The PL excitation of KBa_2I_5:Eu 4% and K_2BaI_4:Eu 7% spectrum comprises multiple unresolved overlapping bands from 280 nm to 433 nm measured by monitoring the 444 and 448 nm emissions respectively. Both crystals exhibit a sharp PL emission band with peak maximum around 444 and 448 nm, using any excitation wavelength in the range of 300–410 nm.

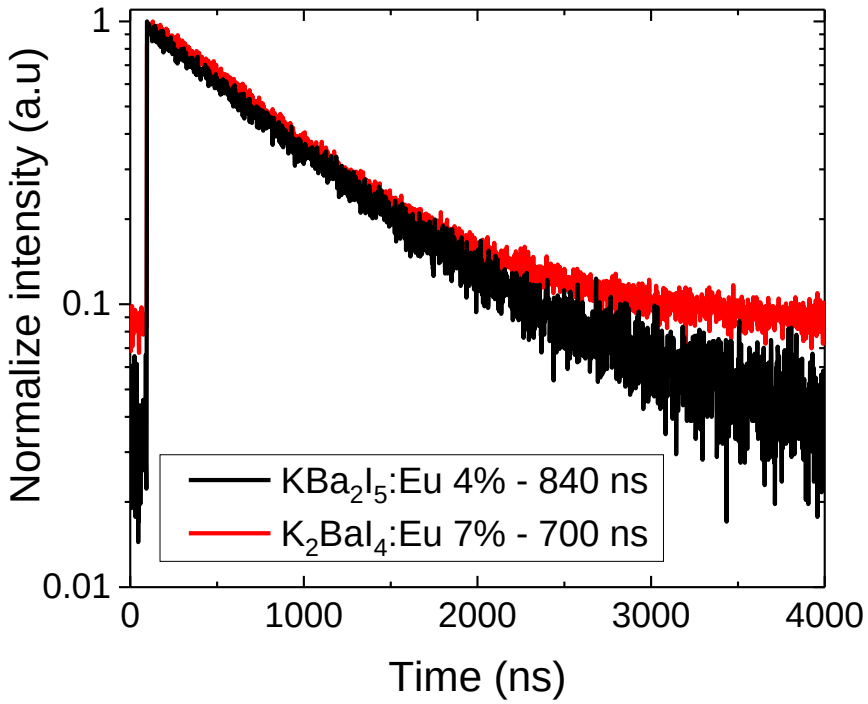

Figure 33. The Eu^{2+} lifetime of 840 ns and 700 ns were measured for KBa_2I_5:Eu 4% and K_2BaI_4:Eu 7% (370 nm was used as the excitation wavelength).

spectra suggest that Eu^{2+} primarily occupies only one of the Ba sites, although it is not possible to say with certainty which site is occupied. The results obtained from the RL and RL measurements are commonly seen in europium doped scintillators due to the 5d-4f radiative transition in Eu^{2+} [21, 22, 61, 62]. No evidence of emission from perturbed Eu was observed.

The measured scintillation light yield and energy resolution of KBa_2I_5:Eu 4% and K_2BaI_4:Eu 7% are summarized in Table 11. The light yield of a 2 × 2 × 1 mm^3 sample of KBa_2I_5:Eu 4% was 90,000 ph/MeV with 2.4% energy resolution at 661.7 keV as shown in Figure 34a. For a similar size sample of K_2BaI_4:Eu 7%, a light yield of 63,000 ph/MeV and an energy resolution of 2.9% were measured Figure 35a). The pulse height spectra were also recorded at lower energies, using ^{57}Co (122 keV) and ^{241}Am (59.5 keV) sealed sources. At 122 keV the energy resolution was 5.4% for KBa_2I_5:Eu 4% and 6.9% for K_2BaI_4:Eu 7%. The energy resolution at 59.5 keV was 7.6% and 8.7% respectively. Larger specimens of both crystals were measured using a ^{137}Cs source. In spite of the lack of transparency of KBa_2I_5:Eu 4% and using a larger 5 × 8 × 13 mm^3 specimen, we were able to measure an energy resolution of 2.7%. For K_2BaI_4:Eu 7%, we used a 5 × 5 × 7 mm^3 specimen and we measured an energy resolution of 3.0%, shown in Figure 34b and Figure 35b, respectively.

These results are very promising for national security applications, where scintillators are required to have excellent energy resolution to provide unambiguous identification of radioactive sources and discrimination of potential threat sources from non-threat sources. The light yield and energy resolution obtained for KBa_2I_5:Eu^{2+} are comparable to SrI_2:Eu^{2+} and $CsBa_2I_5$:Eu^{2+}, all having light yields above 90,000 ph/MeV and energy resolution lower than 3.0% [44, 63]. K_2BaI_4:Eu^{2+} has a much lower light yield, but nevertheless an excellent energy resolution was measured.

For the scintillation light yield non-proportionality measurements, a set of γ-ray sources was used to obtain various γ-ray excitation energies. The relative light

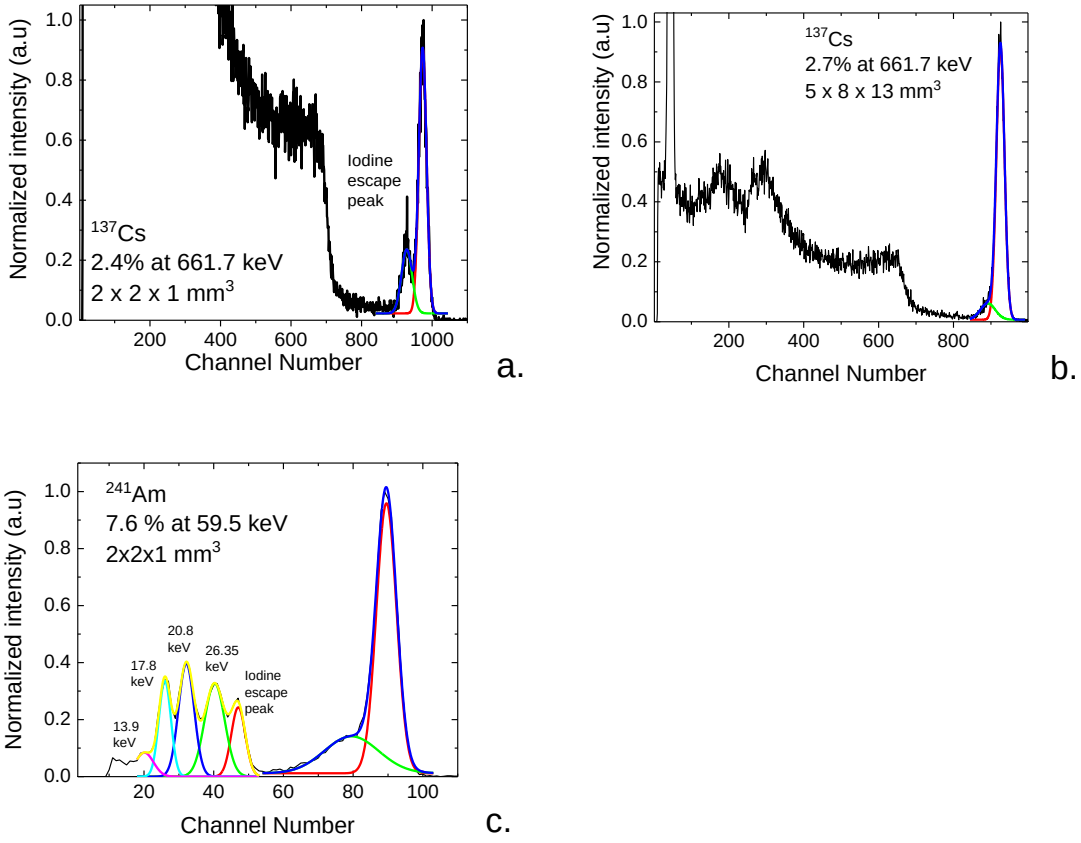

Figure 34a. Pulse height spectra measured for KBa_2I_5:Eu 4% at 661.7 keV with an energy resolution 2.4% of a cleaved piece (~ 2 × 2 × 1 mm^3) and (b) 2.7% energy resolution of a 5 × 8 × 13 mm^3 specimen. (c). The energy resolution of the 59.5 keV full absorption peak is 7.6%. One can also clearly distinguish the 13.95 keV, 17.8 keV, and 20.8 keV, the Neptunium X-ray photoelectric absorption peaks, the 26.35 keV ^{241}Am peak, and the iodine Kα escape peak.

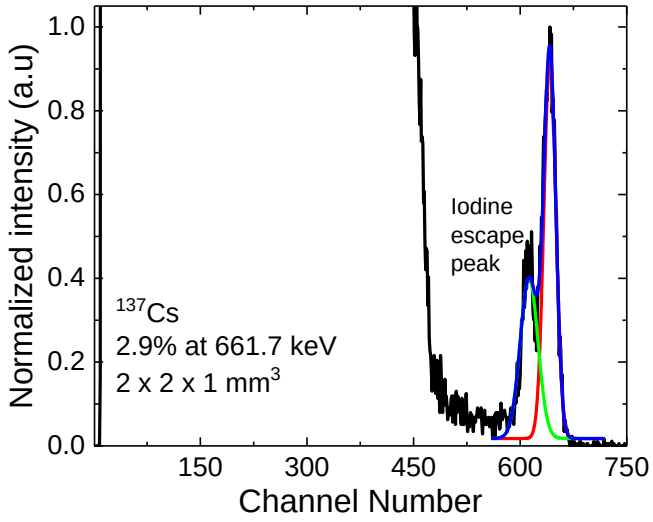

a.

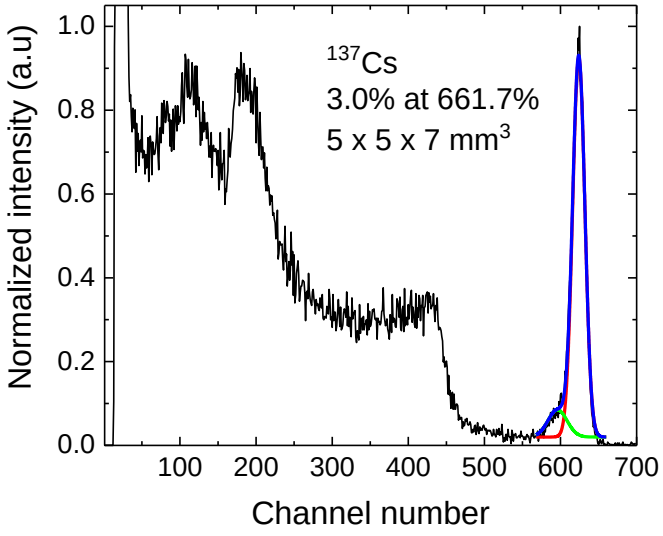

b.

Figure 35a**.** ^{137}Cs pulse height spectra measured for K_2BaI_4:Eu 7% with an energy resolution of 2.9% for a cleaved piece (~ 2 × 2 × 1 mm^3) and (b) 3.0% energy resolution of a 5 × 5 × 7 mm^3 specimen.

yield measured as a function of absorbed γ-ray energy is shown in Figure 36a. The new scintillators, $KBa_2I_5:Eu^{2+}$ and $K_2BaI_4:Eu^{2+}$, showed highly proportional responses that deviate less than 2% from an ideal proportional response over the measured energy range of 14.4 to 662 keV. As we previously stated, the energy resolution R of a scintillator at energy E is experimentally determined from the FWHM of the full energy photopeak in the pulse height spectrum. However, several factors [64] contribute to the peak width such that:

$$R^2 = R_M^2 + R_{nPR}^2 + R_{inh}^2$$

where R_M is the contribution from PMT gain and photoelectron detection Poisson statistics, R_{nPR} is the contribution from the non-proportional response, and R_{inh} is the contribution from crystal inhomogeneity [30]. In other words, in order to achieve energy resolutions lower than 3%, scintillator crystals must be homogeneous and the light yield must be proportional to the absorbed gamma-ray energy and so far this is valid statement for the detector sizes measured in this work.

The scintillation decays of KBa_2I_5:Eu 4% and K_2BaI_4:Eu 7% have primary components of ~1 μs with longer secondary components. The scintillation time profiles of KBa_2I_5:Eu 4% and K_2BaI_4:Eu 7% are shown in Figure 36b. The data were fitted with double exponential decay functions. For KBa_2I_5:Eu 4% the primary decay component of 910 ns accounted for ~81% of the total emitted light while the secondary decay component of 4900 ns accounted for the rest of the light. Similarly, K_2BaI_4:Eu 7% showed a primary component of 720 ns (67%) and secondary component of 3100 ns. The primary component of the decay time for both crystals can be attributed to 5d-4f radiative transition in Eu^{2+}, with a slight delay from the ionization and energy migration process (compared Eu^{2+} PL lifetime), while the secondary long component could be due to the possible presence of shallow charge traps. In general, the scintillation decay time profiles shown for $KBa_2I_5:Eu^{2+}$ and $K_2BaI_4:Eu^{2+}$ are typical for Eu^{2+}-doped scintillators.

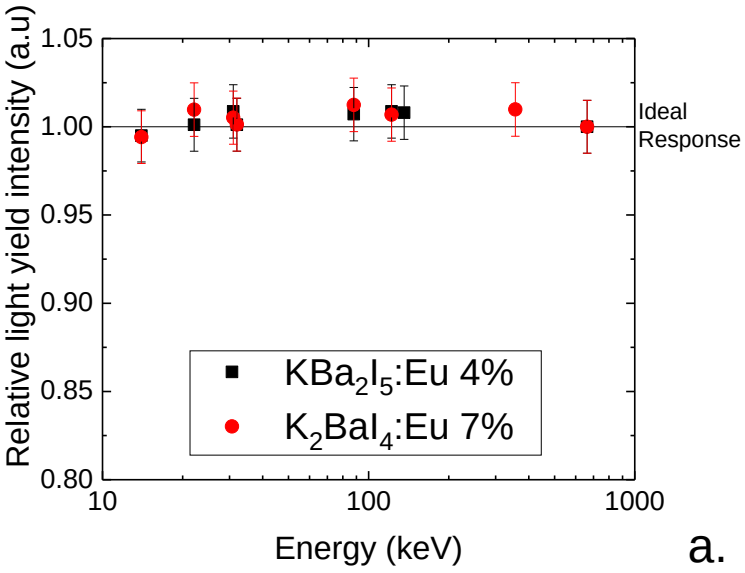

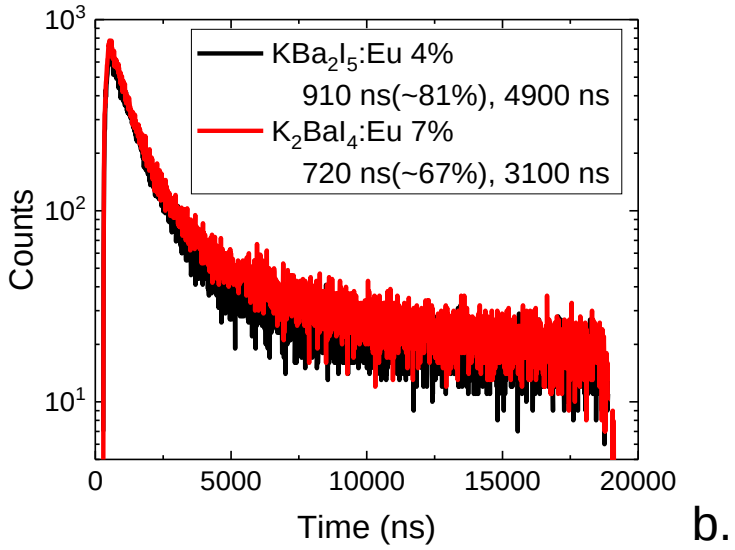

Figure 36a. The light yield proportionality of KBa_2I_5:Eu 4% and K_2BaI_4:Eu 7% showed a deviation of less than 2% from the ideal response. (b). The scintillation decay of KBa_2I_5:Eu 4% and K_2BaI_4:Eu 7% has primary components of ~1 μs with longer secondary components.

4.4. Summary

In this work we report the structural analysis and scintillation properties of two new scintillators, KBa_2I_5:Eu 4% and K_2BaI_4:Eu 7%. A summary of the crystal structure data and single-crystal X-ray diffraction refinement results can be found in Table 8. Both compounds have exceptional scintillation properties, in particular the energy resolutions are lower than 3% at 662 keV. A summary of the scintillation properties is shown in Table 11. $KBa_2I_5:Eu^{2+}$ and $K_2BaI_4:Eu^{2+}$ have highly proportional photon responses which indicate that even better energy resolutions may be achieved as the crystal quality is improved. Future work will focus on the improvement of the optical clarity and the optimization of growth parameters for larger size crystals.

Table 11. Comparison of scintillation properties.

	KBa_2I_5:Eu	*K_2BaI_4:Eu*	*$CsBa_2I_5$:Eu*	*SrI_2:Eu*
RL Emission (nm)	444	448	432	435
Decay time (ns)	910	720	1000	1000
LY (ph/MeV)	90,000	63,000	80,000	100,000
ER at 662 keV	2.4%	2.9%	2.3%	2.6%

Chapter 5
Exploring Growth Conditions and Eu^{2+} Concentration Effects for KSr_2I_5:Eu Scintillator Crystals

A version of this chapter was originally published in peer-reviewed journal by Luis Stand. No additional changes were made other than formatting to conform to the dissertation format.

The full citation is as follows: L. Stand, M. Zhuravleva, G. Camarda, A. Lindsey, J. Johnson, C. Hobbs, C.L. Melcher, Exploring growth conditions and Eu2+ concentration effects for KSr_2I_5:Eu scintillator crystals, Journal of Crystal Growth, 439 (2016) 93-98 [65]. No additional changes were made other than formatting to conform to the dissertation format.

Dr. Camarda (Brookhaven National Laboratory) performed the Micro-Resolution X-ray mapping measurements. J. Johnson and C. Hobbs cut and polished the crystals measured in this work. The remaining co-authors provided valuable research advice during this research.

Abstract

Our current research is focused on understanding dopant optimization, growth rate, homogeneity and their impact on the overall performance of $KSr_2I_5:Eu^{2+}$ single crystal scintillators. In this work we have investigated the effects of Eu^{2+} concentration in the potassium strontium iodide matrix, and we found that the concentration needed to maximize the light yield was 4 mol %. In order to assess the effects of the pulling rate, we grew single crystals at 12, 24 and 120 mm/day via the vertical Bridgman technique. For the sample sizes measured (5 × 5 × 5 mm^3), we found that the crystal grown at the fastest rate of 120 mm/day showed a light yield within ~7% of the more slowly grown boules, and no significant change was observed in the energy resolution. Therefore, light yields from 88,000 to 96,000 ph/MeV and energy resolutions from 2.4 to 3.0% (at 662 keV) were measured for KSr_2I_5:Eu 4% over a relatively wide range of growth conditions. In order to assess the homogeneity of KSr_2I_5:Eu 4%, a newly developed micro-resolution X-ray technique was used to map the light yield as a function of excitation position. In the crystals that we studied, we did not observe any

significant inhomogeneity other than a smooth gradient due to light collection and self-absorption effects.

5.1. Introduction

In the development of new scintillators, divalent europium has proven to be an excellent luminescent activator due to the high quantum efficiency of the dipole-allowed 5d-4f transition, providing emission wavelengths compatible with common photomultipliers, with light yields and energy resolutions approaching the fundamental limits of scintillators [6]. In general, the excellent energy resolutions obtained from metal halide scintillators make these crystals promising candidates for nuclear nonproliferation applications [7]. For this reason, in recent years great efforts have been made to discover and develop metal halide scintillators. Crystals such as: SrI_2:Eu [18], $CsBa_2I_5$:Eu [46], BaBrI:Eu [47], $CsSrI_3$:Eu [66], KSr_2I_5:Eu [67] and $LaBr_3$:Ce,Sr [17] have light yields ≥ 60,000 ph/MeV, and energy resolutions between 2 – 4%.

There are a few challenges surrounding the development of this new generation of high light yield/high resolution scintillators; for example, the high cost of production due to low crystal yield and slow growth process, and crystal inhomogeneity, either caused by dopant segregation or composition inconsistencies. If we take commercially available SrI_2:Eu and $La(Br/Cl)_3$:Ce, for example, the literature indicates that these crystals are grown using solidification rates between 5 to 30 mm/day (SrI_2:Eu - 5 to 19 mm/day [25, 43] and $La(Br/Cl)_3$:Ce - 5 to 30 mm/day [28]) in order to achieve high quality, transparent crystals. Other crystals such as BaBrI:Eu and $CsSrI_3$:Eu were grown at 24 mm/day and the results were translucent crystals [47, 66], suggesting slower rates are needed in order to obtain higher quality crystals. In general, optimal performance of many scintillators is achieved only when growth rates of no more than a few mm/day are used.

There has been considerable interest in the $CsBa_2I_5$:Eu^{2+} scintillator due to its excellent energy resolution of 2.3% for small crystals [30]. However, by

evaluating the performance using larger specimens, Shirwadkar *et al* [59], showed that the energy resolution of $CsBa_2I_5:Eu^{2+}$ strongly depends on the crystal size. The energy resolution of a 2 × 2 × 1 mm^3 sample was 2.56%, while the energy resolution of a 1 × 1 × 1 cm^3 sample was 3.9%. In later investigations, by Lam *et al* [60], these unexpected changes in energy resolution were attributed to phase impurities.

All the challenges cited above are expected to be addressed at some point in the development of $KSr_2I_5:Eu^{2+}$. In this work we focused on establishing relationships between dopant optimization, crystal growth processes, homogeneity and the overall performance of $KSr_2I_5:Eu^{2+}$.

5.2. Experimental

5.2.1. Europium Optimization and Crystal Growth

All quartz ampoules used for these experiments were rinsed with deionized water and then baked at 200°C before use. The 99.99% pure KI, SrI_2 and EuI_2 raw materials from Sigma-Aldrich were mixed in stoichiometric quantities and then loaded into quartz ampoules in a dry box with <0.1 ppm moisture and oxygen. The loaded ampoules were dried at 200 °C for 12 hours and sealed under a vacuum of 10^{-6} torr.

The optimum Eu^{2+} activator concentration was determined through small rapidly-synthesized 4g samples with EuI_2 substituting for SrI_2 in molar concentrations ranging from 1 to 7 %. Each sample was synthesized by reacting the raw materials ~20 ºC above the melting points of all the components for 12 hours and then allowed to cool to room temperature over a 10-hour period. To promote complete mixing of the melt, the ampoule was inverted after the first synthesis cycle and the procedure above was repeated [68]. Small single crystals of each composition were selected for scintillation performance characterization.

Following the optimization of Eu^{2+} concentration, large single crystals were grown by the vertical Bridgman method. Three boules of KSr_2I_5:Eu 4% (KSI-1, KSI-

2 and KSI-3) were grown in a two-zone transparent furnace. Pulling rates from 12 to 120 mm/day, and cooling rates from 72 to 240 °C/day were used, with temperature gradients near the solid-liquid growth interface ranging from 35 °C/in to 140°C/in. For KSI-1 and KSI-2, the growth was initiated by a ø 2 mm grain selector connected to the bottom of the ampoule. For KSI-3 a double wall ampoule was used to minimize radial gradients during the growth process and the grain selector was removed. Double wall ampoules have shown some promising results in the single crystal growth of organic materials [69]. Table 12 shows a detailed summary of the growth parameters used for this work.

5.2.2. Scintillation Characterization

The pixels used for the scintillation characterization were cut inside a dry box with ultra-low contents of moisture and oxygen using a low speed wire saw. The specimens were lapped and polished by hand using silicon carbide polishing pads (600 grit to 1200 grit) with Buehler AutoMet™ low viscosity lapping oil.

The scintillation light yield was measured under excitation with 662 keV gamma rays from a ^{137}Cs source by coupling a sample to a Hamamatsu R2059 photomultiplier tube (PMT), while the energy resolution at 59.4 keV, 356 keV, 122 keV and 662 keV was measured with a Hamamatsu R6231-100 PMT. The specimens were placed in a quartz container filled with mineral oil to protect them from moisture during the measurement. Mineral oil was also used as an optical coupling between the quartz container and the PMT. A Spectralon hemispherical diffuse reflector dome to direct scintillation photons toward the PMT, and an amplifier shaping time of 10 μs was used to integrate the scintillation signals. The scintillation photon yield was calculated by convolving the quantum efficiency of the PMT with the X-ray excited emission spectrum of the sample.

The radioluminescence (RL) spectra of small specimens were acquired at room temperature under continuous 30 kV X-ray irradiation. The emission spectra were recorded with a 150-mm focal length monochromator over a wavelength that

Table 12. Summary of growth condition for KSr_2I_5:Eu 4%.

	Size (I.D. mm)	*Pulling rate (mm/day)*	*Gradient (°C/in)*	*Cooling rate (°C/day)*	*Grain selector*
KSI - 1	13	120	~35	240	Yes
KSI - 2	22	24	~140	120	Yes
[+]KSI - 3	13	12	~70	72	No*

[+] Double wall ampoule

* Conical tip

ranged from 200 to 800 nm.

The scintillation decay time was measured with the time-correlated single photon counting technique [40] with excitation by a ^{137}Cs gamma-ray source. Micro-resolution X-ray detector mapping (MXDM) was performed at Brookhaven National Laboratory's (BNL) National Synchrotron Light Source (NSLS) on the X27B beam line [70]. The MXMD measurement is performed using 30 keV monochromatic X-rays collimated to a 10 x 10 μm micro-beam which is rastered over the sample to create an intensity map in 50 μm steps. The crystal was encapsulated in an oil-containing quartz cell to avoid degradation during the measurement. The oil cell was coupled to a PMT and was wrapped with Teflon to ensure light collection.

5.3. Results and discussion

5.3.1. Single Crystal Growth of $KSr_2I_5:Eu^{2+}$

Single crystals of KSr_2I_5:Eu 4% were grown via the vertical Bridgman technique using different growth parameters. Table 12 in the experimental section shows a summary of the growth conditions used. The results were high quality, transparent single crystals, within this range of growth and cooling parameters. KSI-1, a 13 mm diameter boule grown using a pulling rate of 120 mm/day, is shown in Figure 37. KSI-2 was a 22-mm diameter boule (pulling rate 24 mm/day), shown in Figure 38, and KSI-3, a 13-mm diameter boule pulled at 12 mm/day is shown in Figure 39. If we take a closer look at KSI-1, shown in Figure 37, this crystal has a subtle yellow tint and its optical appearance is slightly different compared to KSI-2 and KSI-3. This could be due to light scattering defects created by combining the effects of the small thermal gradient and the fast pulling rate used (5 times faster than KSI-2, and 10 times faster than KSI-3). Also, since all the growth experiments for this work were carried out in a two-zone transparent furnace, we could get real time visual feedback during all growth processes. Thus, it was noticed that the grain selector used in the ampoules for KSI-1 and KSI-2 facilitated the nucleation

Figure 37. Appearance of 13 mm ø of KSr_2I_5:Eu 4%, grown at 120 mm/day.

Figure 38. Appearance of 22 mm ø of KSr_2I_5:Eu 4%, grown at 24 mm/day.

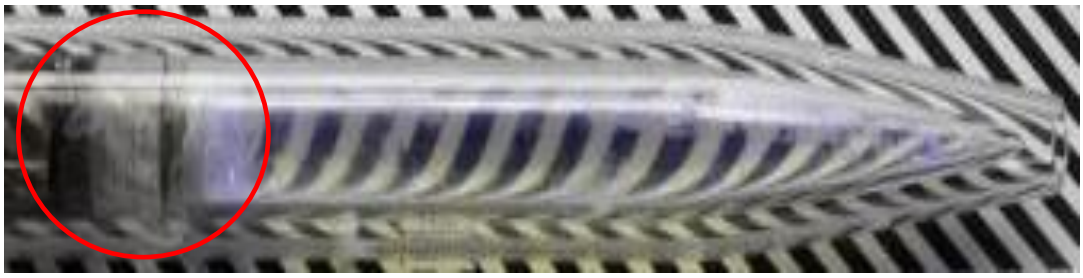

Figure 39. Appearance of 13 mm ø of KSr_2I_5:Eu 4%, grown at 12 mm/day.

and propagation of a single grain, when compared to the conical tip used for KSI-3.

It is worth mentioning that for these growth experiments, aside from the drying process, the precursors materials were used as received from Sigma Aldrich. Neither a filtering process nor a zone refining process was performed before the growth processes. Consequently, black carbon-related impurities in the melt segregated to the last to freeze region. It is believed that these impurities are originated from the precursor materials, and they are inherent in the purification processes of the halide salts. As a result, a small polycrystalline mass was produced in the last to freeze region. For the growth at larger diameter, these impurities are likely to affect the crystal yield and they should be filtered out of the melt.

5.3.2. Europium Optimization and Concentration Effects

The measured scintillation light yield versus Eu concentration for small specimens is shown in Figure 40. The maximum light yield was found to be at 4% Eu^{2+} molar concentration. Of the concentrations tested, we found that the lowest light yield was about 20% less than the maximum with the minimum corresponding to Eu concentrations of 1% and 7%. X-ray excited radioluminescence spectra of KSr_2I_5 with different Eu^{2+} concentration are shown in Figure 41. We found that there was a slight shift of the emission wavelength maximum as the Eu^{2+} concentration increases; at 1% Eu^{2+} the emission peak was centered at 441 nm, and it gradually shifts to 451 nm for the 7% Eu^{2+} sample. The scintillation decay curves are shown in Figure 42. A single exponential decay fit was used to fit time profiles, and the time constants were: 740 ns, 880 ns, 890 ns, 980 ns and 1023 ns for 1%, 2.5%, 4%, 5% and 7% Eu^{2+} concentration respectively. The scintillation decay is shown to increase along with the Eu^{2+} concentration. Similar trends have been observed in other Eu^{2+}-doped scintillators, and they are attributed to self-absorption [56, 57].

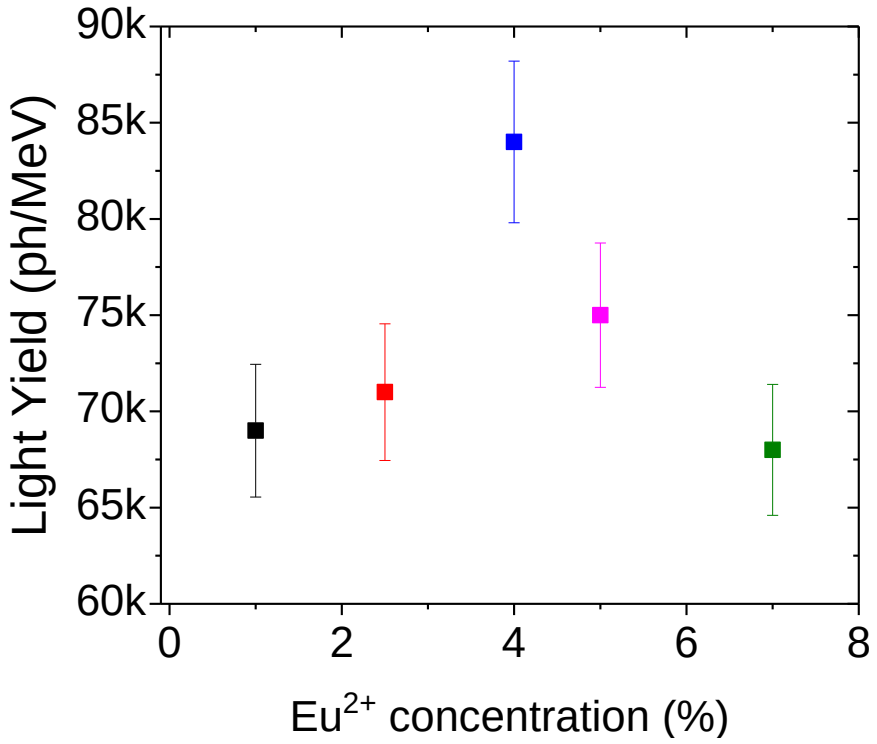

Figure 40. Light yield of $KSr_2I_5:Eu^{2+}$ with different Eu^{2+} concentrations.

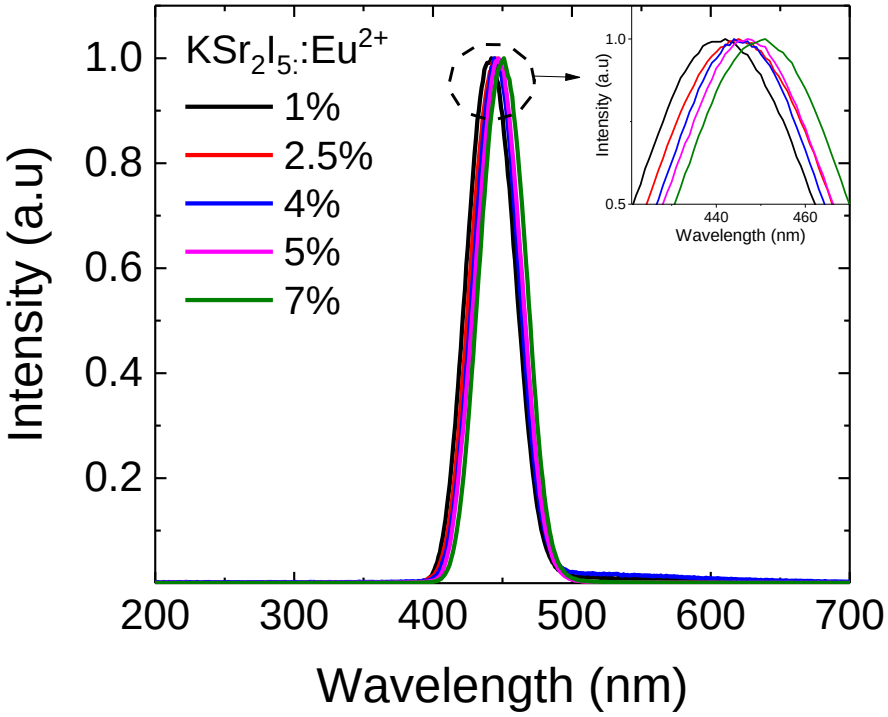

Figure 41. X-ray excited emission vs. Eu^{2+} concentration in KSr_2I_5.

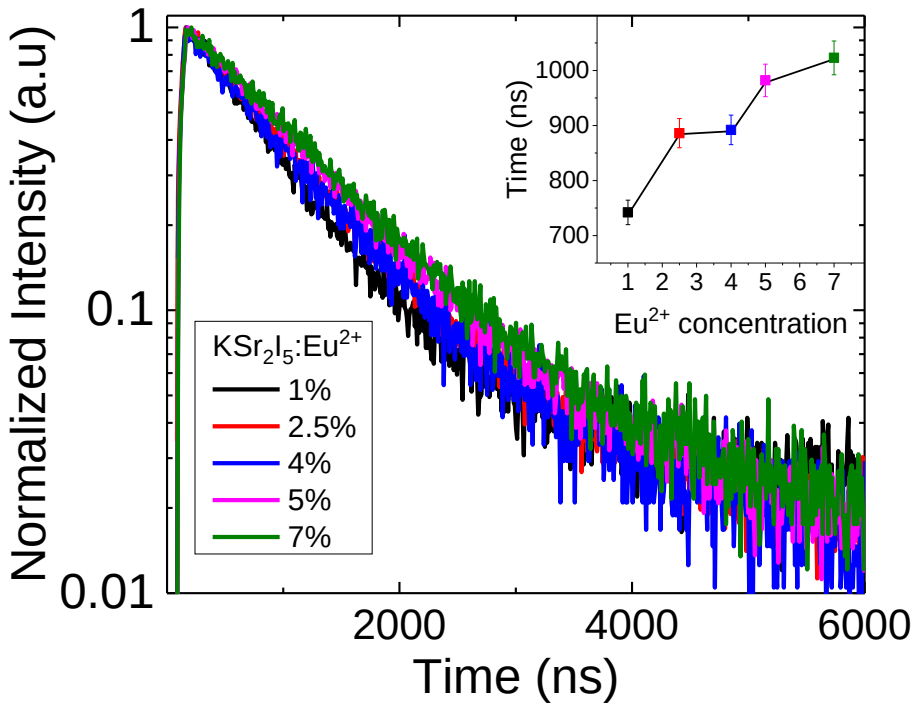

Figure 42. Scintillation decay time with various Eu^{2+} concentrations. The insert shows decay time constant vs. Eu^{2+} concentration. Typical self-absorption trends were observed as the concentrations of Eu^{2+} increased.

Self-absorption is known to have a negative effect on Eu^{2+} activated scintillator as it increases with crystal size. Since larger volumes (≥ $1in^3$) are required for many detector applications, the optimal europium concentration that gave the maximum light yield (4%) in this study may not be the optimum for significantly larger crystals. A lower Eu^{2+} concentration will be considered.

5.3.3. Light Yield and Energy Resolution

For small specimens (~ 2 × 1 × 1 mm^3) of KSr_2I_5:Eu 4%, a light yield of 94,000 ph/MeV and an energy resolution of 2.4% was measured at 662 keV [67]. Performance of small samples is useful because it provides information regarding the inherently achievable characteristics of the scintillator compound. On the other hand, synthesis and characterization of larger samples are needed to better judge the potential effects of point defects as well as structural and compositional inhomogeneity. To this end, larger samples of KSr_2I_5:Eu 4%, measuring 5 × 5 × 5 mm^3 were prepared from the conical section of each boule, as shown in Figure 43. All samples were cut, lapped and measured using the same procedure. It is notable that the light yield of the most rapidly grown crystal (120 mm/day) was within 7% of the much more slowly grown crystals (12 and 24 mm/day). The small difference in light yield and the slight discoloration may be due to increased self-absorption as well as to the introduction of light scattering defects created by the small axial thermal gradient (35 °C/in) and faster pulling rate. The gamma-ray spectra and energy resolution at 662 keV are shown in Figure 44a and b. Spectra were also recorded using ^{133}Ba, ^{57}Co, and ^{241}Am sources. Table 13 shows a summary of the energy resolution at different energies recorded for the KSI series. At 662 keV, the energy resolution differences between the three boules are insignificant (from 2.8 to 2.9%), but at low energies specifically at 59.4 keV, the difference becomes slightly larger; the energy resolution ranges from 7.6 to 7.9%.

The relative light yield measured as a function of absorbed γ-ray energy (non-proportional response) was plotted for 5 × 5 × 5 mm^3 specimens as shown in

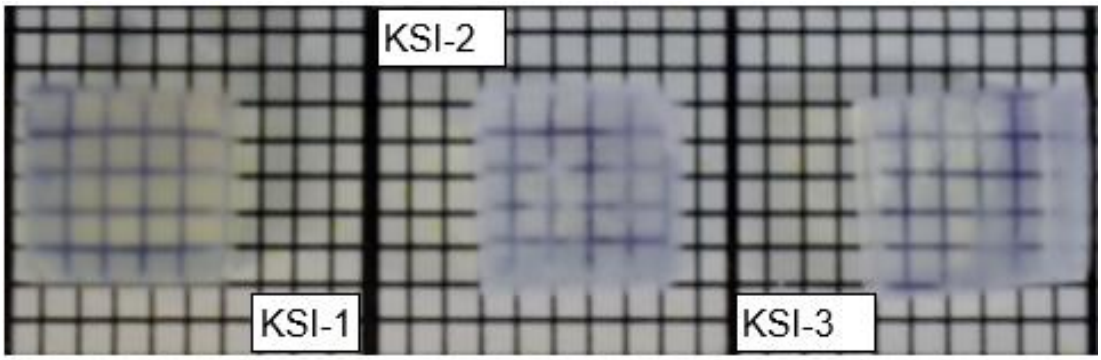

Figure 43. 5 × 5 × 5 mm^3 samples of KSr_2I_5:Eu 4%, KSI-1 grown at 120 mm/day, KSI-2 grown at 24 mm/day and KSI-3 grown at 12 mm/day.

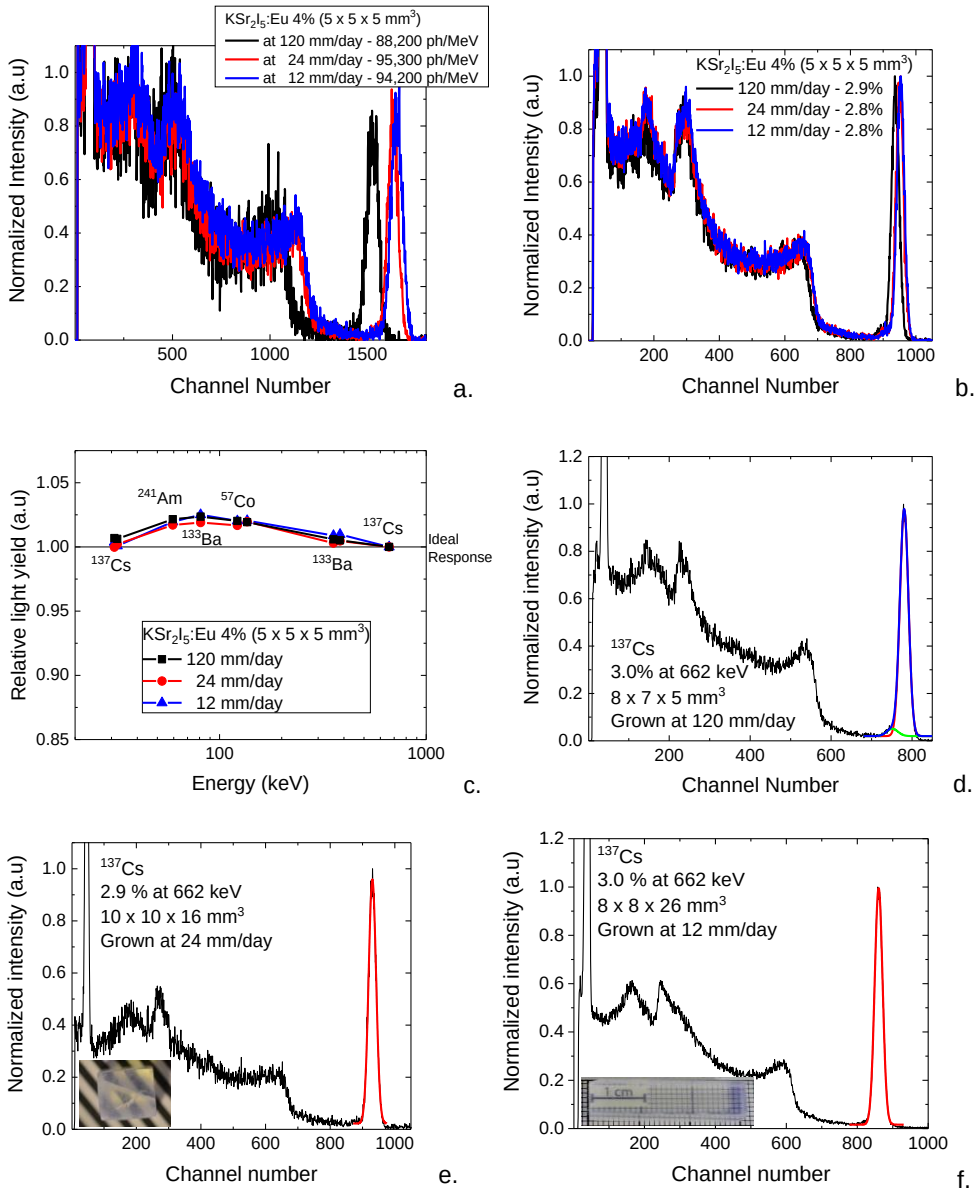

Figure 44a. Light yield measurements, (b) energy resolution measurements, (c) non-proportionality response of 5× 5 × 5 mm^3 samples from KSI-1, KSI-2, KSI-3, (d) energy resolution of a 8 × 7 × 5 mm^3 specimen from KSI-1, (e) energy resolution of a 10× 10 × 15 mm^3 specimen from KS1-2 and, (f) energy resolution of a 8 × 8 × 26 mm^3 specimen from KS1-3. Light yields from 88,000 to 96,000 ph/MeV and energy resolutions from 2.4 to 3.0% (at 662 keV) were measured for KSr_2I_5:Eu 4% over a relatively wide range of growth conditions.

Table 13. Light Yield and Energy resolution of KSr_2I_5:Eu 4% (5 × 5 × 5 mm^3) .

Growth Rate (mm/day)	*LY (Ph/MeV)*	*ER at 662 keV*	*ER at 356 keV*	*ER at 122 keV*	*ER at 59.4 keV*
120	88,200	2.9	3.8	5.8	7.9
24	95,300	2.8	3.7	5.8	7.7
12	94,200	2.8	3.6	5.7	7.6

in Figure 44c. The non-proportional curves showed an almost identical response over the measured energy range; a slight deviation upward (~3% from the ideal) that peaks at 81 keV was observed on KSI-1, KSI-2 and KSI-3.

In order to further evaluate volume effects on crystal quality and uniformity, we prepared larger sample sizes of 8 × 7 × 5 mm^3, 10 × 10 × 16 mm^3 and 8 × 8 × 26 mm^3 for KSI-1, KSI-2 and KSI-3, respectively. At 662 keV, energy resolutions of 3.0%, 2.9% and 3.0% were measured for KSI-1 (Figure 44d), KSI-2 (Figure 44e) and KSI-3 (Figure 44f). The results obtained from the volumetric studies are encouraging because they show that $KSr_2I_5:Eu^{2+}$ has the potential to perform adequately in larger sizes. We need to mention that the light yield of KSr_2I_5:Eu is expected to decrease to some extent with increasing volume, mainly due to self-absorption. This is typically seen in Eu^{2+} activated crystals [56, 57]. Further evaluation is needed to quantitatively address this effect on potassium strontium iodide.

5.3.4. Micro-resolution X-ray Detector Mapping.

The micro-resolution X-ray Detector mapping (MXDM) technique has the potential to become an important tool for the scintillator community because it could be used to evaluate the light yield homogeneity of large size scintillator materials. Other techniques commonly used such as UV microscopy are able to describe the uniformity of the dopant distribution, but this information is not a complete measurement of scintillation homogeneity because in the UV excitation process, electron-hole creation and recombination are not present. On the other hand, X-rays produce ionization, and therefore the information obtained is more relevant to the uniformity of the scintillation process.

For MXDM measurements, a sample measuring 8 × 8 × 26 mm^3 was prepared from KSI-3. It had an energy resolution of 3% at 662 keV as shown in Figure 44f. The scan was performed by rastering the X-ray beam spot over one of the 8 × 26 mm^2 faces. Spectra were collected every 50 μm, and a 10 μm X-ray

beam size was used. The 2D X-ray response map is shown in Figure 45(left). The grayscale image correlates to the channel number of the photopeak centroid in the X-ray pulse height spectrum at each beam spot. A lighter shade indicates higher light yield. The difference between the lightest and darkest gray shades corresponds to a 20% difference in measured light yield. The same information is displayed in 3D format in Figure 45 (right), where the x and y axes are the areal position, and the z-axis is the normalized centroid position. The primary change in the measured light intensity is a smooth decrease as a function of distance from the PMT, which we attribute to a combination of a geometrical light collection effect and some degree of self-absorption of the Eu^{2+} emission. There is little evidence of inhomogeneity that could be attributed to structural or compositional inhomogeneity of the crystal. These results are encouraging, because many ternary alkali halide and alkaline earth halide scintillators are known to have uniformity problems that affect their performance and limit their wide spread utilization [47, 58-60, 66].

5.4. Conclusion

In this work we focused on understanding fundamental material properties related to: dopant optimization, crystal growth processes, homogeneity and overall performance of KSr_2I_5:Eu.

- We found that 4 molar % is the Eu^{2+} concentration needed to maximized the light yield in the KSr_2I_5 matrix for crystal sizes up to roughly 1-2 cm^3. Typical self-absorption was observed with the increase in europium concentration.
- We have shown that it is possible to grow high performing single crystals of KSr_2I_5:Eu at faster rates (12 mm/day -120 mm/day) than commonly used for other halide scintillators (5 to 30 mm/day).
- We learned that having a grain selector at the bottom of the ampoule facilitated the nucleation and propagation of a single grain.

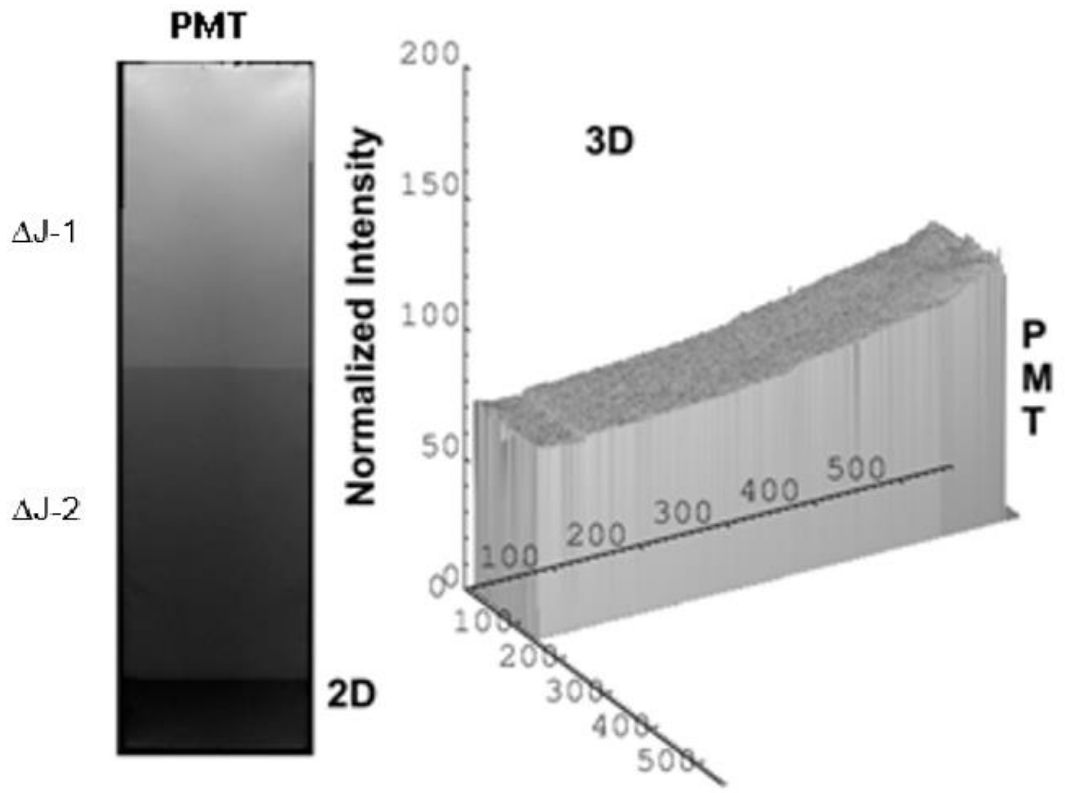

Figure 45. Micro-resolution X-ray mapping, Left - 2D X-ray response map. Right - 3D X-ray response map. Changes is the beam flux are shown in the figure as ΔJ-1 and ΔJ-2.

- In crystals measuring 5 × 5 × 5 mm^3, we found that the boule grown at 120 mm/day showed light output within 7% of the boules grown at 24 and 12 mm/day. This small difference may be due to an increase in the defect density in that crystal caused by the faster growth rate. Insignificant changes were seen in the energy resolution. Therefore, light yields between 88,000 and 96,000 ph/MeV and energy resolutions from 2.4 to 3.0% were observed for the range of growth parameter used.
- Using a new technique, micro-resolution X-ray mapping, we were able to evaluate the uniformity of scintillation response in $KSr_2I_5:Eu^{2+}$. No obvious inhomogeneities that could compromise the performance were found in the measured crystal.

At this point we can say that KSr_2I_5:Eu scintillator crystals are more tolerant of growth conditions than some other high performance scintillators. We obtained excellent performance for crystals grown at rates ranging from 12 to 120 mm/day and with thermal gradients at the growth interface of 35 to 140 °C/in. The optimal Eu^{2+} concentration is a function of crystal size and is ~4% for 1-2 cm^3 crystals. It will likely be less for larger crystals in order to manage the self-absorption effects. These results are encouraging, and future work will focus on the rapid crystal growth (120 mm/day or faster) and characterization of larger size crystals (≥ 1 in^3) in addition to co-doping studies to further improve the performance on $KSr_2I_5:Eu^{2+}$.

Chapter 6
Exploring Growth Conditions and Eu^{2+} Concentration Effects for KSr_2I_5:Eu Scintillator Crystals II: Ø 25 mm Crystals

A version of this chapter was originally published in peer-reviewed journal by Luis Stand. No additional changes were made other than formatting to conform to the dissertation format.

The full citation is as follows L. Stand, M. Zhuravleva, J. Johnson, M. Koschan, Y. Wu, S. Donnald, K. Vaigneur, E. Lukosi, C.L. Melcher, Exploring growth conditions and Eu^{2+} concentration effects for KSr_2I_5:Eu scintillator crystals II: Ø 25 mm crystals, Journal of Crystal Growth, 483 (2018) 301-307 [71].

J. Johnson cut and polished the crystals used for this work. Agile technologies inc. (Dr. Donnald and Vaigneur) encapsulated the crystal shown in section 6.3.5. The remaining co-authors provided valuable research advice during this research.

Abstract

Europium doped potassium strontium iodide is a very promising scintillator for national security applications due to its ease of growth and excellent scintillation properties. For this work the crystal growth and scintillation properties of 1-inch diameter single crystals of $KSr_2I_5:Eu^{2+}$ were investigated. We focused our efforts on optimizing the growth parameters required to produce one-inch diameter crystals without decreasing the previously reported fast pulling rate of 5 mm/h. Cracking was minimized by replacing the quartz ampoules with carbon coated quartz ampoules; thus, several crack free single crystals of KSI with varying Eu^{2+} concentrations were grown, including a Ø 1" by 6" long boule of with 2.5% Eu.

The maximum achievable performance of each crystal was measured using 0.012 cm^3 specimens and the volumetric dependencies of the light yield, energy resolution and decay time were evaluated using specimens of KSI:Eu 2% with volumes ranging from 0.012 cm^3 to 18 cm^3. For large volumes (≥ 9 cm^3), the performance was comparable to other high performing scintillators, with light yields up to 78,200 ph/MeV and energy resolutions as good as 3.2% at 662 keV. The

initial version of a hermetic package has been developed, and the stability of the sealed crystal is promising.

6.1. Introduction

Scintillators for national security applications require high light yields and excellent energy resolutions to provide unambiguous identification of radioactive sources and discrimination of potential threat sources from non-threat sources [32]. In recent years, several metal halide scintillators from $BX_2:Eu^{2+}$, $CX_3:Ce^{3+}$, $ABX_3:Eu^{2+}$ and $AB_2X_5:Eu^{2+}$ (where A = alkaline metals, B = alkaline earth metals, C = lanthanides and X= one or more halides) compositional families have been studied due to their high light yields and excellent energy resolutions, approaching the fundamental limits of scintillators [6, 9, 15, 18, 23, 29, 31, 36, 45, 72]. Halide scintillators such as SrI_2:Eu, $CeBr_3$ and $LaBr_3$:Ce are the most promising candidates for many gamma ray detection applications, but due to their high cost related to their low production yield and slow growth processes, NaI:Tl is still preferred due to lower cost.

Intensive investigations were undertaken by several laboratories to improve the mechanical properties and the yield of detector quality SrI_2:Eu. Techniques such as zone refining, melt filtration and vacuum melt pumping have been evaluated to remove O^{-2}, OH^-, CO_3^{-2} and oxyhalides impurities that are known to have a detrimental effect on the crystal quality [23, 25, 73]. Although it is unclear which technique or combination of techniques is currently used for the fabrication of commercial-grade SrI_2:Eu, the work presented by Boatner et al. suggests that a combination of all three techniques is the most likely to yield high quality crystals reproducibly [25].

Boatner's synthesis guideline is expected to also improve the yield of KSI:Eu. On the other hand, the purpose of our work is to produce a high performing scintillator at an affordable cost, therefore the steps related to the removal of impurities from the precursor materials or the molten salt were minimized. Instead,

the typical quartz ampoule was replaced by a carbon coated quartz ampoule expecting that the carbon would act as a scavenger of oxygen (O_2) and water (H_2O) impurities, and as a protective buffer between the molten salt and the quartz [74]. In fact, carbon coated ampoules have proven to be effective at reducing the adhesion between the ingot and the sidewalls of the quartz ampoule for many semiconductors materials [74-76], and for scintillators such as CsI:Tl and NaI:Tl which are known to interact aggressively with quartz. Recent work on CaI_2:Eu, $KCaI_3$:Eu and $K(Ca,Sr)I_3$:Eu has shown that using carbon coated ampoules could improve quality of the boules [25, 77, 78].

We have previously shown that crack free Ø15 mm KSI:Eu can be grown using thermal gradients ranging from 15 to 55 °C/cm and solidification rates ranging from 0.5 to 5 mm/h without affecting the scintillation properties [65]. For this work, the growth parameters were optimized to produce high quality, high performing 1-inch diameter single crystals of Eu^{2+}-doped potassium strontium iodide at much faster rates than those typically used for other metal halide such as SrI_2:Eu, $LaBr_3$:Ce and $CeBr_3$ (0.2 to 1 mm/h) [18, 23, 25, 26, 28, 44, 73, 79-82]. The ability to grow high performing detector quality scintillator crystals at much faster rates should decrease the production cost by reducing overhead and direct labor expenses enough to meet the cost requirements for national security applications.

6.2. Experimental

6.2.1. Crystal Growth

Single crystals of $KSr_{2(1-x)}Eu_{2x}I_5$ (where $0 \leq \times \leq 0.06$) were grown via the vertical Bridgman technique. Anhydrous 99.999% pure beads of KI and EuI_2 and 99.995% pure beads of SrI_2 from APL Engineered Materials Inc. were mixed and loaded into 22 mm diameter quartz ampoules and 25 mm diameter carbon coated quartz ampoules inside a dry box with <0.01 ppm moisture and oxygen. The loaded ampoules were dried at 200 ˚C for 12 hours and sealed under a dynamic vacuum

of 10^{-6} torr. Prior to the growth experiments, a melt-synthesis step was carried out by reacting the raw materials at 720 ˚C for 12 hours and then cooling to room temperature over a 5-hour period. The crystals were grown using a two-zone transparent furnace (TF) and a 24-zone electrodynamic gradient (EDG) Mellen furnace. To obtain the desired thermal gradient, a diaphragm was placed between the hot zone and cool zone [83, 84]. The growth process was initiated in a Ø 2 mm grain selector connected to the bottom of the ampoule where the self-seeding process took place. Solidification rates of 0.8, 3 and 5 mm/h and cooling times of 40, 53 and 130 hours were used. Table 14 shows a summary of the growth parameters used for each of the crystals grown for this work. The single crystal boules were cut to size using a low speed wire saw and were lapped by hand using silicon carbide polishing pads (600 grit to 1200 grit) with Buehler AutoMet™ low viscosity lapping oil inside the drybox.

6.2.2. Characterization

For the light yield, energy resolution and non-proportionality measurements, specimen sizes ranging from 0.012 to18 cm^3 were measured using an analog signal processing chain consisting of a Hamamatsu photomultiplier tube, a Canberra model 2005 pre-amplifier, an Ortec 672 amplifier, and a Tukan 8K multi-channel analyzer. The absolute light yield was measured via the single photoelectron technique using a Hamamatsu R2059 photomultiplier tube (PMT) [85]. The number of photoelectrons was calculated from the relative positions of the 662 keV photopeak and the peak from single photoelectrons. The conversion from the number of measured photoelectrons to the number of photons/MeV emitted by the scintillator was accomplished by convolving the quantum efficiency of the PMT as a function of wavelength (measured by Hamamatsu) with the X-ray excited emission spectrum of the sample. Mineral oil was used as a couplant between the specimen and PMT. A hemispherical dome of Spectralon was used to improve the scintillation light collection and a shaping time of 10 μs was used to

Table 14. Summary of the growth condition.

Eu^{2+} conc. (%)	*Diameter (mm)*	*Pulling rate (mm/h)*	*Furnace type*	*Cooling time (hours)*	*Carbon coating?*
0, 6	22	0.8	TF	130	×
0.25	22	5	EDG	40	✓
1, 2, 4	25	5	EDG	40	✓
2.5	25	3	EDG	53	✓

ensure the complete integration of the light pulse. For the energy resolution and the non-proportionality measurements, a Hamamatsu R6231-100 Super Bialkali PMT was used. The specimens were placed in a quartz container filled with mineral oil to protect them from moisture during the measurement; mineral oil was also used couplant between the quartz container and PMT. Radioisotopic sources of ^{60}Co, ^{137}Cs, ^{133}Ba, ^{57}Co and ^{241}Am were used as the excitation mode. A shaping time of 10 μs was used. The scintillation decay time was measured under irradiation from a ^{137}Cs sealed source with the time-correlated single photon counting technique [40]. The decay curves were fitted with a two-component exponential function.

Characterization of the undoped KSI crystal and the one inch diameter by six inch long crystal of KSr_2I_5:Eu 2.5 % will be reported elsewhere.

6.3. Results and Discussion

6.3.1. Crystal Growth

To evaluate the cracking behavior of KSI:Eu^{2+} at fast pulling rates, a 22 mm diameter boule of KSI:Eu 4% was grown 3 times at 10, 7 and 5 mm/h under a 140 °C /in thermal gradient and a 40 hour cooldown. The highest crystal quality was obtained when grown at 5 mm/h as shown in Figure 46. Although this crystal had excellent optical quality, few cracks were present towards the last-to-freeze region, shown circled in blue in Figure 46. These cracks likely originated during the cooldown stage from stresses produced by the polycrystalline last-to-freeze region and by the crystal detaching from the quartz ampoule. When the crystal contracts more than the ampoule, the degree of wetting between the crystal and the ampoule is the major factor determining the stress in the crystal. The chemical bonding between the molten salt and the quartz is likely caused by presence of foreign compounds formed during synthesis by OH^-, O^{-2} and CO_3^{-2} contaminants. A viable solution to minimize the molten salt-ampoule interactions was to replace the regular quartz ampoules with carbon coated quartz ampoules.

Figure 46. 22 mm diameter boules of KSr_2I_5:Eu 4% grown via the vertical Bridgman technique using an EDG furnace and using 10, 7 and 5 mm/h as pulling rates. The last-to-freeze region is circled in blue.

Nearly crack free one-inch diameter single crystals of KSr_2I_5 with varying Eu^{2+} concentrations were grown using carbon coated quartz ampoules with the growth parameters previously discussed; 5 mm/h – pulling rate, 140 °C /in – thermal gradient and 40 h – cooldown, as shown in Figure 47a. By using carbon coated quartz ampoules, the crystal yield of KSI:Eu was significantly improved compared to the crystals grown in regular quartz ampoules, see Figure 46 and Figure 47. It worth mentioning that undoped KSI and KSI:Eu 6% could not be grown under the conditions used for the other Eu^{2+} concentrations. Nevertheless, nearly crack free crystals were grown by using a conservative approach, shown in Figure 47b.

Although these results are very promising, producing one detector per growth run is not a practical nor cost-effective process for large scale manufacturing. To make the process economically viable, more detectors per boule would be needed. Therefore, we decided to test the procedure investigated in this work by growing a one-inch diameter by six inch long boule. To ensure the success of this experiment, the pulling rate was reduced from 5 to 3 mm/h and the cooldown was increased from 40 to 53 hours, resulting in a 10-day growth run. The result was an excellent quality, crack free single crystal as shown in Figure 48.

6.3.2. Maximum Achievable Performance

The maximum achievable performance of each boule was measured using 0.012 cm^3 specimens to minimize potential homogeneity and self-absorption effects. The light yield, energy resolution and non-proportional response of small $KSr_2I_5:Eu^{2+}$ crystals were not heavily dependent upon the dopant concentration. The highest light yield of 90,700 ph/MeV and the best energy resolution of 2.5% at 662 keV were measured for a europium concentration of 6%, while the lowest light yield and worst energy resolution of 75,300 ph/MeV and 3.0% were measured for a concentration 0.25%. The light yield and energy resolution vs. Eu^{2+} concentration trends are shown in Figure 49 and Figure 50, respectively. Figure 51 shows the

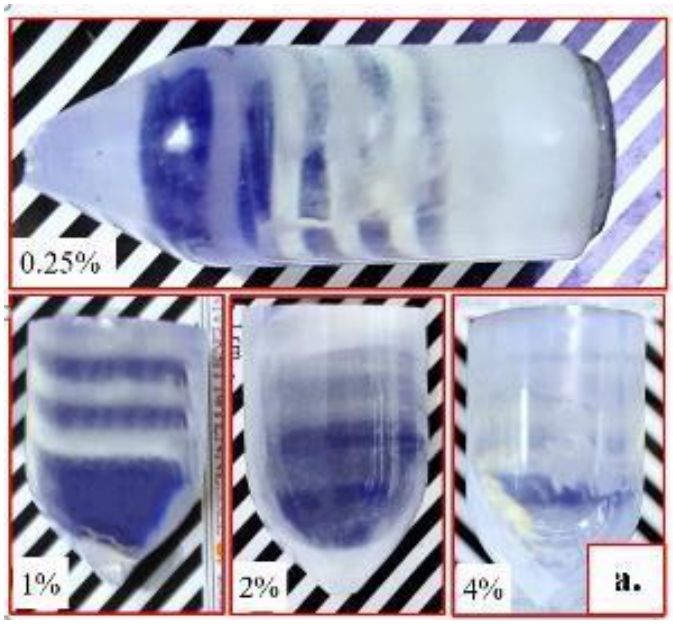

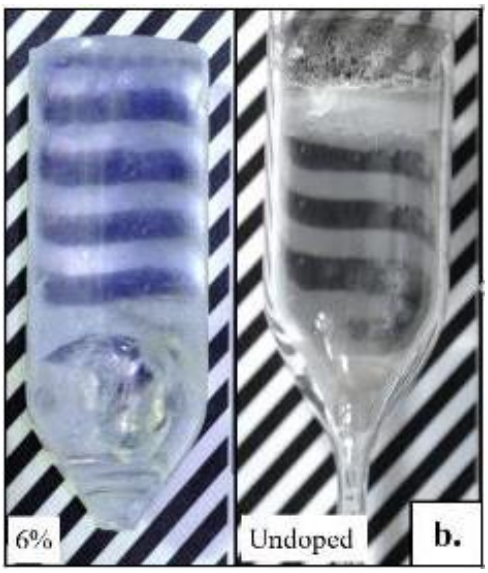

Figure 47a. 25 mm diameter single crystals of $KSr_2I_5:Eu^{2+}$ under white fluorescence light (The Eu^{2+} concentration is indicated in the lower left corner). The crystals were grown at 5 mm/h and cooled down over 40 hours. (b) 22 mm diameter crystals of undoped-KSI and KSI:Eu 6% were grown at 0.8 mm/h and cooled down in 130 hours.

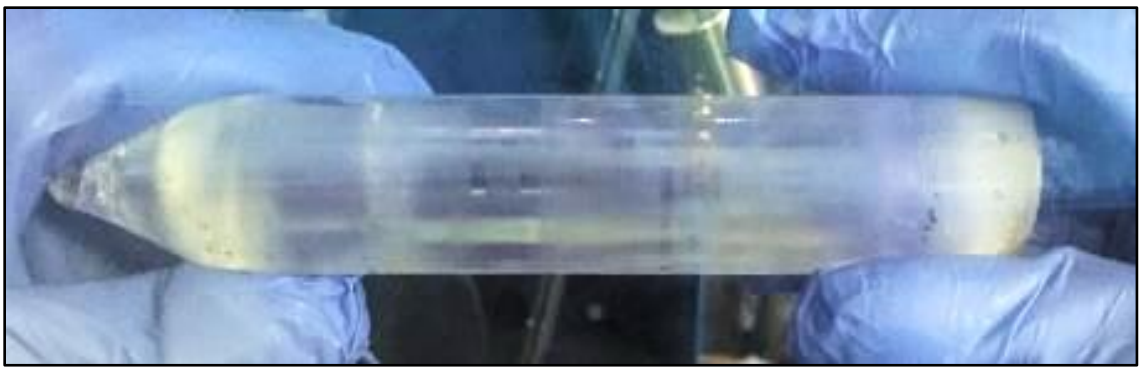

Figure 48. One inch diameter by six inch long crack free single crystal of KSr_2I_5:Eu 2.5 %

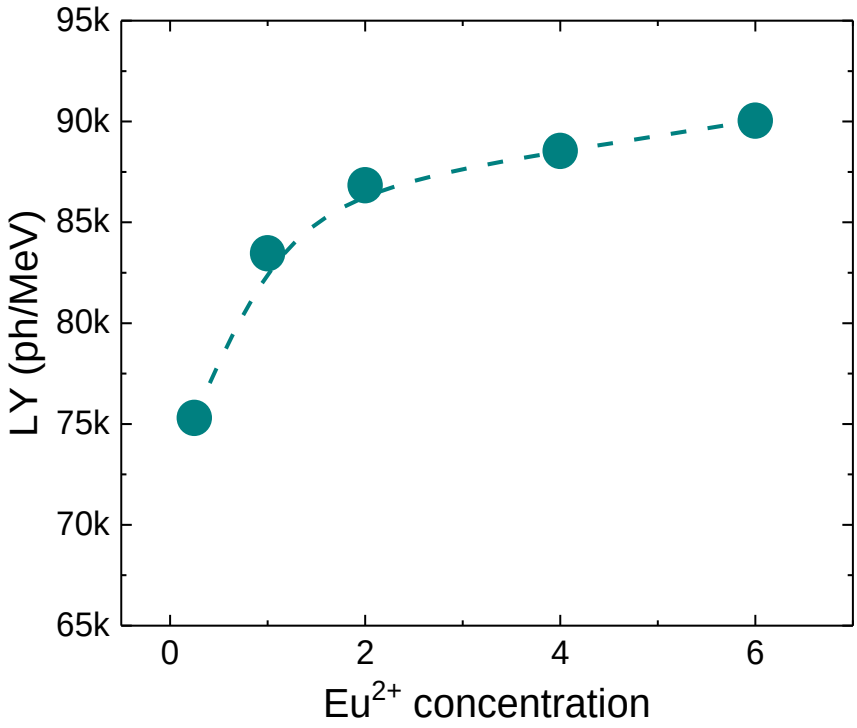

Figure 49. Light yield of each 0.012 cm^3 specimen.

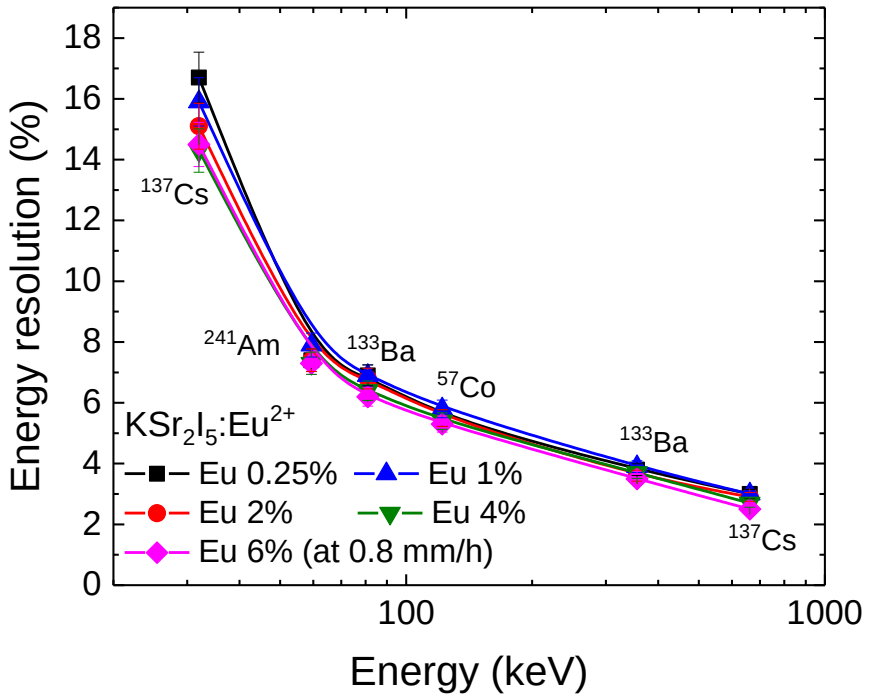

Figure 50. Energy resolution of each 0.012 cm^3 specimen. The highest light yield and lowest energy resolution at 662 keV was measured for an Eu^{2+} concentration of 6%.

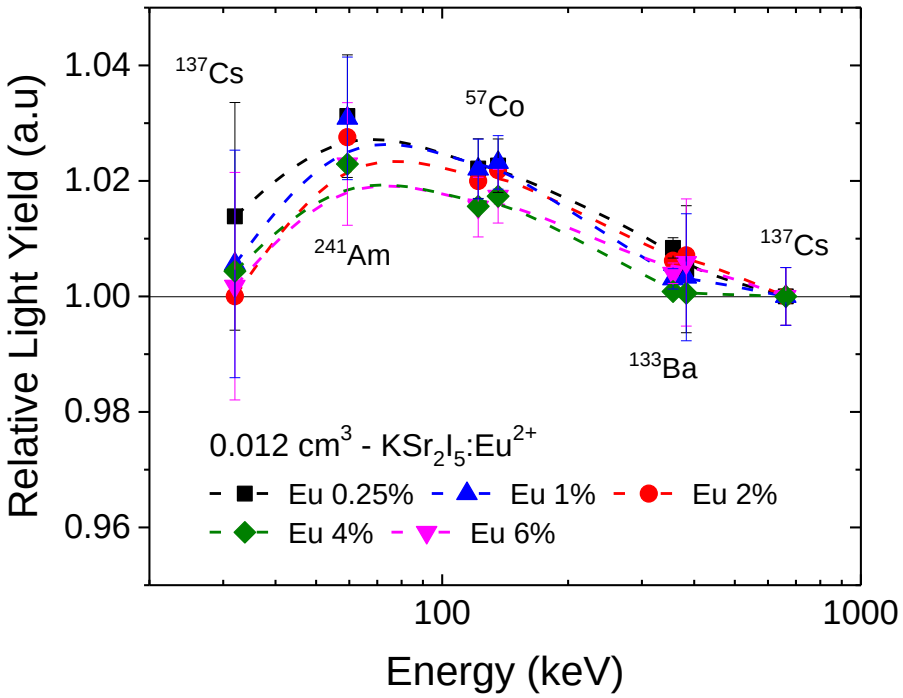

Figure 51. Non-proportional response curves of KSI:Eu^{2+} (0.25% to 6%) show a deviation of ~3% from the ideal.

non-proportional response curves of KSr_2I_5 which deviated 3% from the ideal at the intermediate energies (~60 keV), regardless of the Eu^{2+} concentration. A summary of the results from the specimens measured in this section are shown Table 15.

6.3.3. Volumetric Effects on KSr_2I_5:Eu 2%

Artifacts such as compositional inhomogeneities, growth defects and, in the case of most Eu^{2+} doped crystals, self-absorption are often responsible for performance degradation with increasing volume [12, 44, 56, 86]. In this section the volumetric dependencies of the light yield, energy resolution, and decay time were evaluated for KSr_2I_5:Eu 2% by comparing specimens with volumes of 0.012 cm^3, 1cm^3, 5 cm^3, 14 cm^3 and 18 cm^3. The light yield and energy resolution of KSI:Eu 2% showed only minor volumetric dependencies; the largest variation was observed when the crystal volume was increased from 0.012 cm^3 to 1 cm^3. The LY decreased by ~17%, from 87,900 ph/MeV at 0.012 cm^3 to 73,200 ph/MeV at 18 cm^3 and the energy resolution increased from 2.9% at 0.012 cm^3 to 3.8% at 18 cm^3 at 662 keV, as shown in Figure 52. High energy tailing of the ^{137}Cs photopeak was observed for crystals measuring 14 cm^3 and 18 cm^3 as shown by the red arrow in Figure 53. The degree of asymmetry of the Gaussian peak intensified with increasing volume due to the incomplete signal integration of our analog electronics. As expected the scintillation decay time lengthened as the volume of crystals increased, a two-component exponential function provided a good fit to the decay curves as shown in Figure 54. The first component of the scintillation decay ranged from 0.850 µs at 0.012 cm^3 to 1.92 µs at 18 cm^3 and consisted of ~85% of the total light. The remainder of the scintillation light had a time constant that ranged from 3.85 to 14.07 µs. Microsecond-long decay times are typically measured for Eu^{2+} doped crystals due 4f-5d transitions [56, 57]. There are two main factors known to lengthen the scintillation decay time; light scattering centers

Table 15. Summary of the light yields and energy resolutions measured from the 0.012 cm^3 crystals.

Eu^{2+} conc.	*LY (ph/MeV)*	*ER at 662 keV*	*ER at 122 keV*	*ER at 59.4 keV*
0.25%	75,300	3	5.5	7.4
1%	83,400	3	5.8	7.9
2%	86,800	2.9	5.5	7.4
4%	88,500	2.6	5.4	7.3
$^{+}$6%	90,700	2.5	5.3	7.2

+Grown at 0.8 mm/h

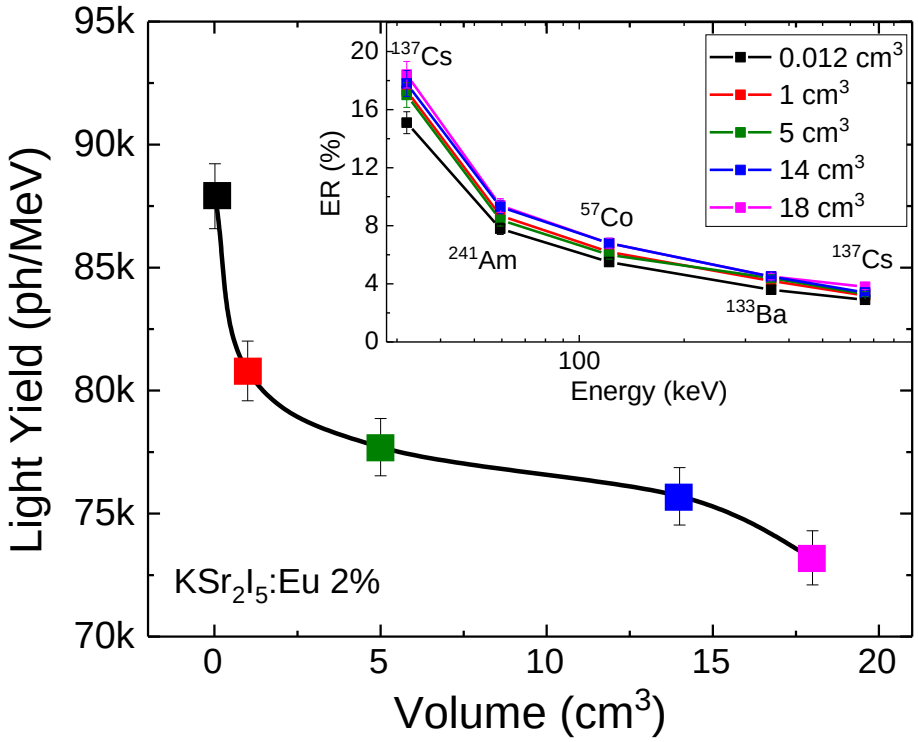

Figure 52. The light yield and energy resolution (insert) of KSr_2I_5:Eu 2% measured for 0.012 cm^3, 1 cm^3, 5cm^3, 14 cm^3 and 18 cm^3 crystals.

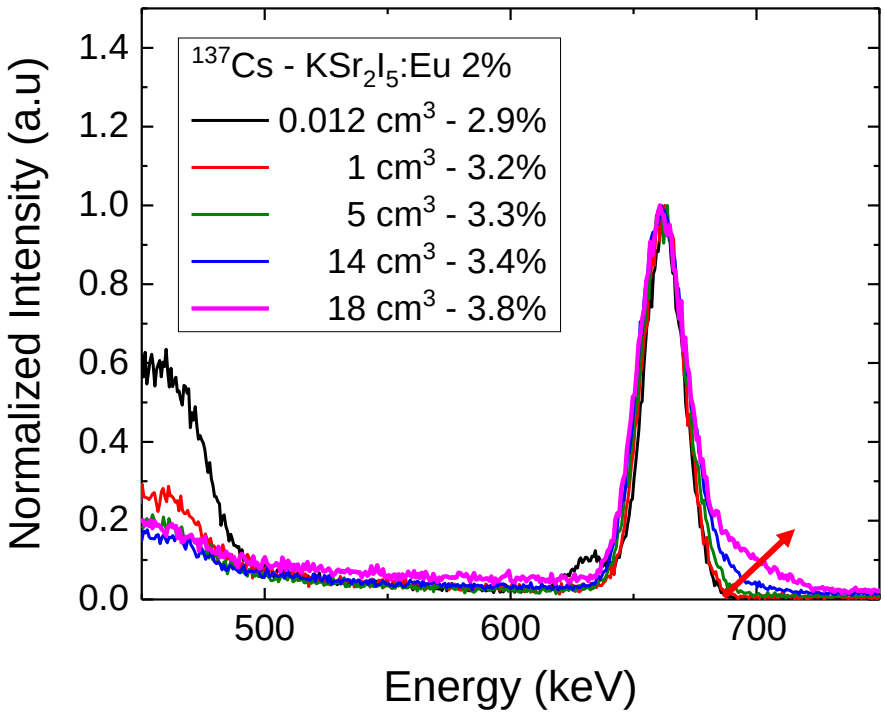

Figure 53. ^{137}Cs spectra showing the energy resolution at 662 keV broadening from 2.9% at 0.012 cm^3 to 3.8% at 18 cm^3. The red arrow shows high energy tailing related to the incomplete light collection of the analog electronics.

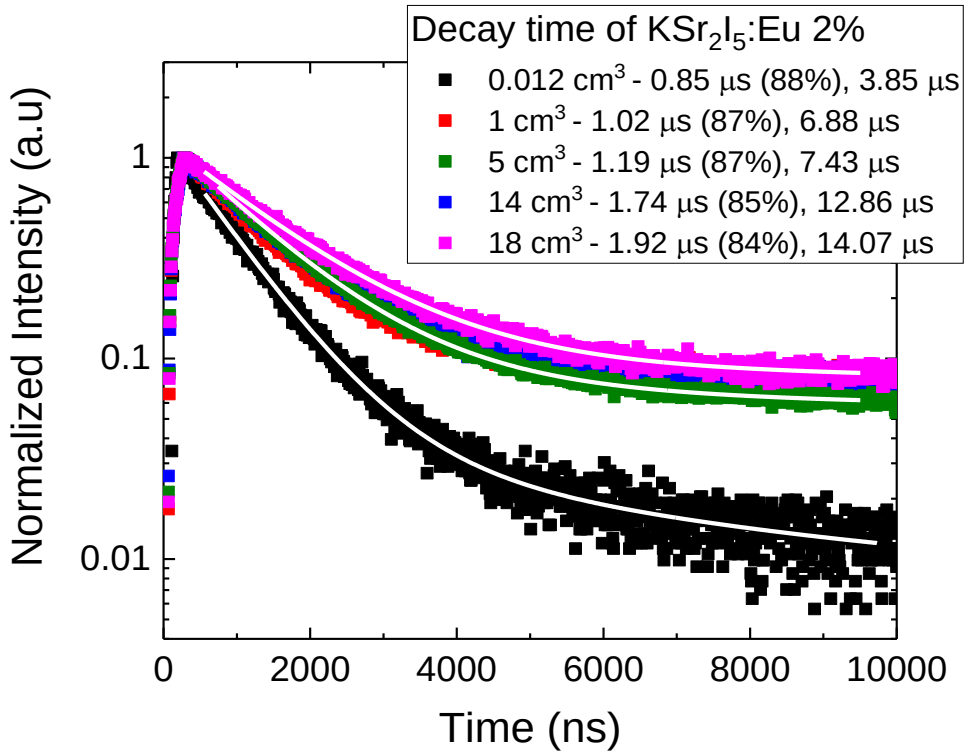

Figure 54. Scintillation decay time profiles for all of the crystal volumes tested. (6b) Probability of self-absorption of the scintillation decay time.

produced by growth defects and self-absorption caused by re-absorption and re-emission of the scintillation light in the luminescence centers. Since the same crystal was used, we could assume that the contribution of the scattering centers and the self-absorption per unit length are constant through the crystal. Therefore, the probability of self-absorption *a* shown in Figure 55 was calculated by applying the self-absorption model proposed by Alekhin et. al [56, 87], using Eq. 1.

$$a = 1 - \tau/\tau_{eff}$$

Since the scint. decay time at 1 cm^3 was used for τ_{eff}, the calculated value of *a* represents the combined effect from defects and radiation trapping. The probability of self-absorption increased with volume from 0.2 at 5 cm^3 to 0.5 at 18 cm^3. As expected, the probability of self-absorption was comparable for both components of the scintillation decay time.

The reduction of the light yield, the slight variation of the energy resolution and the lengthening of the decay time observed with increasing volume can be attributed mostly to self-absorption caused by re-absorption and re-emission of light by Eu^{2+} centers in the crystal. These effects has been previously reported for SrI_2:Eu and $CsBa_2I_5$:Eu [12, 44, 56, 57, 87]. Table 16 shows a summary of the results obtained from this section.

6.3.4. Performance of Large Crystals

The scintillation properties were measured using a 9 cm^3 crystal of KSI:Eu 0.25%, a 14 cm^3 crystals of KSI:Eu 1%, KSI:Eu 2% and KSI:Eu 4%, and a 11 cm^3 crystal of KSI:Eu 6%. The relationships between light yield and Eu^{2+} concentration and between energy resolution and Eu^{2+} concentration are shown in Figure 56. Light yields between 62,500 and 78,200 ph/MeV and energy resolutions between 3.2% and 3.7% were measured at 662 keV. The ^{137}Cs energy spectra are shown in Figure 57. The performance measured for the large crystals is promising. The light yield and energy resolution of the rapidly grown $KSr_2I_5:Eu^{2+}$ crystals are. comparable to commercial already comparable to SrI_2:Eu scintillators, which are

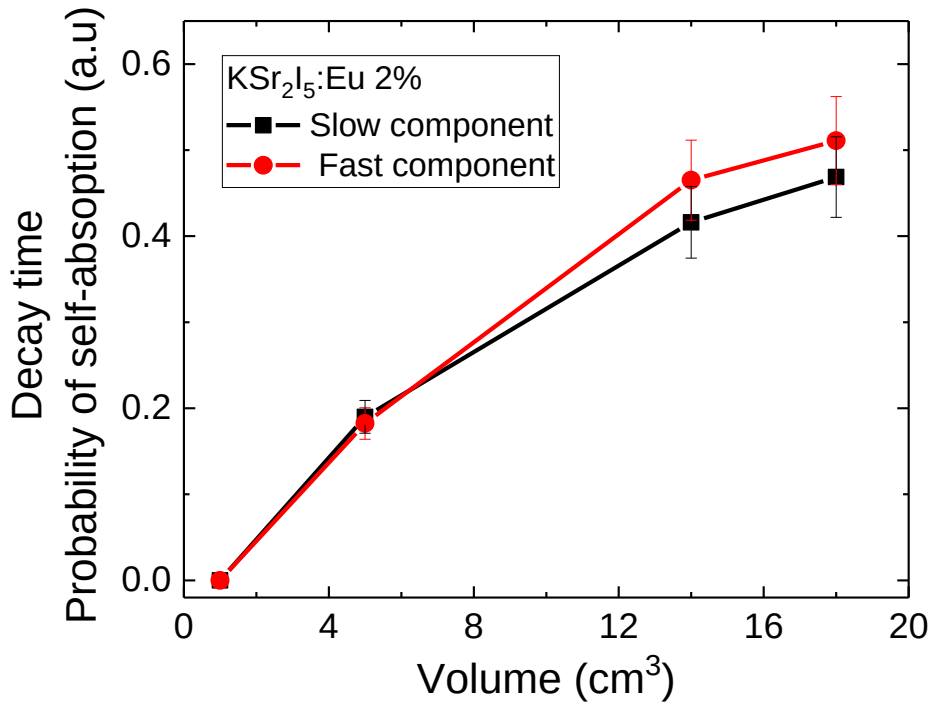

Figure 55. Probability of self-absorption of the scintillation decay time.

Table 16. Summary of scintillation properties of KSr_2I_5:Eu 2% measured at volumes ranging from 0.012 cm^3 to 18 cm^3.

Volume (cm^3)	*LY (ph/MeV)*	*ER at 662 keV*	*ER at 122 keV*	*ER at 59.4 keV*	*Scintillation Decay time (μs)*
0.012	87,900	2.9	5.5	7.8	0.85 (86%), 3.83
1	80,800	3.2	6.2	8.7	1.02 (87%), 6.88
5	77,700	3.3	6.0	8.4	1.29 (87%), 7.43
14	75,700	3.4	6.8	9.3	1.69 (85%), 12.86
18	73,200	3.8	6.8	9.4	1.92 (85%), 14.07

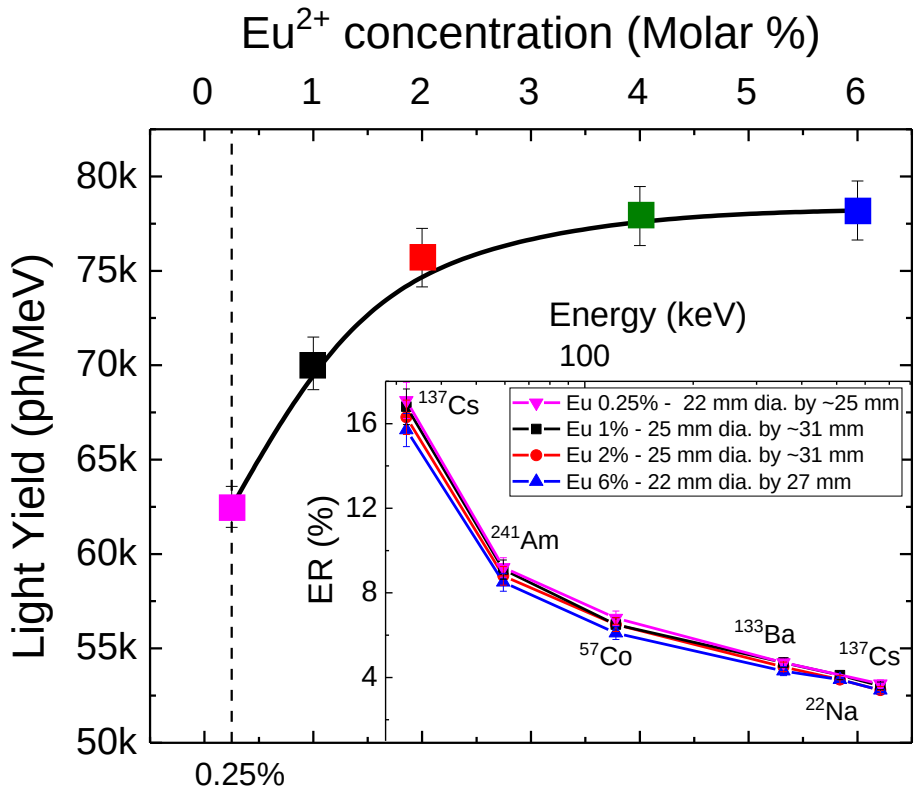

Figure 56. The highest light yield (~78,000 ph/MeV) was measured for KSI doped with Eu 6% (Worst – 62,500 and 3.7% @ Eu 0.25%).

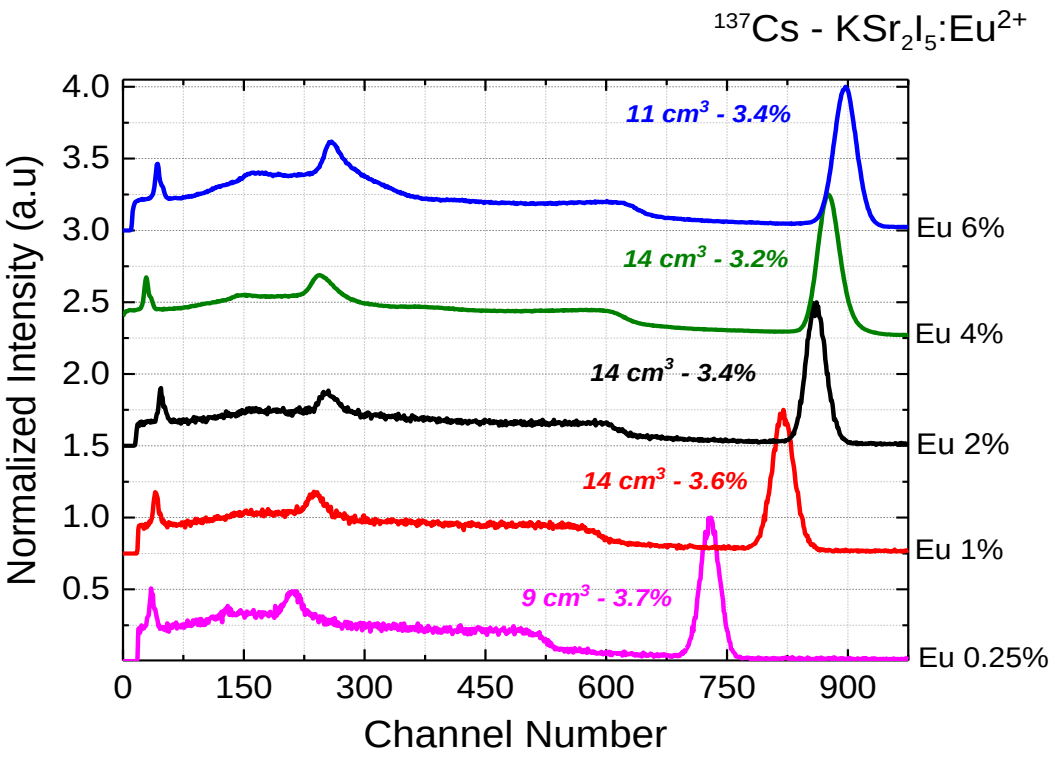

Figure 57. ^{137}Cs spectra of large volume KSr_2I_5 at different Eu^{2+} concentration.

typically grown ~10 times more slowly [12, 18, 23, 25, 26, 44, 56, 73, 80-82, 88]

Excellent non-proportional responses were observed for all the Eu^{2+} concentrations investigated. Like the 0.012 cm^3 specimens, the non-proportional response curves of the large crystals were independent of the europium concentration and showed a slight deviation of ~3% from the ideal response as shown in Figure 58.

The scintillation decay time curves were fitted using a two-component exponential decay function. The principal time constants ranged from 1.32 to 2.29 µs and accounted for ~85% of the scintillation light while the secondary component ranged from 6.8 to 17.4 µs. A summary of the results from this section is shown in Table 17.

6.3.5. Hermetic Encapsulation

The first hermetically sealed package of KSr_2I_5:Eu was developed. Hermetic encapsulation is required to protect the physical integrity of metal halide scintillator crystals when stored under ambient conditions. There are two main challenges around this process; (1) the durability of the hermetic encapsulation and (2) the stability of the scintillation performance.

A 14 cm^3 crystal of KSI:Eu 2% was encapsulated and measured as shown in Figure 59. The energy resolution at 662 keV was 3.6 to 3.9%. A range is given because of the high energy tailing produced by an intensified Eu^{2+} self-absorption due to the close proximity of the reflector to the crystal [89]. This effect can be suppressed by slightly reducing the volume of the crystal, tapering crystal or by using digital pulse processing [12, 88]. Nonetheless, the energy resolution of the encapsulated crystal is only slightly worse than the 3.4% measured before the encapsulation.

6.3.6. Summary

In this work, we have shown that high quality, high performing single crystals of Eu^{2+} doped potassium strontium iodide can be grown at much faster

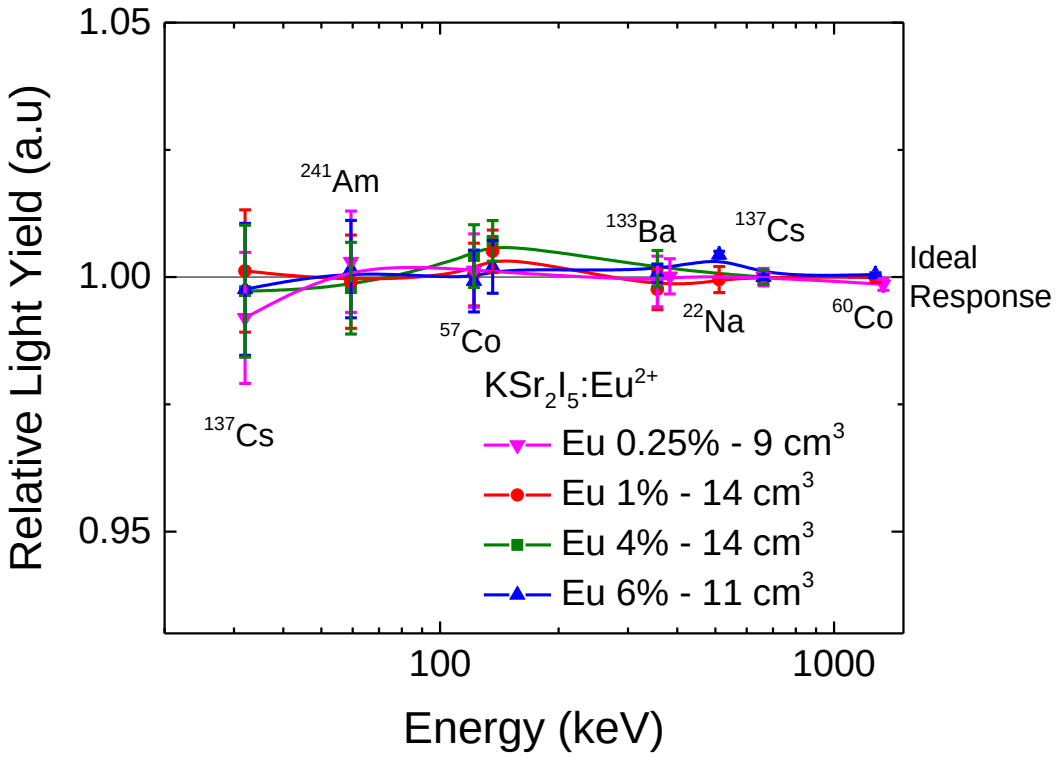

Figure 58. Non-proportional response from each of Eu^{2+} concentration grown; all crystals had a nearly flat response independent of europium concentration.

Table 17. Summary of the scintillation properties of 9 cm^3 KSI:Eu 0.25%, 14 cm^3 KSI:Eu 1%, KSI:Eu 2%, KSI:Eu 4% and 11 cm^3 - KSI:Eu 6%.

Eu^{2+} conc.	*Vol. (cm^3)*	*LY (ph/MeV)*	*ER at 662 keV*	*ER at 122 keV*	*ER at 59.4 keV*	*Scint. Decay time (µs)*
0.25%	9	62,500	3.7	7.1	10.9	1.32 (90%), 6.8
1%	14	70,100	3.6	6.4	9.1	1.51 (85%), 11.7
2%	14	75,700	3.4	6.5	8.8	1.62 (86%), 12.8
4%	14	77,900	3.2	6.0	8.3	1.78 (86%), 13.5
$^{+}$6%	11	78,200	3.4	6.1	8.5	2.29 (86%), 17.4

+Grown at 0.8 mm/h

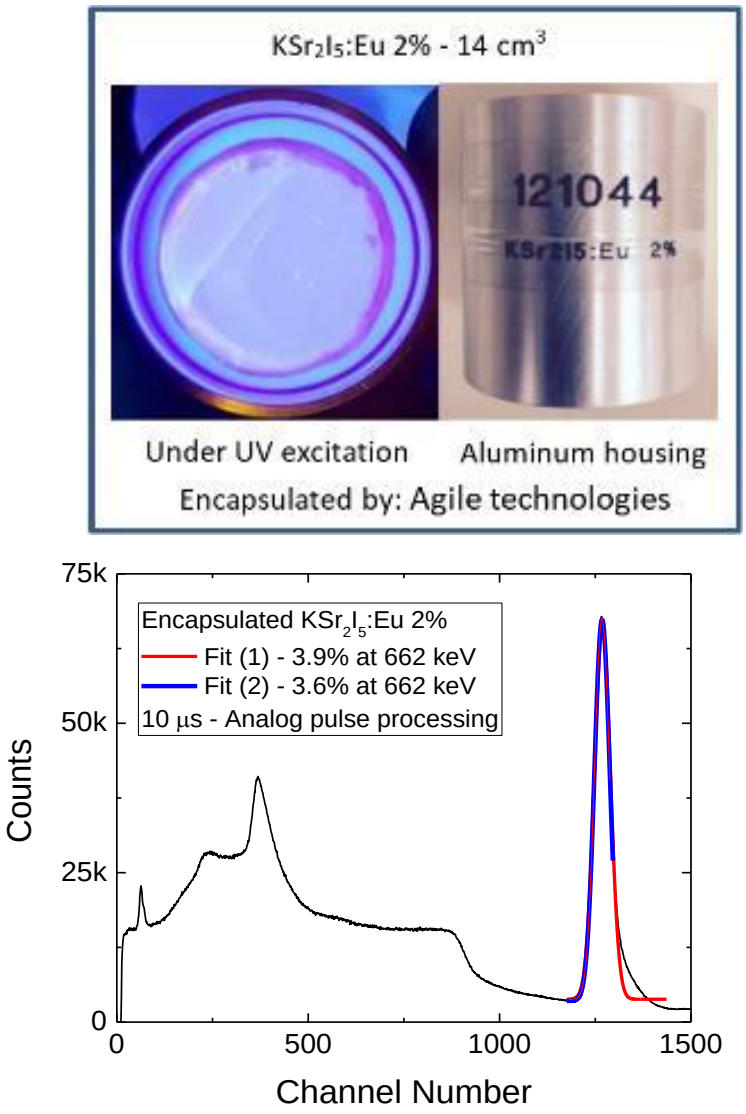

Figure 59a. The 14 cm^3 crystal of KSI:Eu 2% encapsulated in an aluminum housing. (b) The ^{137}Cs spectrum with an energy resolution between 3.6 % - Gaussian fit shown in blue, and 3.9% - Gaussian peak shown in red. The Gaussian fit shown in red includes most of the asymmetry of the full energy peak produced by self-absorption on the energy resolution, while Gaussian fit shown in blue excludes these effects.

rates than typically used for other metal halide scintillators without compromising the performance. The crystal yield was significantly increased by replacing the typical quartz ampoules with carbon coated quartz ampoules. As a result, several crack free Ø 1" boules of KSr_2I_5 with varying Eu^{2+} concentrations were grown, including a Ø 1" × 6" boule.

The volumetric dependencies of the light yield, energy resolution and decay time were evaluated for KSr_2I_5:Eu 2%. The light yield decreased from 87,900 ph/MeV to 73,200 ph/MeV and the energy resolution increased from 2.9% to 3.8% at 662 keV, as the volume increased from 0.012 cm^3 to 18 cm^3. High energy tailing was observed in the ^{137}Cs spectra of the 14 cm^3 and 18 cm^3 crystals.

The scintillation properties were also evaluated for a 9 cm^3 of KSI:0.25%, 14 cm^3 of KSI:Eu 1%, KSI:Eu 2%, KSI:Eu 4% and 11 cm^3 of KSI:Eu 6%. The light yield steadily increased with Eu^{2+} concentration from 62,500 ph/MeV to 78,200 ph/MeV, while the best energy resolutions at 662 keV were 3.2% for KSI:Eu 4% and 3.4% for KSI:Eu 2% and KSI:Eu 6%. The initial version of a hermetic package was developed and the performance of the sealed crystal is promising.

Future work will focus on studying the effects of the intrinsic radioactivity produced by ^{40}K on crystals of appreciable sizes (≥ 1 in^3) for national security applications.

Chapter 7
Characterization of Large-Volume $KSr_2I_5:Eu^{2+}$ Scintillators

Abstract

In this work we present the crystal growth and characterization of large $KSr_2I_5:Eu^{2+}$ (KSI:Eu) single crystals. High quality, Ø 1 × 6 inch long boules of KSI:Eu 2.5% and KSI:Eu 4% were grown in carbon coated quartz ampoules via the vertical Bridgman technique using pulling rates of 3 and 5 mm/h. Multiple characterization techniques were used to evaluate the scintillation properties and the non-uniformities of the light collection of crystals with volumes ranging from 12.5 to 60 cm^3. At 60 cm^3, KSI:Eu 2.5% had a light yield of 53,500 ph/MeV with an energy resolution of 5.1% at 662 keV, and KSI:Eu 4% had 40,300 ph/MeV with an energy resolution of 4.6% at 662 keV. Four 12.5 cm^3 specimens were prepared from each boule. The specimens obtained from KSI:Eu 4% had a light yield that ranged from 70,400 to 82,100 ph/MeV, with an energy resolution that ranged from 3.1% to 3.5% at 662 keV, and the specimens obtained from KSI:Eu 2.5% had a light yield that varied from 69,500 ph/MeV to 77,200 ph/MeV, with an energy resolution that ranged only from 3.4 to 3.6% at 662 keV.

7.1. Introduction

Scintillator-based radiation detectors have broad applications in today's world. Scintillator materials are often developed to match the requirements for a specific application. Radiation-detection technology used for nonproliferation and national security applications, e.g. hand-held gamma ray spectrometers, requires low-cost scintillator materials with excellent capabilities to accurately search for, locate and discriminate illicit radioactive materials from legitimate radionuclides [8, 32]. For such applications, scintillator crystals between 12 and 100 cm^3 in volume are often required. In the last two decades, several new scintillator materials from the halide family have been introduced as potential radiation detectors for national security applications. These materials have high light yields and excellent energy resolutions, approaching the fundamental limits of scintillators [6, 9, 15, 18, 23, 29, 31, 36, 45, 72]. Scintillators such as SrI_2:Eu, $CeBr_3$ and $LaBr_3$:Ce are the most

promising radiation detectors for national security applications, but due to their high production cost NaI:Tl is still preferred because it offers an acceptable energy resolution at a much lower cost.

In 2013, Eu^{2+}-doped potassium strontium iodide was introduced to the scintillator community. Its ease of growth and excellent scintillation properties made KSr_2I_5:Eu (KSI:Eu) a promising scintillator material that could potentially be used as a radiation detector for national security applications [15, 90]. High quality single crystals of KSI:Eu can be grown using a wide variety of parameters, including pulling rates up to 10 times faster than those typically used for other high-performing halide scintillators [25, 28, 43, 65, 91]. Although these results were promising for small scale laboratory experiments, producing one detector per growth run is not a cost-effective process for large-scale manufacturing and wide spread utilization. Thus, for this work we focused our efforts on optimizing the growth procedure to produce more detectors per boule, per growth run at a faster rate and we present the rapid crystal growth of two Ø 1inch × 6 inch long single crystal boules of KSI:Eu and their characterization.

7.2. Experimental Methods

7.2.1. Crystal Growth

Single crystal boules of KSr_2I_5:Eu 2.5% and KSr_2I_5:Eu 4% were grown via the vertical Bridgman technique. The anhydrous 99.999% pure beads of KI and EuI_2 and 99.995% pure beads of SrI_2 from APL Engineered Materials Inc. were loaded in stoichiometric quantities into a Ø 25 mm carbon coated quartz ampoule inside an Mbraun glovebox with <0.01 ppm moisture and oxygen levels [25, 74-78]. The loaded ampoule was transferred to a vacuum system, where the growth charge was dried at 200 ^oC for 12 hours using a single zone furnace, and then sealed at 10^{-6} torr using an oxyhydrogen torch. To homogenize the growth charge, a mixing step was carried out by melting the raw materials at 740 ^oC for 12 hours. The boules were grown using a 24-zone electro dynamic gradient (EDG) Mellen furnace in

which a one-inch diaphragm was placed between the hot zone and cool zone to achieve a thermal gradient of 55 °C/cm [83, 84]. The growth process was initiated above the diaphragm and self-seeding took place in a 2 mm diameter × 25 mm long grain selector connected to the bottom of the ampoule. A pulling rate of 3 and 5 mm/h and cooling time of 53 and 40 hours were used for KSI:Eu 2.5% and KSI:Eu 4%, respectively.

The single crystal boules were cut to size using a low-speed wire saw and lapped by hand using silicon carbide polishing pads with Buehler AutoMet™ low viscosity lapping oil inside a glovebox. Specimens ranging from 12.5 to 60 cm^3 in volume were prepared to evaluate the scintillation properties of the grown crystals. A detailed description of the crystals' dimensions is shown in Table 18.Since the scintillation characterization took place outside the glovebox, the specimens were placed inside a quartz container filled with mineral oil to protect them from moisture during the measurements. To ensure the light collection, the quartz container holding the crystal was wrapped with several layers of Teflon.

7.2.2. Characterization

The scintillation properties were measured using a variety of techniques. The light yield (LY), energy resolution (ER) and the non-proportionality (nPR) were measured using an analog signal processing chain consisting of a Hamamatsu photomultiplier tube, a Canberra model 2005 pre-amplifier, an Ortec 672 amplifier set to 10 μs shaping time, and a Tukan 8K multi-channel analyzer. The light yield in photons per MeV at 662 keV was measured using the single photo-electron technique with a QE calibrated R2059 photomultiplier tube (PMT) [92, 93]. The energy resolution and the scintillation light yield non-proportionality were measured with a Hamamatsu R6231-100 PMT using 10 μCi sealed sources of ^{137}Cs, ^{22}Na ^{133}Ba, ^{57}Co and ^{241}Am. The energy resolution was defined as the Full Width Half Maximum over the centroid of the photopeak of energy E (R=ΔE(FWHM)/E [55]). The nPR or relative light yield was defined as the ratio

Table 18. Dimensions of the crystals prepared for this work

Diameter	2.5 cm			
Height	12 cm	7.6 cm	5.1 cm	2.54 cm
Volume	60 cm^3	37.5 cm^3	25 cm^3	12.5 cm^3

between centroid position of a photopeak of energy E and centroid position at 662 keV. The scintillation decay times (DT) were acquired using an Agilent Technologies digital oscilloscope (DSO6104A – 1GHz) connected directly to the R6231-100 PMT. Thousands of scintillation traces were averaged together and then fitted with a two-component exponential function. A ^{137}Cs gamma ray source was used. An illustration of the setup used for the measurements in this section is shown in Figure 60 – Left.

The non-uniformity of the light collection was evaluated by performing a volumetric study on KSI:Eu 2.5% and a collimation study on KSI:Eu 4%. The volumetric study was carried out by collecting pulse high spectra under ^{137}Cs irradiation using crystals that ranged from 12.5 cm^3 to 60 cm^3 in volume. For the collimation study, a ^{137}Cs source was placed behind two lead bricks with a 3-mm separation. The collimated beam was projected horizontally across the crystal. The pulse height spectra and decay time curves were acquired at each planar position, along the z-axis. The data was collected every 2.5 cm, starting at 1 cm above the PMT and finishing next to the seed section of the crystal at 11 cm, using a 60 cm^3 crystal. An illustration of the setup used for the collimation study is shown in Figure 60 – Right.

7.3. Results and Discussion

7.3.1. Crystal Growth

Excellent quality, nearly crack-free Ø 1 × 6 inch long single crystal boules of KSI:Eu 2.5% and KSI:Eu 4% were successfully grown via the vertical Bridgman technique using pulling rates up to 5 mm/h, as shown in Figure 61 and Figure 62 [91]. Note that increasing the pulling rate from 3 to 5 mm/h and decreasing the cooling time from 53 to 40 hours did not affect the quality of the boule. It is important to mention that some cracks developed during the multiple stages of sample preparation required to produce the desired detector sizes.

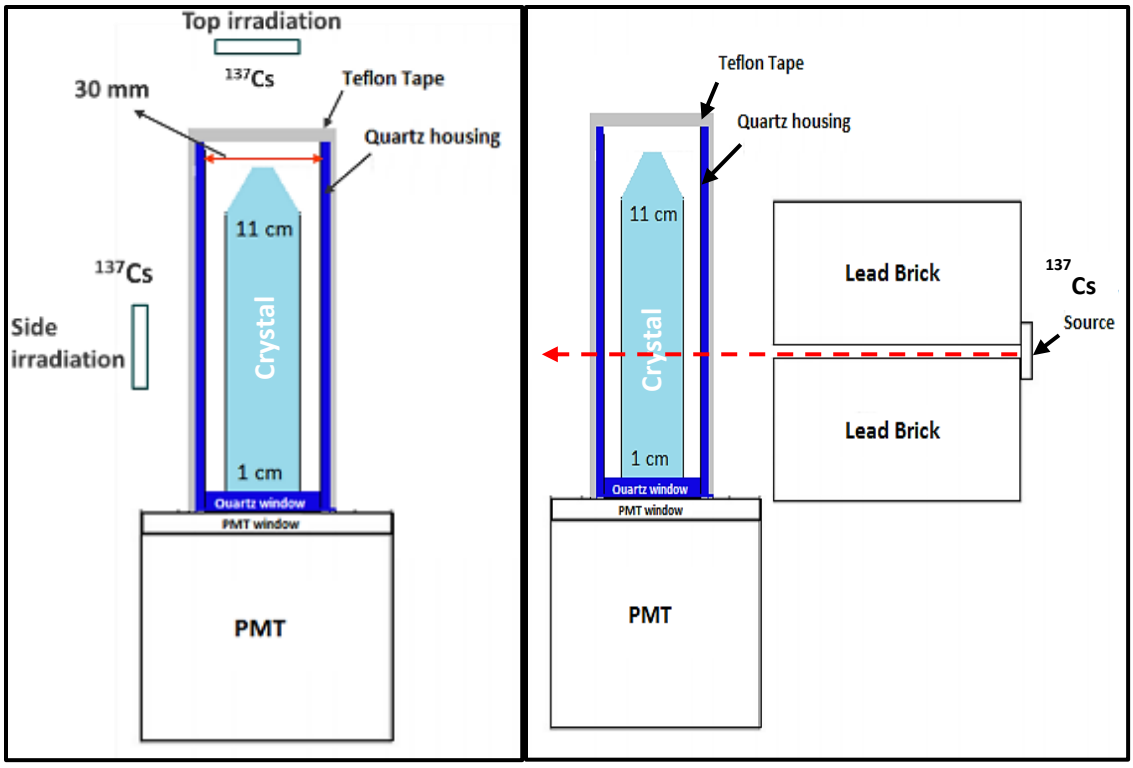

Figure 60. Diagram of the experimental setup and housing/crystal geometry used for the gamma ray spectroscopy measurements. On the left, setup used for LY, ER, nPR, and DT measurements and on the right, the setup used for the collimation study.

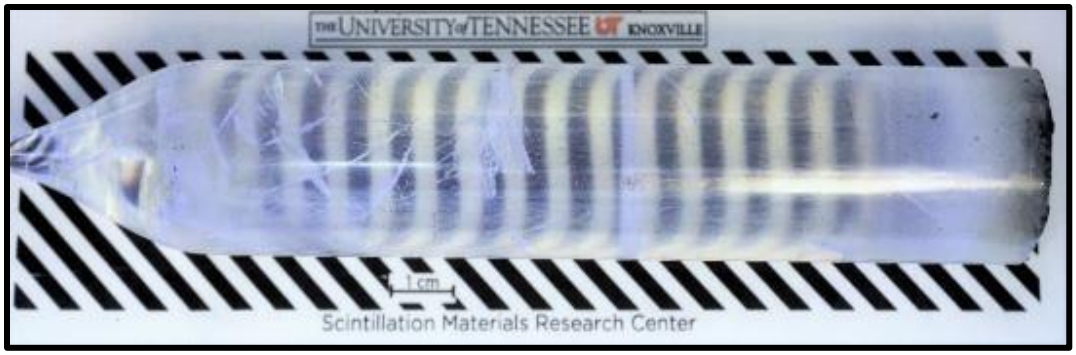

Figure 61. One inch diameter by six inch long single crystal of KSr_2I_5:Eu 2.5 %, under white fluorescent light.

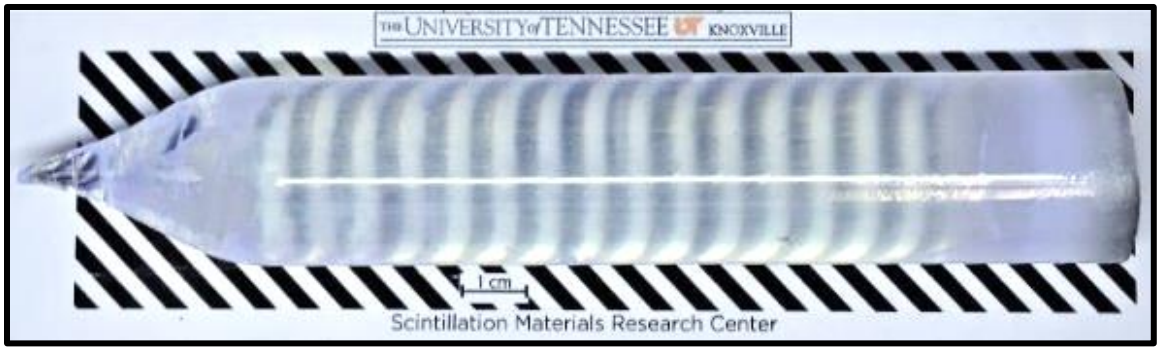

Figure 62. One inch diameter by six inch long single crystal of KSr_2I_5:Eu 4%, under white fluorescent light.

7.3.2. Scintillation Properties of 60 cm^3 crystals

The scintillation light yield, decay time, and non-proportionality of 60 cm^3 KSI:Eu^{2+} cylinders were evaluated to determine the overall performance of the grown boules. The ^{137}Cs spectra and the decay time curves were collected by placing the radiation source on the top and side of the specimen as shown in Figure 60 – Left. When irradiated from the top, KSI:Eu 2.5% had 53,500 ph/MeV with an energy resolution of 5.1% at 662 kev, and KSI:Eu 4% had 40,300 ph/MeV with an energy resolution of 4.6% at 662 keV, as shown in black in Figure 63a and b. Upon side irradiation, the energy resolution of both crystals deteriorated significantly, as shown in red in Figure 64a and b. These differences are due to changes in the light collection efficiency caused by non-uniform light pulses. Note that the mean free path of a 662 keV photon from a ^{137}Cs source is ≈ 3.3 cm. Thus, by placing the radiation source on the side, the entire crystal volume is irradiated. The scintillation decay time curves of KSI:Eu 2.5% and KSI:Eu 4% are shown in Figure 64a and b. The time profiles were fitted using a two-component exponential function. The primary component consisted of ~85% of the total emitted light with time constants of 2.61 μs for KSI:Eu 2.5% and 3.15 μs for KSI:Eu 4%. The remaining scintillation light was collected over 18 and 20 μs, respectively. Unlike the energy resolution, the decay time was not affected by the radiation source placement. The non-proportional response of both 60 cm^3 crystals was nearly flat, with a slight “halide hump” that deviated less than 2% from the ideal, as shown in Figure 65.

7.3.3. Volumetric and Collimation Study

Non–uniformity of the light collection in Eu^{2+} doped scintillators is caused by (1) optical absorption at the crystal’s surface, (2) light absorption and scattering due to impurities in the bulk of the crystal, and (3) self–absorption at the luminescence center Eu^{2+} [12, 30, 44, 94-96]. In this section, the non-uniformities of the light

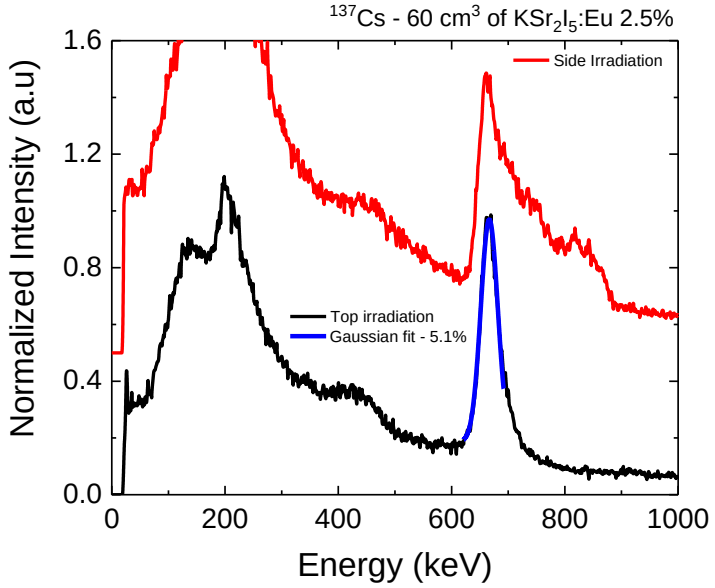

a.

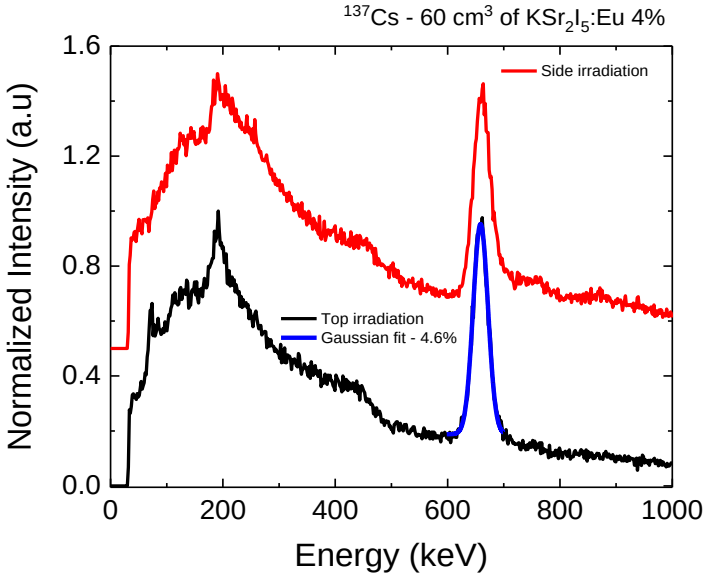

b.

Figure 63a. ^{137}Cs spectra of 60 cm^3 crystals of KSr_2I_5:Eu 2.5% and (b) KSr_2I_5:Eu 4%. The black spectra show the crystals' response when irradiated from the top and the red spectra show the crystals' response when irradiated from the side.

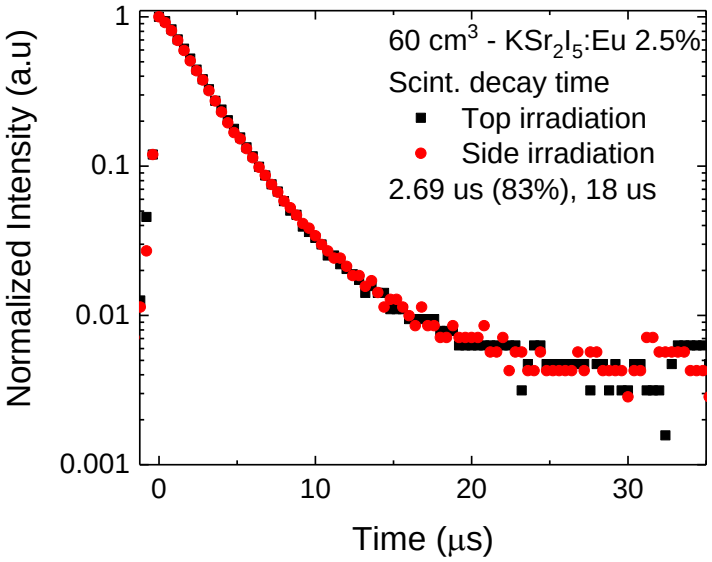

a.

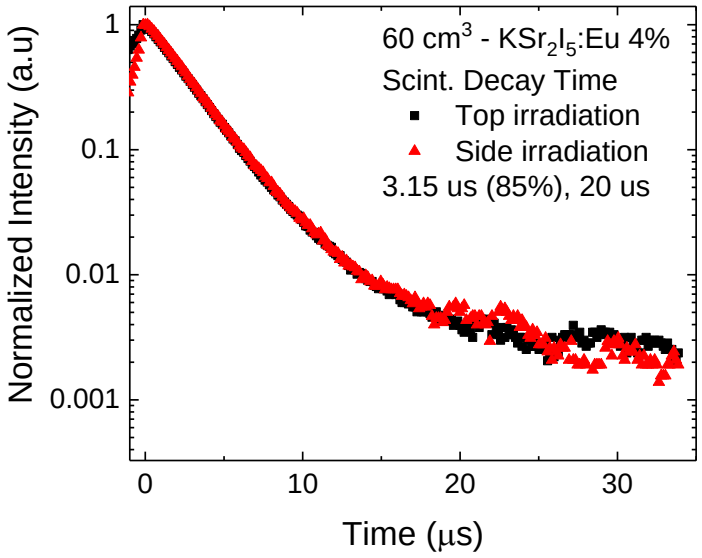

b.

Figure 64a. Scintillation decay time curves of 60 cm^3 crystals of KSr_2I_5:Eu 2.5% and (b) KSr_2I_5:Eu 4%. Top irradiation shown in black and the side irradiation shown in red.

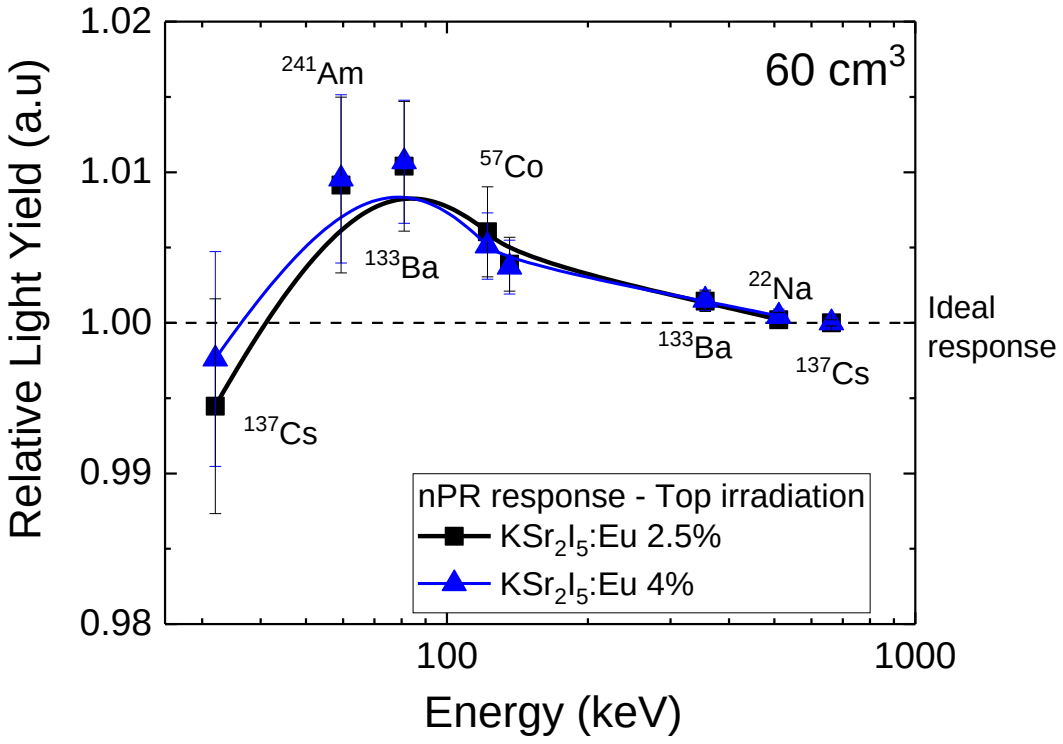

Figure 65. Non-proportional response of a 60 cm^3 specimen of KSr_2I_5:Eu 2.5% and KSr_2I_5:Eu 4%.

collection were investigated by performing a volumetric study on KSr_2I_5:Eu 2.5% and a collimation study on KSr_2I_5:Eu 4%.

The volumetric effects in the light yield and energy resolution were evaluated by measuring 60 cm^3, 37.5 cm^3, 25 cm^3 and 12.5 cm^3 cylindrical specimens of KSI:Eu 2.5%. The ^{137}Cs spectra and the volumetric trends of the light yield and energy resolution are shown in Figure 66. As expected, the performance of the crystal improved as the light path length decreased. The light yield and energy resolution of KSI:Eu 2.5% improved by ~30% from 53,500 ph/MeV and 5.1% to 76,900 ph/MeV and 3.4 % at 662 keV as the volume decreased from 60 cm^3 (12 cm in length) to 12.5 cm^3 (2.5 cm in length).

For KSr_2I_5:Eu 4%, the pulse height spectra and decay time were collected along the z-axis, starting 1 cm above the PMT and finishing 11 cm away from the PMT. ^{137}Cs spectra and decay curves are shown in Figure 67. The light yield increased as the collimated beam was moved in the direction of the PMT, while the energy resolution improved as the collimated beam was moved away from the PMT. These trends are directly related to the photons' mean free path and their different probabilities of self-absorption at the Eu^{2+} centers. The number of photons collected, i.e. the measured light yield, is dictated by the path length travelled by the photons inside of the crystal prior to collection. Thus, as the light's path length decreases, the light yield increases. In contrast, the energy resolution is affected by the variations in the path lengths of the collected photons. Note that similar energy resolution deterioration was observed for the 60 cm^3 crystals by moving the radiation source from the top to the side of boule. Also, similar dependencies of the light yield and energy resolution were observed by Sturm et al. with 24 cm^3 crystals of Eu^{2+} doped SrI_2 [12, 95].

As for the scintillation decay time measurements, no clear trend was observed upon irradiation position along the z-axis. This is likely because the decay curves were obtained by averaging several thousands of traces together rather than by analysis of individual traces. Also, the fact that KSI:Eu has a multicomponent

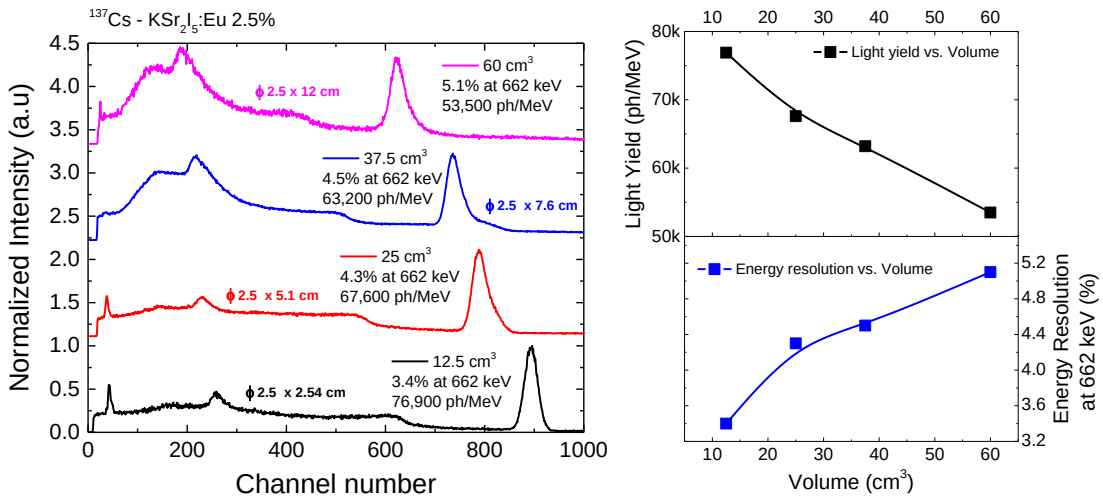

Figure 66. Right - ^{137}Cs spectra of KSr_2I_5:Eu 2.5% measured at different volumes. Left - Volumetric trends for the light yield (black curve) and energy resolution (blue curve).

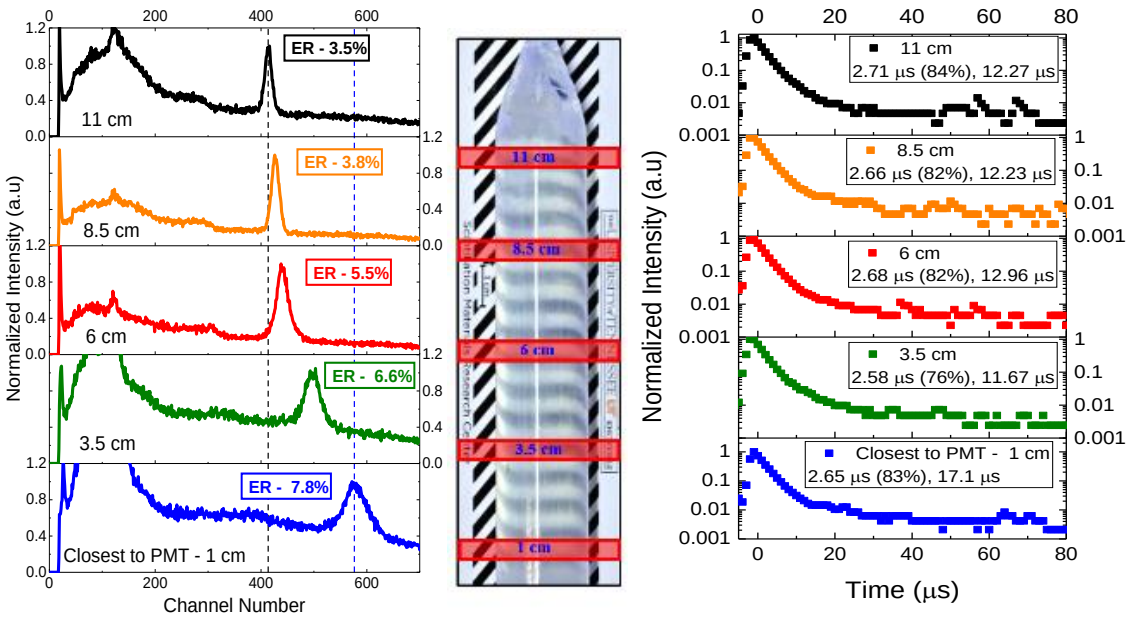

Figure 67. Collimated study of a 60 cm^3 of KSI:Eu 4%, using ^{137}Cs source as an excitation source. ^{137}Cs spectra are shown on the left and the scintillation decay times are shown on the right; 3-mm thick areas are marked on the boule where gamma-rays are impinging, shown in the middle.

exponential decay contributes to the complexity of the analysis of the scintillation pulse, since slight changes in their component distribution could partially mask the decay constant lengthening produced by self-absorption and other defects.

7.3.4. Light Yield and Energy Resolution of 12.5 cm^3 Crystals

In this section, the light yield and energy resolution under ^{137}Cs irradiation of eight 12.5 cm^3 cylindrical detectors (four individual detectors cut from each boule) were measured. The detectors obtained from KSI:Eu 2.5% showed a variation of ~11% in the light yield, ranging from 69,500 ph/MeV to 77,200 ph/MeV with an energy resolution that only ranged from 3.4% to 3.6% at 662 keV, as shown in Figure 68. The detectors obtained from KSI:Eu 4% showed a slightly higher variation on both the light yield and energy resolution. The light yield ranged from 70,400 ph/MeV to 82,100 ph/MeV (~14%), while energy resolution ranged from 3.1% to 3.5% at 662 keV, as shown Figure 69.

7.4. Summary

Excellent quality, high-performance Ø 1 × 6” long scintillator crystals of KSI:Eu 2.5% and KSI:Eu 4% were successfully grown via the vertical Bridgman technique using pulling rates of 3 and 5 mm/h. At 60 cm^3, KSI:Eu 2.5% had 53,500 ph/MeV with an energy resolution 5.1%, and KSI:Eu 4% had 40,300 ph/MeV with an energy resolution of 4.6% at 662 keV. In detectors of this size, most non-uniformities in the light collection of KSI:Eu^{2+} are caused by scintillation photons having different probabilities of self-absorption, where the light yield (ph/MeV) is affected by the photons’ path length and the energy resolution is affected by the path length variations of the collected photons. Thus, the reduction of the light yield and variation of the energy resolution observed with increasing volume are mostly due to the re-absorption and re-emission of light at the luminescence center, which is an intrinsic property of Eu^{2+}.

We were able to obtain four 12.5 cm^3 specimens from each of the boules grown for this work. The detectors obtained from KSI:Eu 2.5% had light yield that

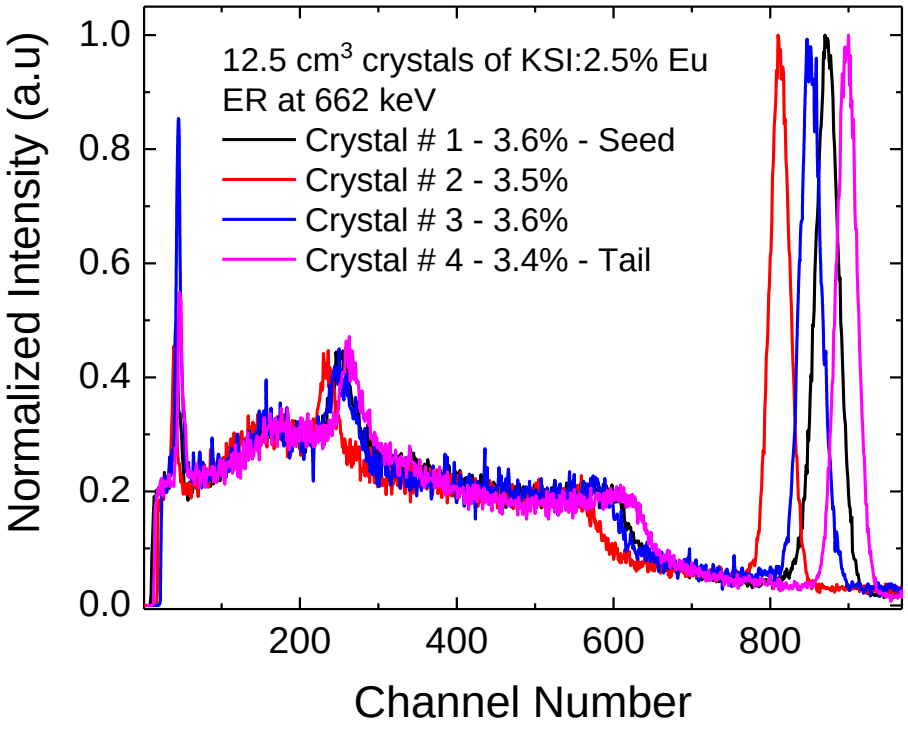

Figure 68. ^{137}Cs spectra of four 12.5 cm^3 crystals obtained from a one inch diameter by six inch long boule of KSr_2I_5:Eu 2.5%.

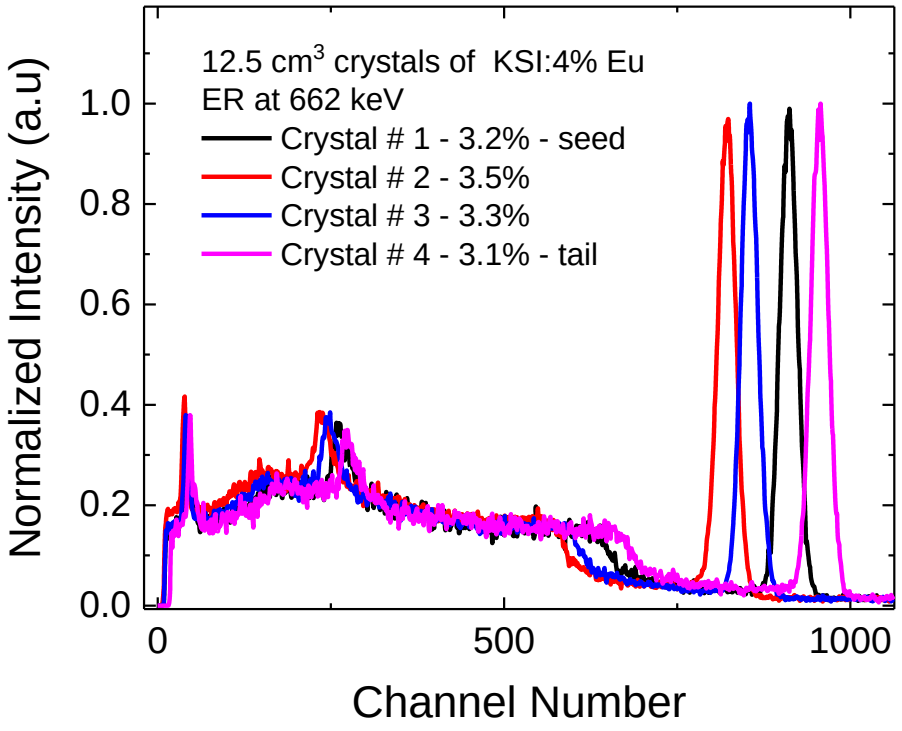

Figure 69. ^{137}Cs spectra of four 12.5 cm^3 crystals obtained from a one inch diameter by six inch long boule of KSr_2I_5:Eu 4%.

ranged from 69,500 ph/MeV to 77,200 ph/MeV while the energy resolution had less variation, only ranging from 3.4% to 3.6% at 662 keV and the detectors obtained from KSI:Eu 4% had light yield that ranged from 70,400 ph/MeV to 82,100 ph/MeV with an energy resolution range from 3.1% to 3.5% at 662 keV.

Chapter 8
Crystal Growth and Scintillation Characterization of High Performing $KSr_2Br_xI_{(5-x)}:Eu^{2+}$ and $KSr_{1.3}Ba_{0.7}I_5:Eu^{2+}$ Solid Solutions

Abstract

For this work we investigated anion and cation substitution to enhance the light yield and energy resolution of KSr_2I_5:Eu. Transparent single crystals of solid solutions of $KSr_2Br_xI_{(5-x)}$:Eu 4% and $KSr_{1.30}Ba_{0.7}I_5$:Eu 4% were grown via the vertical Bridgman technique using a two-zone transparent furnace. The scintillation properties of the mixed compounds were investigated and compared to the unmixed compound using a wide variety of techniques. We found that: (1) replacing some of the matrix iodine atoms in KSr_2I_5:Eu with bromine increased the light yield by 10% while maintaining similar energy resolution. The highest light yield was measured for $KSr_2Br_{0.10}I_{4.90}$:Eu 4% with 97,900 ph/MeV and 3.0% at 662 keV. The addition of bromine blue-shifted the x-ray excited emission from 450 to 446 nm, increased the light yield by ~11% and decreased the scintillation decay time by suppressing its secondary component (≥ 3μs - 15%), while maintaining energy resolution comparable to the unmixed crystal. Thermoluminescence glow curves showed that the addition of bromine modified the shallow trap configuration located between 25 K and 55 K, suggesting that these traps are responsible for the decay time lengthening in KSr_2I_5:Eu. In large sizes (10.3 cm^3), $KSr_2Br_{0.10}I_{4.90}$:Eu 2% had a light yield of 79,000 ph/MeV and energy resolution of 3.2% at 662 keV, while KSr_2BrI_4:Eu 2% had light yield of 62,800 ph/MeV and 3.8% energy resolution at 662 keV. (2) The addition of barium increased the light yield and improved the energy resolution. The light yield increased from 84,000 to 120,000 ph/MeV and the energy resolution improved from 3.0% to 2.3% for a 1 cm^3 sample.

8.1. Introduction

In recent years, several metal halide scintillators from the AB_2X_5:Eu^{2+} (where A = alkaline metals, B = alkaline earth metals, and X= one or more halides) compositional family have been studied due to their excellent scintillation properties [15, 29, 31, 49, 65, 87, 97]. These scintillators have been reported to have light yields up to 100,000 ph/MeV and energy resolutions as low as 2.3% at 662 keV,

making them promising for national security applications where scintillators with high light yields and excellent energy resolutions are required to provide identification and discrimination of potential threats from non-threat radioactive sources [32].

Techniques such as codoping and compositional engineering have shown to be a promising method of enhancing the properties of scintillator materials. The compositional engineering approach has been successfully used to improve the scintillation properties of many oxide and metal halide scintillators. In garnet scintillators such as $(Y,Gd)_3(Ga,Al)_5O_{12}:Ce^{3+}$ and $(Lu,Gd)_3(Ga,Al)_5O_{12}:Ce^{3+}$, this technique improved the bulk performance of crystals by increasing the Stokes shift and by reducing the effects of shallow traps [98, 99]. For metal halide scintillators, the most promising results were obtained by forming solid solutions between BaI_2 and $BaBr_2$. The light yield of $BaBr_{(x)}I_{(2-x)}:Eu^{2+}$ improved by ~50% when compared to the unmixed compounds [29, 47, 100]. Other solid solutions such as $LaBr_{(3-x)}Cl_{(x)}:Ce^{3+}$, $LaBr_{(3-x)}I_{(x)}:Ce^{3+}$ and $CeBr_{(3-x)}Cl_{(x)}$ have also shown promising results [39, 101, 102].

The purpose of this study is to further enhance the scintillation properties of $KSr_2I_5:Eu^{2+}$ by forming solid solutions. In this work, we present the crystal growth and scintillation properties of $KSr_2Br_xI_{(5-x)}$:Eu 4% (where $0.05 \leq x \leq 1$) and $KSr_{1.3}Ba_{0.7}I_5$:Eu 4%.

8.2. Experimental

8.2.1. Crystal Growth

Single crystals of $KSr_2Br_xI_{(5-x)}$:Eu and $KSr_{1.3}Ba_{0.7}I_5$:Eu were grown via the vertical Bridgman technique. Due to the hygroscopic nature of the reactants and products of these experiments, handling took place inside an ultra-dry Mbraun glovebox with <0.01 ppm H_2O and O_2. Each charge was prepared with different ratios of bromine replacing iodine atoms in KSr_2I_5:Eu 4%. The source of bromine was KBr which replaced KI. Anhydrous 99.9% pure beads of KBr from Sigma

Aldrich, 99.995% pure beads of SrI_2, and 99.999% pure beads of KI and EuI_2 from APL Engineered Materials Inc. were mixed and loaded into quartz ampoules. The loaded ampoules were dried at 200^oC and sealed under a dynamic vacuum of 10^{-6} torr. Prior to the crystal growth experiments, a mixing step was carried out by melting the raw materials at 750 ^oC for 24 hours and then cooling to room temperature over a 10-hour period. The crystal growth experiments were carried out in a two-zone transparent furnace. A diaphragm was placed between the hot zone and cool zone to sharpen the thermal gradient at the growth interface [83, 84]. The growth process was initiated at a grain selector connected to the bottom of the ampoule where the self-seeding process took place [103].

For the Br/I ration optimization experiments,15 mm diameter $KSr_2Br_xI_{(5-x.)}$:Eu 4% crystals (where x = 0.05, 0.10, 0.25, 0.50, 0.75 and 1) were grown, and from these experiments $KSr_2Br_{0.10}I_{4.90}$:Eu 2% and KSr_2BrI_4:Eu 2% were selected to be grown at 22 mm diameter. The europium concentration was reduced from 4 to 2 molar % to decrease self-absorption effects. Note that the europium and bromine concentrations mentioned in the text are the nominal concentration in the melt. Table 19 shows in detail the growth parameters used in this work.

For the cation substitution experiments, we grew Ø 7 mm single crystals of $KSr_{1.3}Ba_{0.7}I_5$:Eu 2%, $KSr_{1.3}Ba_{0.7}I_5$:Eu 4%, and $KSr_{1.3}Ba_{0.7}I_5$:Eu 6% and a Ø 15 mm single crystal of $KSr_{1.3}Ba_{0.7}I_5$:Eu 4%.

Small 0.125 cm^3 (0.5 $\times$ 0.5 $\times$ 0.5 cm) specimens were cut using a low speed wire saw and lapped by hand using 600, 800 and 1200 grit silicon carbide polishing pads with Buehler AutoMet™ low viscosity lapping oil. To avoid inconsistencies in the characterization results all specimens were prepared from the same axial position in the boule, and during the measurements were placed inside a quartz container filled with mineral oil to protect them from moisture.

Various techniques were used to characterize the optical and scintillation

Table 19. Parameters used for the crystal growth experiments.

Composition	*Diameter (mm)*	*Pulling rate (mm/h)*	*Gradient at diaphragm (°C/cm)*	*Cooldown (h)*
$KSr_2Br_xI_{(5-x)}$*:Eu 4%*	15	5	20	40
$KSr_2Br_{0.10}I_{4.90}$*:Eu 2%*	22	1	30	85
KSr_2BrI_4*:Eu 2%*	22	1	30	85

properties of these crystals. The radioluminescence (RL) measurements were done under continuous 30 keV X-ray irradiation using a CMX003 X-ray generator. The emission spectra were recorded in reflection mode with a 150-mm focal length monochromator over a 200 to 800 nm wavelength range. The steady state photoluminescence (PL) spectra were measured with a Horiba Jobin Yvon Fluorolog 3 Spectrofluorometer equipped with a Xe lamp and dual scanning monochromators. The PL lifetimes were measured using the time correlated single photon counting technique. A Horiba Jobin Yvon NanoLed with an emission wavelength of 370 nm and a pulse width of ~1 ns was used as an excitation source. The emission monochromator wavelength was set to monitor the respective Eu^{2+} emissions of $KSr_2Br_xI_{(5-x.)}$:Eu 4% crystals.

The pulse height spectra of a variety of sealed radioactive sources were collected using a standard bialkali Hamamatsu R2059 photomultiplier tube (PMT) or super bialkali R6231 - 100 PMT connected to a Canberra 2006 pre-amplifier, an Ortec 672 amplifier, and a Tukan 8K multi-channel analyzer. Since Eu^{2+} doped scintillators are known for having microsecond-long pulses, a shaping time of 10 μs was used. Several layers of Teflon and a hemispherical dome of Spectralon were used as reflectors. The absolute light yield in photons per MeV (ph/MeV) was measured via the single photoelectron technique using the R2059 - PMT. The number of photoelectrons per MeV of absorbed γ-ray energy (phe/MeV) was calculated from the centroid position of the 662 keV photopeak and the single photoelectron peak. The conversion from the number of measured phe/MeV to the number of ph/MeV emitted by the scintillator was calculated by convolving the quantum efficiency of the PMT as a function of wavelength (measured by the Hamamatsu PMT) with the X-ray excited emission spectrum of the sample [92, 93]. The energy resolution and the non-proportionality (nPR) of the crystals were measured using the R6231-100 PMT with a standard set of γ-ray sources (^{137}Cs, ^{22}Na, ^{133}Ba, ^{57}Co and ^{241}Am). The energy resolution was defined as the Full Width Half Maximum over the centroid of the photopeak of energy E (R=ΔE(FWHM)/E

[55]). The nPR or relative light yield was defined as the ratio between centroid position of a photopeak of energy E and centroid position at 662 keV.

The scintillation decay time was measured under ^{137}Cs irradiation. The decay curve consisted of several thousand traces of the scintillation pulse averaged together. Scintillation pulses were collected directly from the R6231-100 PMT using an Agilent Technologies digital oscilloscope (DSO6104A – 1GHz). The time constants were obtained by fitting an exponential function to the decay curves. Several layers of Teflon and a Spectralon dome were used as reflectors.

For the thermoluminescence measurements, a 0.125 cm^3 crystal was bonded to a copper sample holder using a two-part thermal epoxy (Epotek - H20E). The sample holder was attached to the cold finger from a DE202AE cryostat (Advance Research System, inc.) and placed under vacuum. While under 20 mTorr vacuum, the crystal was heated to 550 K to release the previously stored luminescence and then cooled down to 10 K, where the irradiation took place. The crystal was irradiated with X-rays (35 kV, 0.1 mA) for 15 min. The sample was heated at a rate of 0.15 K/s from 10 K to 550 K using a Lakeshore 331 temperature controller. The luminescence emitted from the crystal was collected using a R2059 PMT. The current signal from the PMT was transformed into a voltage signal using standard NIM electronics. A National Instruments 6002-E data acquisition card was used to digitize the signal and a LabVIEW-based program developed in-house was used to collect the desired curves. The luminescence signal arises from electrons that thermally escape from traps and migrate to luminescence centers. Peaks in the spectrum provide evidence of discrete trapping levels.

8.3. Results and Discussion

8.3.1. Optimization of Bromine to Iodine Ratio

8.3.1.1. Crystal Growth

Transparent Ø 15 mm single crystals of $KSr_2Br_xI_{(5-x)}$:Eu 4% (x = 0.05, 0.10, 0.25, 0.50, 0.75 and 1) were grown for the bromine optimization experiments, as

shown in Figure 70. As the bromine concentration increased, the amount of halide gas condensate between the crystals and the ampoule walls also increased, giving the crystals a translucence appearance. A similar effect has been observed in $KSr_2Br_5:Eu^{2+}$ [31]. It is worth noting that no trends between cracking and bromine concentration were observed.

8.3.1.2. Characterization of $KSr_2Br_xI_{(5-x)}$:Eu 4%

The luminescence properties of $KSr_2Br_xI_{(5-x)}$:Eu 4% are ascribed to the 5d - 4f radiative transition in Eu^{2+} [21, 22, 61, 62]. Both the x-ray excited emission and the photoluminescence emission/excitation of the solid solutions shifted to higher energy as the bromine concentration increased, as shown in Figure 71a and b. The RL and PL emission consisted of a single peak that shifted 5 nm, over the bromine concentrations studied [21, 100], and the photoluminescence excitation spectra consisted a broad region of poorly resolved bands from ~250 nm to ~430 nm.

All the Br – containing crystals had a slightly faster photoluminescence and scintillation decay response than the KSr_2I_5:Eu 4% reference crystal. The relationship between the photoluminescence and scintillation decay time constants and the bromine concentration is shown in Figure 72. The lifetime of the Eu^{2+} 5d1 excited state ranged from 0.80 to 0.95 μs, and a single exponential function provided a good fit to all lifetime curves. The scintillation decay time ranged from 0.95 to 1.1 μs. A two-component exponential function provided a good fit to the decay curves for the crystals that contained 0, 0.05 and 0.1 bromine concentrations (x). For all the other concentrations studied ($0.25 \leq x \leq 1$), a single component exponential function provided a good representation of the decay curve. Note that faster scintillation kinetics have also been observed in other mixed anion or cation inorganic scintillators [104].

It is well known that exponential processes dictate the population and depopulation of states, thus the luminescence intensity of a scintillation event can be described by the sum of exponential components [105]. In $KSr_2I_5:Eu^{2+}$, the

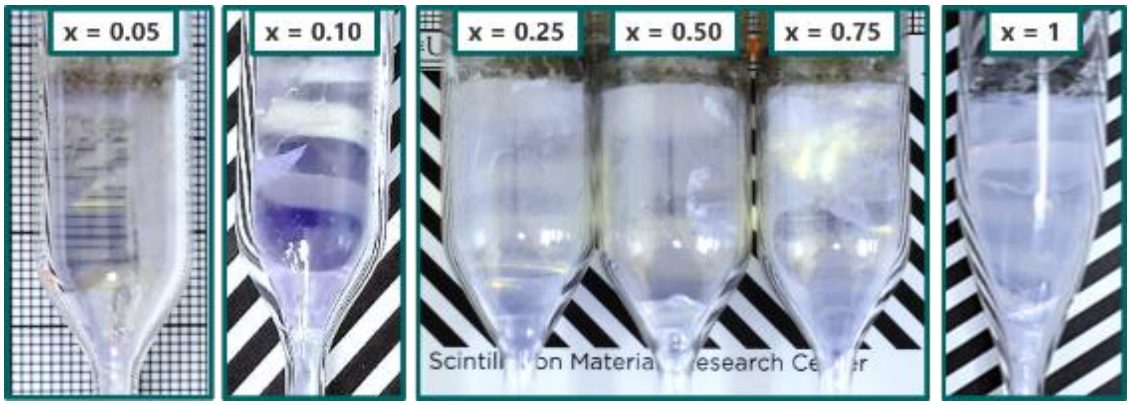

Figure 70. Ø 15 mm single crystals of $KSr_2Br_xI_{(5-x)}$:Eu 4% inside the ampoule, under white ambient light.

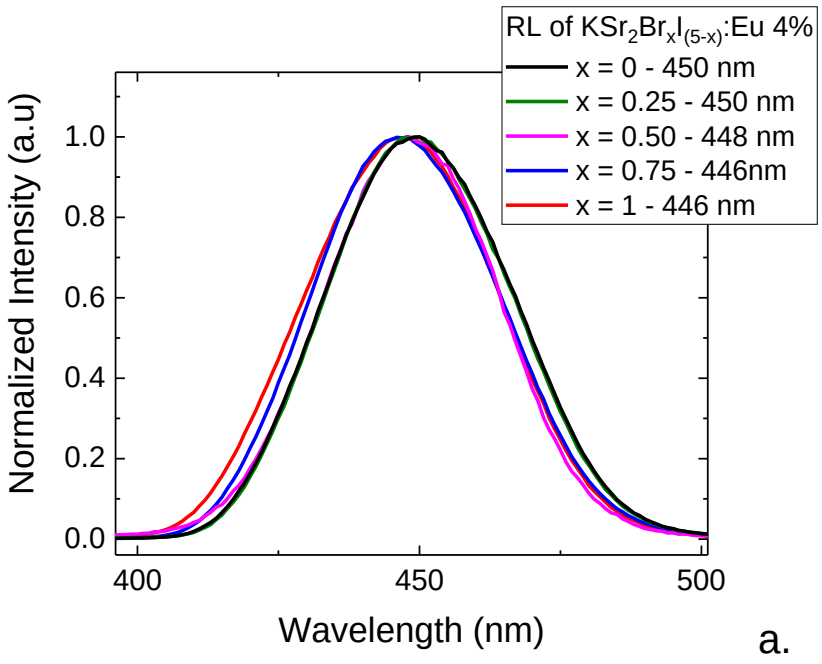

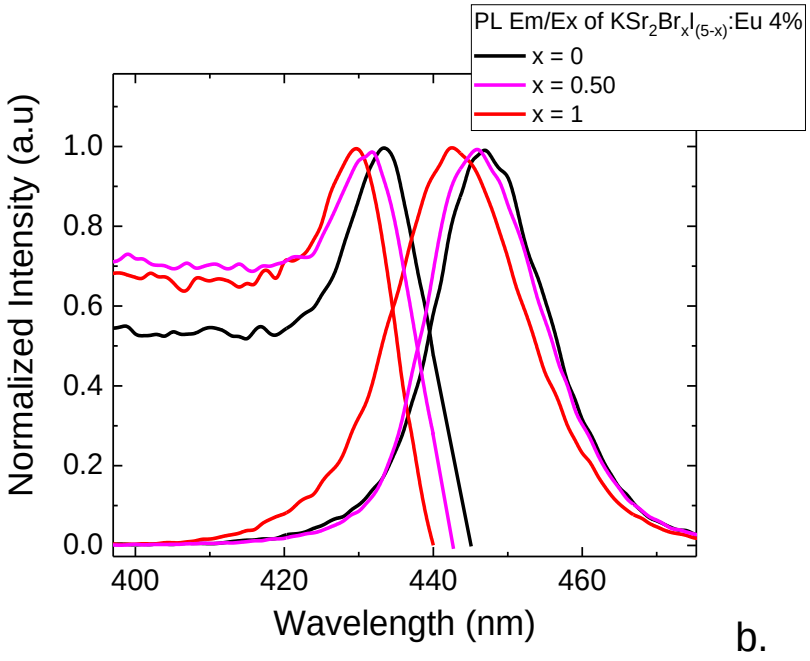

Figure 71a. X-ray excited emission and (b) photoluminescence emission and excitation spectra of $KSr_2Br_xI_{(5-x)}$:Eu 4%.

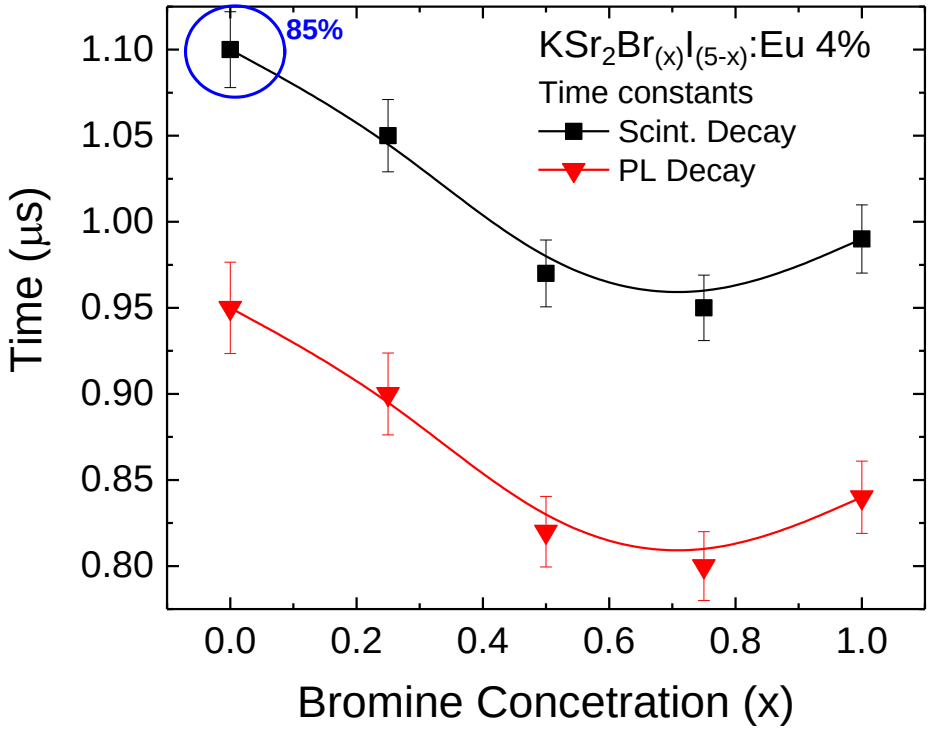

Figure 72. Scintillation and photoluminescence decay time constants versus bromine concentration (x). The scintillation decay time constants are shown by black squares; the blue circle indicates that the principal time consisted of 85% of the scintillation light. The PL decay constants are shown by the red triangles.

scintillation decay time consists of two exponential components with time constants of 1.06 μs (85%) and ≥ 3 μs. The origin of these components is determined by the lifetime of the lowest 5d state in Eu^{2+}, plus a short delay in the e-h recombination process caused by shallow electron traps. These traps are likely related to the iodine vacancies in the crystal [3, 80, 105-107]. The addition of bromine shortened the scintillation decay time by (1) shortening the lifetime of the Eu^{2+} [3] and (2) by altering the shallow trap configuration present between 25K and 55K, which is responsible for the scintillation decay time secondary component in KSI:Eu. Thermoluminescence glow curves of $KSr_2Br_xI_{(5-x)}$:Eu 4% are shown in Figure 73, where the dashed lines show the area of interest.

The light yield and energy resolution trends of 0.125 cm^3 $KSr_2Br_xI_{(5-x)}$:Eu 4% crystals are shown in Figure 5a and the ^{137}Cs spectra are shown in Figure 5b. $KSr_2Br_{0.10}I_{4.90}$:Eu 4% had the highest light yield of 97,900 ph/MeV and an energy resolution of 2.9% at 662 keV, whereas the lowest performing crystals KSr_2BrI_4:Eu 4% and KSr_2I_5:Eu 4% had a light yield of ~88,000 ph/MeV with an energy resolution 3.2% and 2.9% at 662 keV. The improvement in the light yield upon the addition of bromine is likely caused by an improved scintillation efficiency due to the reduction of the number of traps, increasing the number of electron-hole pairs reaching the luminescence centers [104, 108].

The non-proportional response curves of all crystals including the reference were very similar, as shown in Figure 75. The nPR curves had a “halide hump” at 81 keV that deviated 1% - 3% from the ideal response, seemingly increasing with the bromine concentration. More accurate techniques such as SLYNCI and K-dip spectroscopy would offer a better description of the non-proportional response of these scintillators [109-113]. However, we expect the observed trend to be correct since the addition of bromine suppressed the shallow traps which are known to improve the non-proportional response of scintillator materials [108, 113-119].

The best and worst performing composition, $KSr_2Br_{0.10}I_{4.90}$:Eu and KSr_2BrI_4:Eu, were selected to be grown at 22 mm diameter and further evaluate

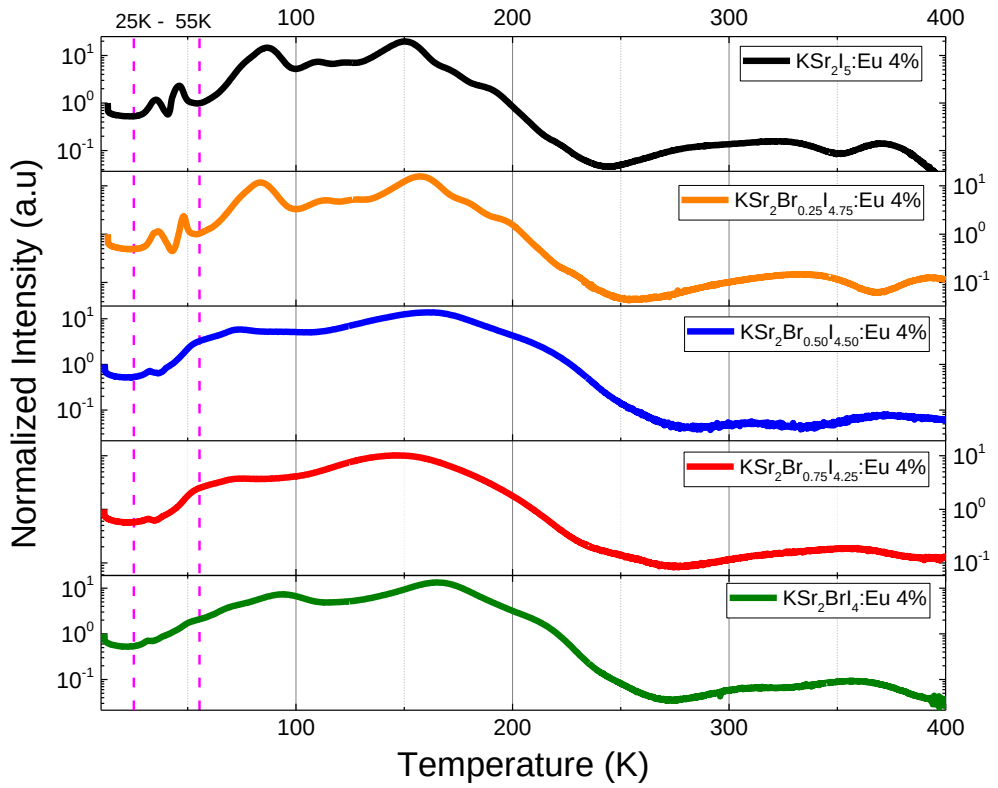

Figure 73. Thermoluminescence glow curves of KSr_2I_5:Eu, $KSr_2Br_{0.25}I_{4.75}$:Eu 4%, $KSr_2Br_{0.50}I_{4.50}$:Eu 4%, $KSr_2Br_{0.75}I_{4.25}$:Eu 4% and KSr_2BrI_4:Eu 4%. The curves are normalized to the steady state luminescence at 15 K.

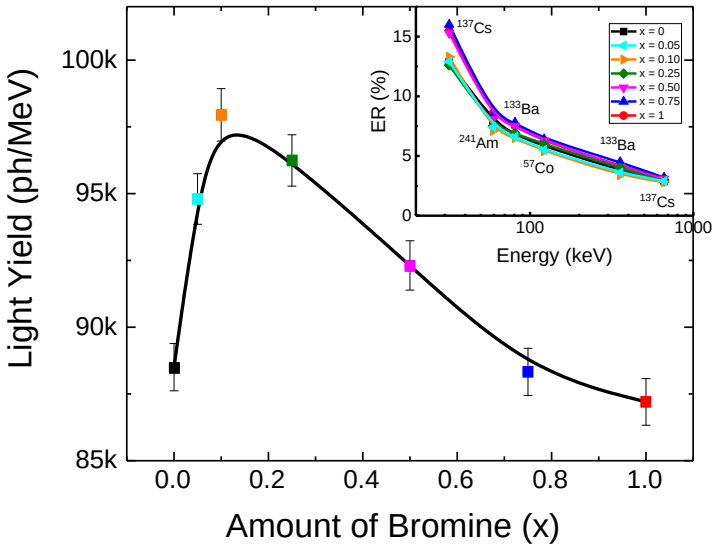

a.

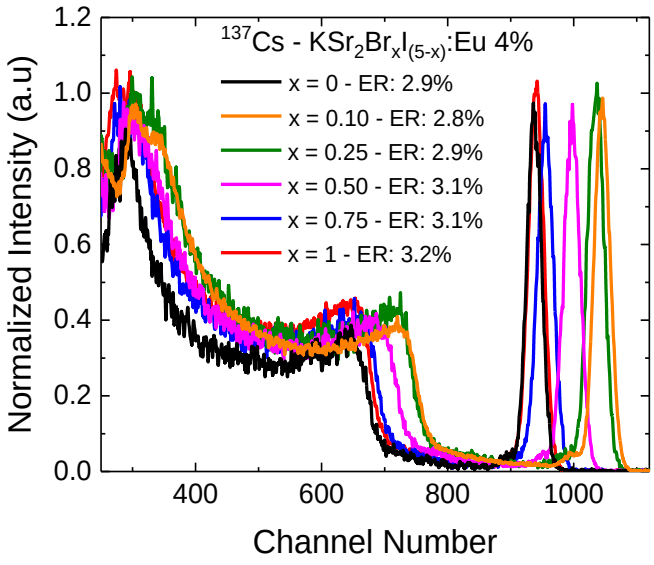

b.

Figure 74a. The light yield and energy resolution (shown in the inset) as a function of bromine concentration and (b) ^{137}Cs pulse height spectra of 0.125 cm^3 of $KSr_2Br_xI_{(5-x)}$:Eu 4%.

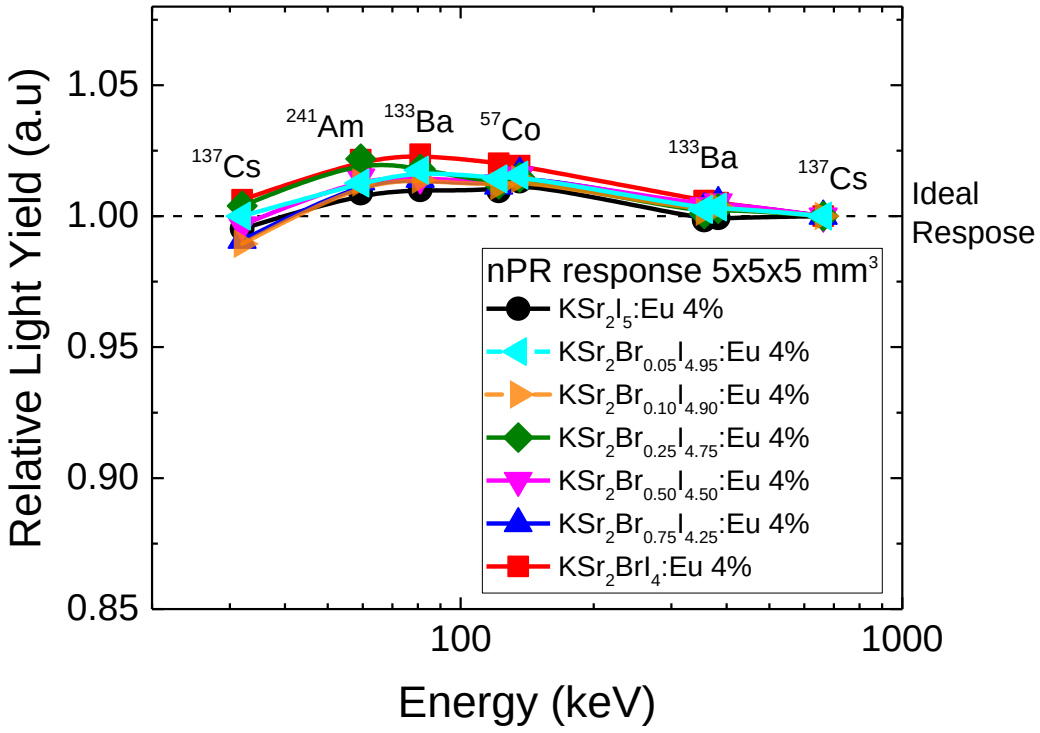

Figure 75. The light yield non-proportionality curves of 0.125 cm^3 specimens of $KSr_2Br_xI_{(5-x)}$:Eu 4%.

the scintillation properties at larger sizes.

8.3.2. Ø 22 mm of $KSr_2Br_{0.10}I_{4.90}$:Eu 2% and KSr_2BrI_4:Eu 2%

8.3.2.1. Growth of 22 mm Diameter Crystals

The results of the 22 mm diameter growth experiments were nearly crack free transparent single crystals of $KSr_2Br_{0.10}I_{4.90}$:Eu 2% and KSr_2BrI_4:Eu 2%, as shown in Figure 76 and Figure 77. The translucent appearance of KSr_2BrI_4:Eu 2% was caused by halide gas condensing between the crystal surface and the ampoule walls during the cooldown procedure. A similar effect was observed in the Ø15 mm $KSr_2Br_xI_{(5-x)}$:Eu crystals for the $x \geq 25$ crystals, shown in Figure 68. Also, note that a lower Eu^{2+} concentration (2%) was used for these crystals to minimize self-absorption.

8.3.2.2. Scintillation Properties of 10.3 cm^3 Crystals

Excellent scintillation properties were measured using Ø 2.2 cm by 2.6 cm tall (10.3 cm^3) cylinders of $KSr_2Br_{0.10}I_{4.90}$:Eu 2% and KSr_2BrI_4:Eu 2%. The ^{137}Cs pulse height spectra and the energy resolution at various gamma-ray energies are shown in Figure 78a and b. As expected, $KSr_2Br_{0.10}I_{4.90}$:Eu 2% performed better than KSr_2BrI_4:Eu 2% with a light yield of 79,000 ph/MeV and 3.2% energy resolution at 662 keV, while KSr_2BrI_4:Eu 2% had 62,800 ph/MeV and 3.8% energy resolution at 662 keV. At 10.3 cm^3, $KSr_2Br_{0.10}I_{4.90}$:Eu performance is marginally better compared to KSr_2I_5:Eu [65, 120]. The relative light yield measured as a function of absorbed γ-ray energy is shown in Figure 79. Both crystals had a nearly flat proportional response with a slight “halide hump” that deviated less than 3% from the ideal, reaching its maximum at 81 keV [112, 121]. The scintillation decay time curves of both crystals are shown in Figure 80. A two-component exponential function with time constants of 1.81 μs (85%) and 12.6 μs provided a good fit to the decay curve of $KSr_2Br_{0.10}I_{4.90}$:Eu 2%, and a single component exponential function with a time constant of 1.64 μs provided a good fit to the decay curve of KSr_2BrI_4:Eu 2%.

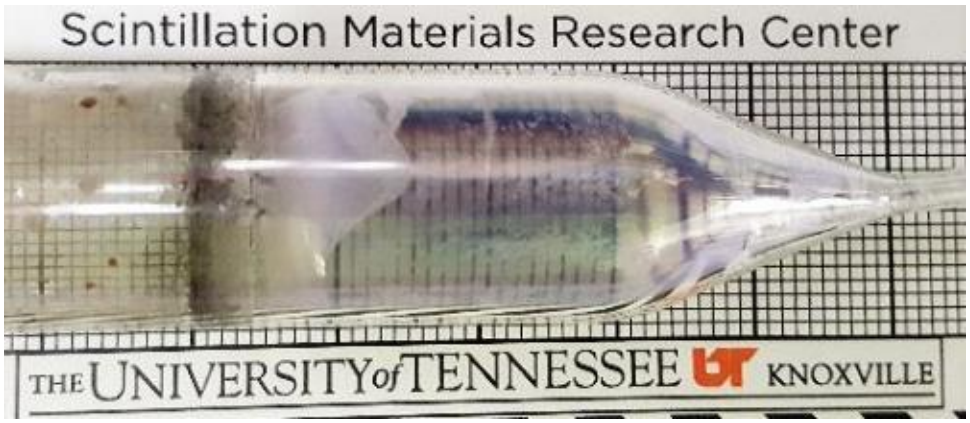

Figure 76. 22 mm diameter single crystal of $KSr_2Br_{0.10}I_{4.90}$:Eu 2% in the ampoule under white fluorescent light.

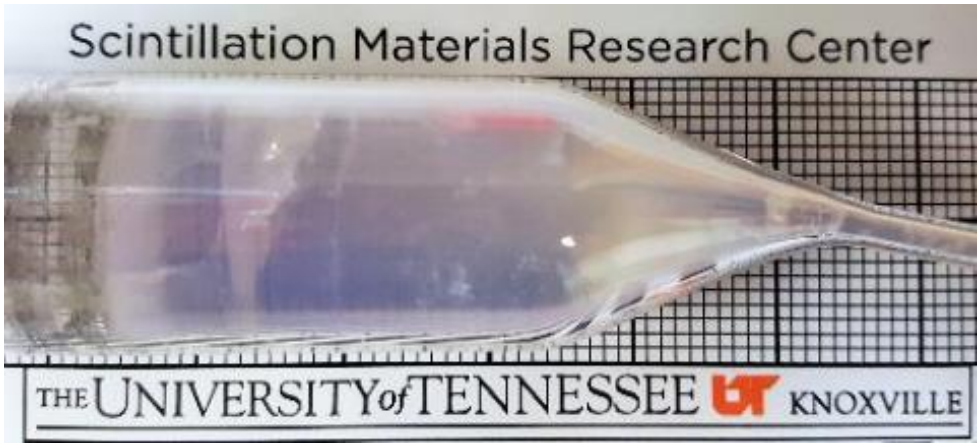

Figure 77. 22 mm diameter single crystal of KSr_2BrI_4:Eu 2% in the ampoule under white fluorescent light.

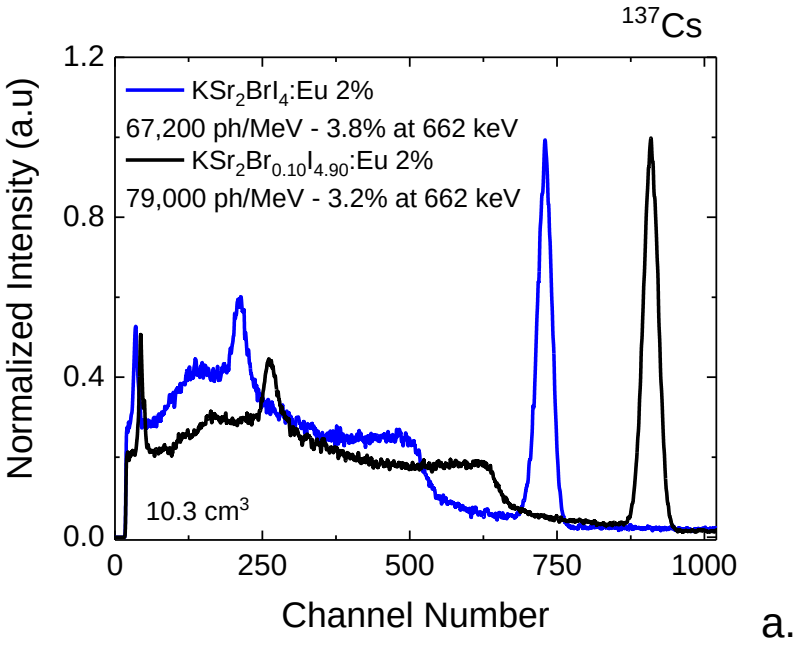

a.

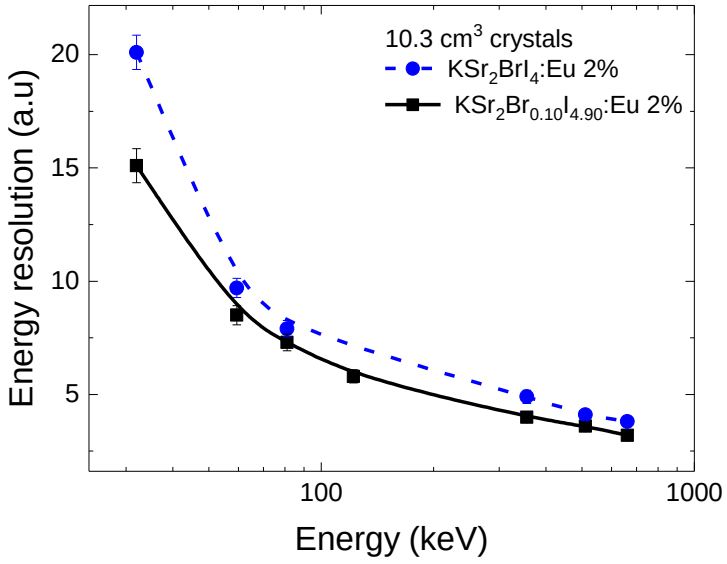

b.

Figure 78a. Pulse height spectra under ^{137}Cs excitation and (b) Energy resolution at various γ-ray excitation energies measured for 10.3 cm^3 specimens of KSr_2BrI_4:Eu 2% and $KSr_2Br_{0.10}I_{4.90}$:Eu 2%.

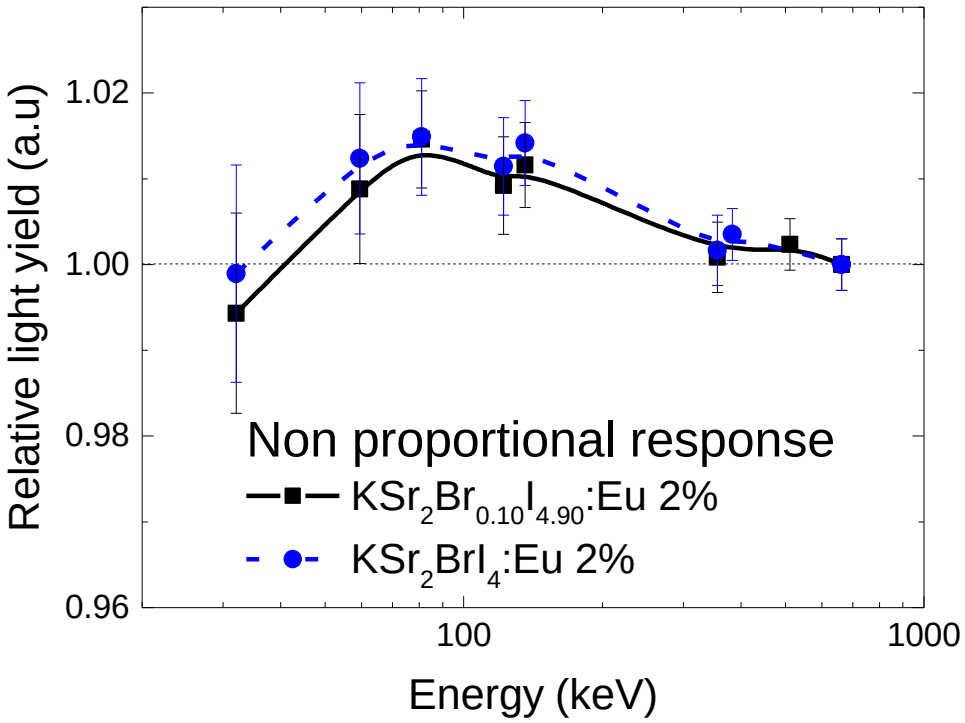

Figure 79. The light yield non-proportionality curves measured for KSr_2BrI_4:Eu 2% and $KSr_2Br_{0.10}I_{4.90}$:Eu 2%.

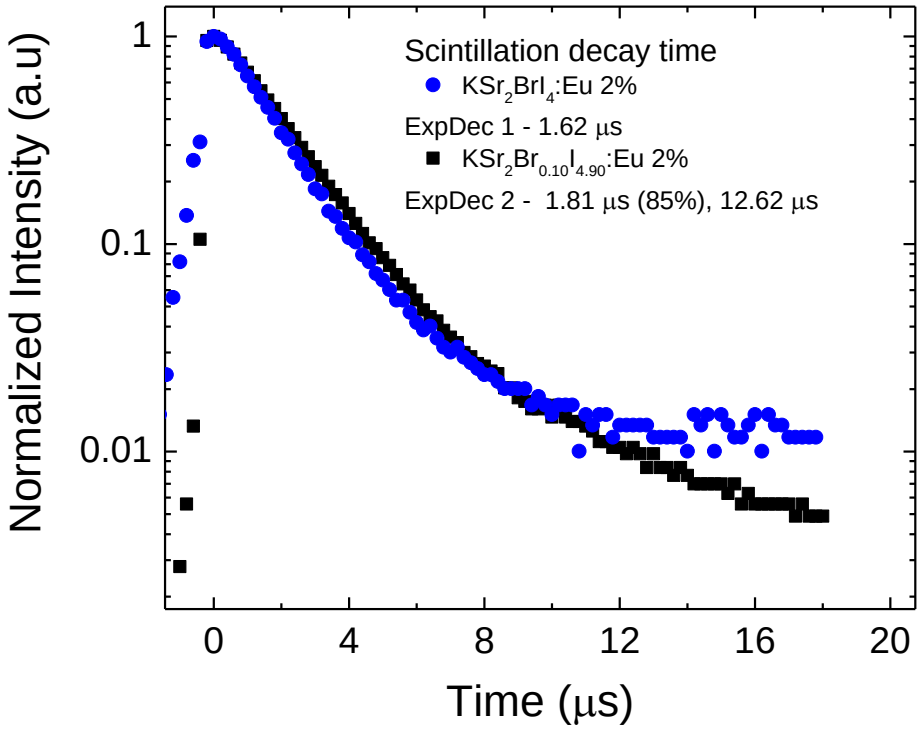

Figure 80. Scintillation decay time curves measured for KSr_2BrI_4:Eu 2% and $KSr_2Br_{0.10}I_{4.90}$:Eu 2%.

8.3.3. Crystal Growth and Scintillation Properties of $KSr_{1.3}Ba_{0.7}I_5:Eu^{2+}$

Small, 7 mm diameter single crystals of $KSr_{1.3}Ba_{0.7}I_5$ with 2%, 4% and 6% molar concentration of Eu^{2+} were grown. The quality of crystals containing 2% and 4% Eu^{2+} was better than the crystal with a concentration of 6%. Also, an excellent quality Ø 15 mm diameter single crystal of $KSr_{1.3}Ba_{0.7}$:Eu 4% was grown. The results of these crystal growth experiments are shown in Figure 81.

$KSr_{1.3}Ba_{0.7}I_5:Eu^{2+}$ is not only one the brightest scintillator ever measured, but also has one of the lowest energy resolution ever measured, just behind $LaBr_3$:Ce,Sr. When compared to KSr_2I_5:Eu, the light yield increased from 84,000 ph/MeV to 120,000 ph/MeV and the energy resolution improved from 2.4% to 2.2% for a 0.012 cm^3 sample. But more importantly the energy resolution of a 1 cm^3 crystal was 2.3% at 662 keV, which is probably the lowest measured energy resolution for a crystal of that volume as shown in Figure 82. Table 20 shows the energy resolution at various γ-ray excitation energies of 1 cm^3 of $KSr_{1.3}Ba_{0.7}I_5$:Eu 4% crystal.

8.3.4. Summary

Excellent quality single crystals were grown for both $KSr_2Br_xI_{(5-x)}:Eu^{2+}$ and $KSr_{1.3}Ba_{0.7}I_5:Eu^{2+}$ solid solutions. For this work the effects of replacing up to 33% of the iodine atoms with bromine in Eu^{2+} doped KSr_2I_5 were investigated. Transparent Ø 15 mm single crystals of $KSr_2Br_xI_{(5-x)}$:Eu 4% (where $0.05 \leq x \leq 1$) and nearly crack free Ø 22 mm single crystals of $KSr_2Br_{0.10}I_{4.90}$:Eu 2% and KSr_2BrI:Eu 2% were successfully grown via the vertical Bridgman technique using a two-zone transparent furnace. The addition of bromine caused a blue-shift of the emission, higher light yields and faster decay times while maintaining energy resolutions similar to those of the unmixed crystal. The secondary component (≥ 3μs - 15%) of the scintillation decay time was suppressed when the bromine content reached 5%. These results, in conjunction with the thermoluminescence glow curves, suggest that the shallow traps between 25K and 55K are responsible

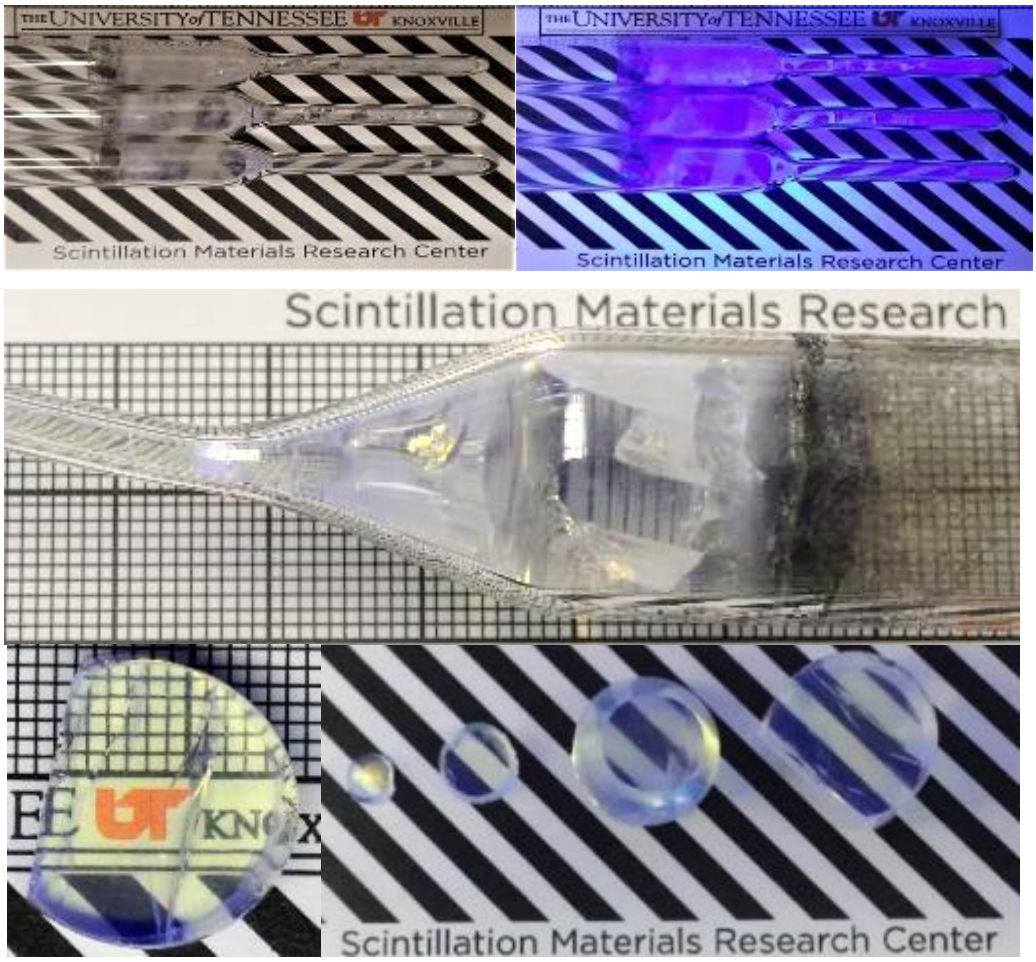

Figure 81. (Top) 7 mm diameter of $KSr_{1.3}Ba_{0.7}I_5$ with 2%, 4% and 6% molar concentration of Eu^{2+} under white fluorescent light on the left and under 365nm UV on the right and, (Bottom) a 15 mm of $KSr_{1.3}Ba_{0.7}I_5$:Eu 4% under white fluorescent light

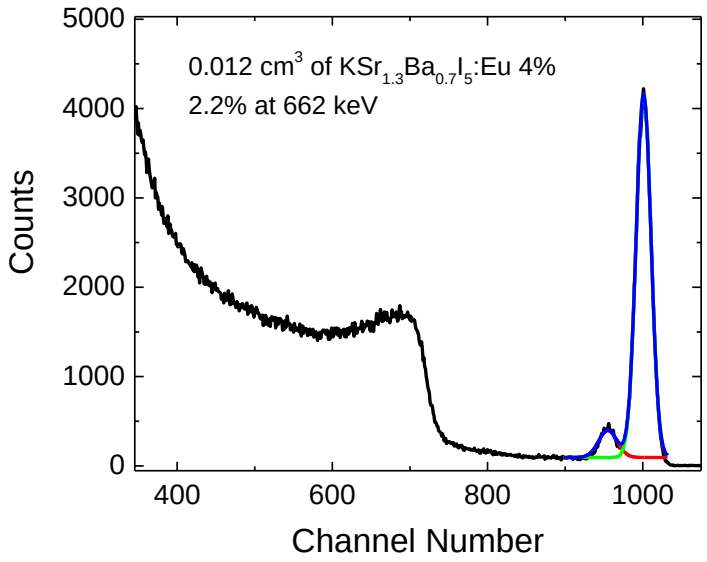

a.

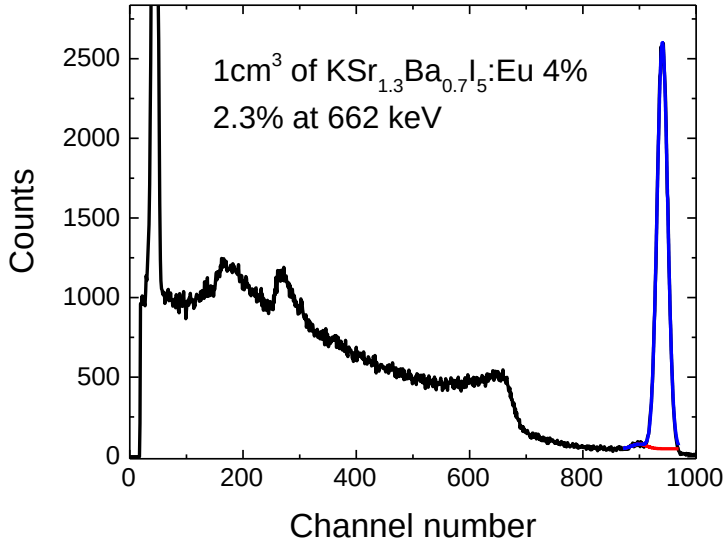

b.

Figure 82. Pulse height spectra of 0.012 cm^3 and 1 cm^3 of $KSr_{1.3}Ba_{0.7}I_5$:Eu 4% under ^{137}Cs excitation.

Table 20. Summary of the energy resolution measured at various γ-ray excitation energies.

γ-ray source	*Energy (keV)*	*Energy resolution (%)*
^{137}Cs	32	12.3
^{241}Am	59.5	7.0
^{133}Ba	81	6.2
^{57}Co	122	4.9
^{133}Ba	356	2.9
^{22}Na	511	2.5
^{137}Cs	662	2.3

for the secondary component of the scintillation decay time of KSr_2I_5:Eu 4% .At 10.3 cm^3, $KSr_2Br_{0.10}I_{4.90}$:Eu 2% performed better than KSr_2BrI_4:Eu 2%, with a light yield of 79,000 ph/MeV and energy resolution of 3.2% at 662 keV, while KSr_2BrI_4:Eu 2% had 62,800 ph/MeV and 3.8% energy resolution at 662 keV.

$KSr_{1.3}Ba_{0.7}I_5$:Eu^{2+} had light yields ranging from 95,200 ph/MeV to 120,000 ph/MeV. At 662 keV, energy resolutions as low as 2.2% were measured for a 0.012 cm^3 specimens, for a 1 cm^3 specimen an energy resolution of 2.3% was measured. The performance of both scintillators is promising and future investigation will be focus on improving the crystal's performance by tuning the europium concentration.

Chapter 9
Summary and Future Outlook

9.1. Summary

In this work we investigated the crystal growth and characterized newly discovered Eu^{2+} doped scintillators from the AB_2X_5 and A_2BX_4 compositional family, where A was potassium, B was strontium and barium, and X was bromine and Iodine. High quality single crystals of KSr_2I_5:Eu, $KSr_2Br_xI_{(5-x)}$:Eu, KSr_2Br_5:Eu, KBa_2I_5:Eu $KSr_{1.3}Br_{0.7}I$:Eu and K_2BaI_4:Eu were grown via the vertical Bridgman technique. Single crystalline specimens were characterized using a wide variety of techniques. These materials have a density ranging from 3.9 to 4.5 g/ cm^3, a Z_{eff} ranging from 35.2 to 53.1, a melting point ranging from 470 to 570 °C and as most halide scintillators are hygroscopic. These scintillator materials have light yield ranging 75,000 to 120,000 ph/MeV and energy resolutions well below 3.5% at 662 keV. Typical luminescence properties due to the Eu^{2+} $4f^6 5d^1$- $4f^7$ transition were observed under UV and x-ray excitation. The investigated crystals also have highly proportional photon responses that deviated less than 3% from the ideal over the energies tested (from 32 keV – 662 keV).

Although all the investigated scintillators have excellent scintillation properties, we found that KSr_2I_5:Eu was more tolerant of growth conditions than most high performance scintillators. Thus, we focused on understanding fundamental material properties related to: dopant optimization, crystal growth processes, homogeneity and overall performance of KSr_2I_5:Eu, and learned that:

- A grain selector at the bottom of the ampoule facilitated the nucleation and propagation of a single grain.
- It is possible to grow high performing single crystals of KSr_2I_5:Eu at faster rates (0.5 mm/h - 5 mm/h) than commonly used for other halide scintillators, without compromising the performance.
- The crystal yield was significantly increased by replacing the typical quartz ampoules with carbon coated quartz ampoules and high-performance, crack free Ø 1 × 6” long scintillator crystals of K can be grown using pulling rates of 3 and 5 mm/h.

- In large sized detectors, most non-uniformities in the light collection of $KSr_2I_5:Eu^{2+}$ are caused by scintillation photons having different probabilities of self-absorption. Thus, the reduction of the light yield, variation of the energy resolution and lengthen scintillation decay time observed with increasing volume are mostly due to the re-absorption and re-emission of light at the luminescence center, which is an intrinsic property of Eu^{2+}.
- 12.5 cm^3 cylindrical $KSr_2I_5:Eu^{2+}$crystals had light yield that ranged from 69,500 to 82,100 ph/MeV, with energy resolution only ranging from 3.1 to 3.6% at 662 keV.
- Higher light yield, lower energy resolutions, and faster scintillation decay times can be obtained by forming $KSr_2Br_xI_{(5-x)}:Eu^{2+}$ and $KSr_{1.3}Ba_{0.7}I_5:Eu^{2+}$ solid solutions.
    - The addition of bromine caused a blue-shift of the emission, higher light yields and faster decay times while maintaining energy resolutions similar to those of the unmixed crystal.
    - $KSr_{1.3}Ba_{0.7}I_5:Eu^{2+}$ had light yields up to 120,000 ph/MeV and energy resolutions as low as 2.2% were measured for a 0.012 cm^3 and 2.3% for a 1 cm^3 crystals.

9.2. Future Outlook

The primary drawback of K-based scintillators is the internal radioactivity due to their ^{40}K content. Future research should focus on finding solid solutions that could partially (or fully) replace potassium to significantly reduce the crystal's background. Also, in order to satisfy the requirements for national security applications further work is needed to (1) enhance the energy resolution to achieve even higher radio-isotopic discrimination and (2) produce Ø 1.5 x 1.5-inch cylindrical detector with energy resolutions below 4% at 662 keV.

References

[1] G.F. Knoll, Radiation Detection and Measurement, John Wiley & Sons, 2010.
[2] P.A. Rodnyi, Physical processes in inorganic scintillators, CRC press, 1997.
[3] P. Dorenbos, Fundamental Limitations in the Performance of Ce3+, Pr3+, and Eu2+ Activated Scintillators, IEEE Transactions on Nuclear Science, 57 (2010) 1162-1167.
[4] E. Rutherford, James Chadwick,, C.D. Ellis., Radiations from Radioactive Substances, Cambridge University Press, 1930.
[5] R. Hofstadter, M.H. Stein, Twenty Five Years of Scintillation Counting, Nuclear Science, IEEE Transactions on, 22 (1975) 13-25.
[6] S.E. Derenzo, M.J. Weber, E. Bourret-Courchesne, M.K. Klintenberg, The quest for the ideal inorganic scintillator, Nuclear Instruments and Methods in Physics Research Section A: Accelerators, Spectrometers, Detectors and Associated Equipment, 505 (2003) 111-117.
[7] K.E. NELSON, T.B. GOSNELL, D.A. KNAPP, LLNL-TR-411374 The Effect of Gamma-Ray Detector Energy Resolution on the Ability to Identify Radioactive Sources, (2009).
[8] W.W. Moses, Scintillator requirements for medical imaging, in: Proc. Int. Conf. on Inorganic Scintillators and Their Applicat.:SCINT99, Moscow, Russia, 1999, pp. 11-21.
[9] E.V.D. Van Loef, P. Dorenbos, C.W.E. Van Eijk, K. Kramer, H.U. Gudel, High-energy-resolution scintillator: Ce^{3+} activated $LaBr_3$, Applied Physics Letters, 79 (2001) 1573-1575.
[10] J. Cox, J. Hovgaard, K. Duftschmid, A new generation hand held identifier for customs applications, C&SPapersSeries, (2002) 553.
[11] M. Moszynski, M. Balcerzyk, W. Czarnacki, M. Kapusta, W. Klamra, P. Schotanus, A. Syntfeld, M. Szawlowski, Study of pure NaI at room and liquid nitrogen temperatures, in: Nuclear Science Symposium Conference Record, 2002 IEEE, 2002, pp. 346-351 vol.341.
[12] B.W. Sturm, N.J. Cherepy, O.B. Drury, P.A. Thelin, S.E. Fisher, S.A. Payne, A. Burger, L.A. Boatner, J.O. Ramey, K.S. Shah, R. Hawrami, Effects of packaging SrI2(Eu) scintillator crystals, Nuclear Instruments and Methods in Physics Research Section A: Accelerators, Spectrometers, Detectors and Associated Equipment, 652 (2011) 242-246.
[13] Ortec, Gamma-Ray Spectra of Natural Background, in, AMETEK, Inc, Web.
[14] G. Meyer, S. Masselmann, The Alkali-Poor Part of the Pseudoternary Triangle AX/BX2/MX3: Crystal Structures, Properties, and Potentials of (Alkali)/Alkaline-Earth/Rare-Earth Chloride Materials, Chemistry of Materials, 10 (1998) 2994-3004.

[15] L. Stand, M. Zhuravleva, A. Lindsey, C.L. Melcher, Growth and characterization of potassium strontium iodide: A new high light yield scintillator with 2.4% energy resolution, Nuclear Instruments and Methods in Physics Research Section A: Accelerators, Spectrometers, Detectors and Associated Equipment, 780 (2015) 40-44.
[16] C.W.E. van Eijk, Inorganic scintillators in medical imaging detectors, Nuclear Instruments and Methods in Physics Research Section A: Accelerators, Spectrometers, Detectors and Associated Equipment, 509 (2003) 17-25.
[17] M.S. Alekhin, S. Weber, K.W. Krämer, P. Dorenbos, Optical properties and defect structure of Sr2+ co-doped LaBr3:5%Ce scintillation crystals, Journal of Luminescence, 145 (2014) 518-524.
[18] N.J. Cherepy, B.W. Sturm, O.B. Drury, T.A. Hurst, S.A. Sheets, L.E. Ahle, C.K. Saw, M.A. Pearson, S.A. Payne, A. Burger, L.A. Boatner, J.O. Ramey, E.V. van Loef, J. Glodo, R. Hawrami, W.M. Higgins, K.S. Shah, W.W. Moses, SrI2 scintillator for gamma ray spectroscopy, in, 2009, pp. 74490F-74490F-74496.
[19] G. Schilling, G. Meyer, Ternäre Bromide und Iodide zweiwertiger Lanthanide und ihre Erdalkali-Analoga vom Typ AMX3 und AM2X5, Zeitschrift für anorganische und allgemeine Chemie, 622 (1996) 759-765.
[20] G. Schilling, G. Meyer, Ternäre Bromide und Iodide zweiwertiger Lanthanide und ihre Erdalkali-Analoga vom Typ AMX3 und AM2X5, Zeitschrift für anorganische und allgemeine Chemie, 622 (1996) 759-765.
[21] P. Dorenbos, Energy of the first 4f7→4f65d transition of Eu2+ in inorganic compounds, Journal of Luminescence, 104 (2003) 239-260.
[22] D.H. Gahane, N.S. Kokode, P.L. Muthal, S.M. Dhopte, S.V. Moharil, Luminescence of some Eu2+ activated bromides, Journal of Alloys and Compounds, 484 (2009) 660-664.
[23] R. Hawrami, M. Groza, Y. Cui, A. Burger, M.D. Aggarwal, N. Cherepy, S.A. Payne, SrI2: a novel scintillator crystal for nuclear isotope identifiers, in, 2008, pp. 70790Y-70790Y-70711.
[24] B.W. Sturm, N.J. Cherepy, O.B. Drury, P.A. Thelin, S.E. Fisher, S.P. O'Neal, S.A. Payne, A. Burger, L.A. Boatner, J.O. Ramey, K.S. Shah, R. Hawrami, Characteristics of undoped and europium-doped SrI2 scintillator detectors, in: Nuclear Science Symposium and Medical Imaging Conference (NSS/MIC), 2011 IEEE, 2011, pp. 7-11.
[25] L.A. Boatner, J.O. Ramey, J.A. Kolopus, R. Hawrami, W.M. Higgins, E. van Loef, J. Glodo, K.S. Shah, E. Rowe, P. Bhattacharya, E. Tupitsyn, M. Groza, A. Burger, N.J. Cherepy, S.A. Payne, Bridgman growth of large SrI2:Eu2+ single

crystals: A high-performance scintillator for radiation detection applications, Journal of Crystal Growth, 379 (2013) 63-68.
[26] R. Hawrami, J. Glodo, K.S. Shah, N. Cherepy, S. Payne, A. Burger, L. Boatner, Bridgman bulk growth and scintillation measurements of SrI2:Eu2+, Journal of Crystal Growth, 379 (2013) 69-72.
[27] K.S. Shah, J. Glodo, M. Klugerman, W.W. Moses, S.E. Derenzo, M.J. Weber, LaBr3:Ce scintillators for gamma-ray spectroscopy, Nuclear Science, IEEE Transactions on, 50 (2003) 2410-2413.
[28] W.M. Higgins, J. Glodo, E. Van Loef, M. Klugerman, T. Gupta, L. Cirignano, P. Wong, K.S. Shah, Bridgman growth of LaBr3:Ce and LaCl3:Ce crystals for high-resolution gamma-ray spectrometers, Journal of Crystal Growth, 287 (2006) 239-242.
[29] G. Bizarri, E.D. Bourret-Courchesne, Z. Yan, S.E. Derenzo, Scintillation and Optical Properties of BaBrI: Eu2+ and CsBa2I5:Eu2+, IEEE Transactions on Nuclear Science, 58 (2011) 3403-3410.
[30] M.S. Alekhin, D.A. Biner, K.W. Krämer, P. Dorenbos, Optical and scintillation properties of CsBa2I5:Eu2+, Journal of Luminescence, 145 (2014) 723-728.
[31] L. Stand, M. Zhuravleva, H. Wei, C.L. Melcher, Crystal growth and scintillation properties of potassium strontium bromide, Optical Materials, 46 (2015) 59-63.
[32] T.B.G. K. E. Nelson, and D. A. Knapp, The Effect of Gamma-Ray Detector Energy Resolution on the Ability to Identify Radioactive Sources, LLNL-TR-411374, (2009).
[33] E.V. van Loef, K.S. Shah, Advances in scintillators for medical imaging applications, in: SPIE Optical Engineering+ Applications, International Society for Optics and Photonics, 2014, pp. 92140A-92140A-92145.
[34] N. Cherepy, Strontium and barium iodide high light yield scintillators, in, 2008.
[35] K.S. Shah, J. Glodo, M. Klugerman, W. Higgins, T. Gupta, P. Wong, W.W. Moses, S.E. Derenzo, M.J. Weber, P. Dorenbos, LuI3:Ce-a new scintillator for gamma ray spectroscopy, Nuclear Science, IEEE Transactions on, 51 (2004) 2302-2305.
[36] K. Yang, M. Zhuravleva, C.L. Melcher, Crystal growth and characterization of CsSr1-xEuxI3 high light yield scintillators, Physica Status Solidi (RRL) – Rapid Research Letters, 5 (2011) 43-45.
[37] H. Wei, M. Zhuravleva, M. Tyagi, C.L. Melcher, Scintillation Properties of Cs3LaCl6:Ce3+ and Cs3LaBr6:Ce3+, Ieee T Nucl Sci, 61 (2014) 390-396.
[38] H. Wei, M. Zhuravleva, K. Yang, B. Blalock, C.L. Melcher, Effect of Ba substitution in CsSrI3:Eu2+, Journal of Crystal Growth, 384 (2013) 27-32.

[39] H. Wei, V. Martin, A. Lindsey, M. Zhuravleva, C.L. Melcher, The scintillation properties of CeBr3−xClx single crystals, Journal of Luminescence, 156 (2014) 175-179.
[40] L.M.Bollinger, in: G.E. Thomas (Ed.), Rev. Sci. Instr, 1961, pp. 1044-1050.
[41] C.S. R. Riccardi, G.V. Campari, A. Magistri, Binary Systems Formed by Alkali Bromides with Barium or Strontium Bromide, Zeitschrift Fur Naturforschung A, 25 (1970) 781.
[42] M. Zhuravleva, L. Stand, h. wei, C. Hobbs, L.A. Boatner, J.O. Ramey, K. Shah, A. Burger, E. Rowe, P. Bhattacharya, E. Tupitsyn, C.L. Melcher, Hygroscopicity evaluation of halide scintillators, in: Nuclear Science Symposium and Medical Imaging Conference (NSS/MIC), 2013 IEEE, 2013, pp. 1-5.
[43] E.V. van Loef, C.M. Wilson, N.J. Cherepy, G. Hull, S.A. Payne, C. Woon-Seng, W.W. Moses, K.S. Shah, Crystal Growth and Scintillation Properties of Strontium Iodide Scintillators, Nuclear Science, IEEE Transactions on, 56 (2009) 869-872.
[44] J. Glodo, E.V. Van Loef, N.J. Cherepy, S.A. Payne, K.S. Shah, Concentration Effects in Eu Doped SrI2, Nuclear Science, IEEE Transactions on, 57 (2010) 1228-1232.
[45] L. Stand, M. Zhuravleva, B. Chakoumakos, J. Johnson, A. Lindsey, C.L. Melcher, Scintillation properties of Eu2+-doped KBa2I5 and K2BaI4, Journal of Luminescence, 169, Part A (2016) 301-307.
[46] E.D. Bourret-Courchesne, G. Bizarri, R. Borade, Z. Yan, S.M. Hanrahan, G. Gundiah, A. Chaudhry, A. Canning, S.E. Derenzo, Eu2+-doped Ba2CsI5, a new high-performance scintillator, Nuclear Instruments and Methods in Physics Research Section A: Accelerators, Spectrometers, Detectors and Associated Equipment, 612 (2009) 138-142.
[47] E.D. Bourret-Courchesne, G. Bizarri, S.M. Hanrahan, G. Gundiah, Z. Yan, S.E. Derenzo, BaBrI:Eu2+, a new bright scintillator, Nuclear Instruments and Methods in Physics Research Section A: Accelerators, Spectrometers, Detectors and Associated Equipment, 613 (2010) 95-97.
[48] E.V. van Loef, K.S. Shah, Advances in scintillators for medical imaging applications, in, 2014, pp. 92140A-92140A-92145.
[49] R. Borade, E. Bourret-Courchesne, S. Derenzo, Scintillation properties of CsBa2Br5:Eu2+, Nuclear Instruments and Methods in Physics Research Section A: Accelerators, Spectrometers, Detectors and Associated Equipment, 652 (2011) 260-263.
[50] G. Gundiah, Z. Yan, G. Bizarri, S.E. Derenzo, E.D. Bourret-Courchesne, Structure and scintillation of Eu2+-activated BaBrCl and solid solutions in the BaCl2–BaBr2 system, Journal of Luminescence, 138 (2013) 143-149.

[51] Rigaku, CrystalClear, in, Rigaku Corporation, Tokyo, Japan, 2005.
[52] T. Higashi, ABSCOR, in, Rigaku Corporation, Tokyo, Japan 2000.
[53] G. Sheldrick, A short history of SHELX, Acta Crystallographica Section A, 64 (2008) 112-122.
[54] K. Momma, F. Izumi, VESTA: a three-dimensional visualization system for electronic and structural analysis, Journal of Applied Crystallography, 41 (2008) 653-658.
[55] C.W.E. van Eijk, P. Dorenbos, E.V.D. van Loef, K. Krämer, H.U. Güdel, Energy resolution of some new inorganic-scintillator gamma-ray detectors, Radiation Measurements, 33 (2001) 521-525.
[56] M.S. Alekhin, J.T.M. de Haas, K.W. Kramer, I.V. Khodyuk, L. de Vries, P. Dorenbos, Scintillation properties and self absorption in SrI2:Eu2+, in: Nuclear Science Symposium Conference Record (NSS/MIC), 2010 IEEE, 2010, pp. 1589-1599.
[57] A.F.M.a.B.P. Oehry, Radiation Trapping in Atomic Vapours, Oxford Science (1999).
[58] U. Shirwadkar, E.V.D. van Loef, R. Hawrami, S. Mukhopadhyay, J. Glodo, K.S. Shah, New promising scintillators for gamma-ray spectroscopy: Cs(Ba,Sr)(Br,I)3, in: Nuclear Science Symposium and Medical Imaging Conference (NSS/MIC), 2011 IEEE, 2011, pp. 1583-1585.
[59] U. Shirwadkar, R. Hawrami, J. Glodo, E.V.D. van Loef, K.S. Shah, Promising Alkaline Earth Halide Scintillators for Gamma-Ray Spectroscopy, Nuclear Science, IEEE Transactions on, 60 (2013) 1011-1015.
[60] S. Lam, S. Swider, J. Fiala, A. Datta, S. Motakef, Microscale luminescence imaging of defects, inhomogeneities, and secondary phases in halide scintillators, Nuclear Instruments and Methods in Physics Research Section A: Accelerators, Spectrometers, Detectors and Associated Equipment.
[61] D.H. Gahane, N.S. Kokode, P.L. Muthal, S.M. Dhopte, S.V. Moharil, Luminescence of Eu2+ in some iodides, Optical Materials, 32 (2009) 18-21.
[62] A. Pushak, V. Vistovskyy, A. Voloshinovskii, T. Demkiv, J. Dacyuk, A. Gektin, S. Myagkota, Luminescence of Eu2+-doped Me-containing aggregates (Me= Ca, Sr, Ba) in KI matrix.
[63] G. Bizarri, E.D. Bourret-Courchesne, Y. Zewu, S.E. Derenzo, Scintillation and Optical Properties of BaBrI:Eu2+ and CsBa2I5: Eu2+, Nuclear Science, IEEE Transactions on, 58 (2011) 3403-3410.
[64] P. Dorenbos, Fundamental Limitations in the Performance of–,–, and–Activated Scintillators, Nuclear Science, IEEE Transactions on, 57 (2010) 1162-1167.

[65] L. Stand, M. Zhuravleva, G. Camarda, A. Lindsey, J. Johnson, C. Hobbs, C.L. Melcher, Exploring growth conditions and Eu2+ concentration effects for KSr2I5:Eu scintillator crystals, Journal of Crystal Growth, 439 (2016) 93-98.
[66] Y. Kan, M. Zhuravleva, H. Rothfuss, C.L. Melcher, Optical and scintillation properties of single crystal CsSr(1-x)Eu(x)I3, in: Nuclear Science Symposium Conference Record (NSS/MIC), 2010 IEEE, 2010, pp. 1603-1606.
[67] L. Stand, M. Zhuravleva, A. Lindsey, C.L. Melcher, Growth and characterization of potassium strontium iodide: A new high light yield scintillator with 2.4% energy resolution, Nuclear Instruments and Methods in Physics Research Section A: Accelerators, Spectrometers, Detectors and Associated Equipment.
[68] H. Wei, M. Zhuravleva, K. Yang, B. Blalock, C.L. Melcher, Effect of Ba substitution in CsSrI3: Eu2+, Journal of Crystal Growth.
[69] T. Suthan, P.V. Dhanaraj, N.P. Rajesh, C.K. Mahadevan, G. Bhagavannarayana, Growth and characterization of benzil single crystals using nanotranslation by the modified vertical Bridgman technique, CrystEngComm, 13 (2011) 4018-4024.
[70] G.S. Camarda, E.M. Kakuno, G. Carini, A.E. Bolotnikov, G.W. Wright, R.B. James, D.P. Siddons, Micro-scale 2D mapping of cadmium-zinc telluride strip detectors, in: Nuclear Science Symposium Conference Record, 2003 IEEE, 2003, pp. 3503-3506 Vol.3505.
[71] L. Stand, M. Zhuravleva, J. Johnson, M. Koschan, Y. Wu, S. Donnald, K. Vaigneur, E. Lukosi, C.L. Melcher, Exploring growth conditions and Eu2+ concentration effects for KSr2I5:Eu scintillator crystals II: Ø 25 mm crystals, Journal of Crystal Growth, 483 (2018) 301-307.
[72] A.C. Lindsey, M. Zhuravleva, L. Stand, Y. Wu, C.L. Melcher, Crystal growth and characterization of europium doped KCaI3, a high light yield scintillator, Optical Materials, 48 (2015) 1-6.
[73] L.A. Boatner, J.O. Ramey, J.A. Kolopus, J.S. Neal, N.J. Cherepy, P.R. Beck, S.A. Payne, A. Burger, E. Rowe, P. Bhattacharya, Advances in the growth of alkaline-Earth halide single crystals for scintillator detectors, in, 2014, pp. 92130J-92130J-92111.
[74] M.J. Harrison, A.P. Graebner, W.J. McNeil, D.S. McGregor, Carbon coating of fused silica ampoules, Journal of Crystal Growth, 290 (2006) 597-601.
[75] L.S. Yip, I. Shih, C.H. Champness, Method of avoiding ampoule adhesion of ingots in Bridgman growth of CuInSe2, Journal of Crystal Growth, 129 (1993) 102-106.

[76] R. Shetty, W.R. Wilcox, L.L. Regel, Influence of ampoule coatings on cadmium telluride solidification, Journal of Crystal Growth, 153 (1995) 103-109.
[77] Y. Wu, A.C. Lindsey, M. Zhuravleva, M. Koschan, C.L. Melcher, Large-size KCa0.8Sr0.2I3:Eu2+ Crystals: Growth and Characterization of Scintillation Properties, Crystal Growth & Design, (2016).
[78] A.C. Lindsey, M. Zhuravleva, Y. Wu, L. Stand, M. Loyd, S. Gokhale, M. Koschan, C.L. Melcher, Effects of Increasing Size and Changing Europium Activator Concentration in KCaI3 Scintillator Crystals, Journal of Crystal Growth.
[79] W.M. Higgins, A. Churilov, E. van Loef, J. Glodo, M. Squillante, K. Shah, Crystal growth of large diameter LaBr3:Ce and CeBr3, Journal of Crystal Growth, 310 (2008) 2085-2089.
[80] Y. Wu, L.A. Boatner, A.C. Lindsey, M. Zhuravleva, S. Jones, J.D. Auxier, H.L. Hall, C.L. Melcher, Defect Engineering in SrI2:Eu2+ Single Crystal Scintillators, Crystal Growth & Design, 15 (2015) 3929-3938.
[81] N.J. Cherepy, G. Hull, A.D. Drobshoff, S.A. Payne, E. Van Loef, C.M. Wilson, K.S. Shah, U.N. Roy, A. Burger, L.A. Boatner, C. Woon-Seng, W.W. Moses, Strontium and barium iodide high light yield scintillators, Applied Physics Letters, 92 (2008) 083508-083508-083503.
[82] N.J. Cherepy, P.R. Beck, S.A. Payne, E.L. Swanberg, B.M. Wihl, S.E. Fisher, S. Hunter, P.A. Thelin, C.J. Delzer, S. Shahbazi, A. Burger, K.S. Shah, R. Hawrami, L.A. Boatner, M. Momayezi, K. Stevens, M.H. Randles, D. Solodovnikov, History and current status of strontium iodide scintillators, in: SPIE Optical Engineering + Applications, SPIE, 2017, pp. 7.
[83] C.E. Chang, W.R. Wilcox, Control of Interface Shape in Vertical Bridgman-Stockbarger Technique, Journal of Crystal Growth, 21 (1974) 135-140.
[84] T.W. Fu, W.R. Wilcox, Influence of Insulation on Stability of Interface Shape and Position in the Vertical Bridgman-Stockbarger Technique, Journal of Crystal Growth, 48 (1980) 416-424.
[85] M. Moszynski, T. Szczesniak, M. Kapusta, M. Szawlowski, J. Iwanowska, M. Gierlik, A. Syntfeld-Kazuch, S. Ł, C.L. Melcher, L.A. Eriksson, J. Glodo, Characterization of Scintillators by Modern Photomultipliers; A New Source of Errors, IEEE Transactions on Nuclear Science, 57 (2010) 2886-2896.
[86] S. Lam, S. Swider, J. Fiala, A. Datta, S. Motakef, Microscale luminescence imaging of defects, inhomogeneities, and secondary phases in halide scintillators, Nuclear Instruments and Methods in Physics Research Section A: Accelerators, Spectrometers, Detectors and Associated Equipment, 784 (2015) 23-28.
[87] M.S. Alekhin, D.A. Biner, K.W. Krämer, P. Dorenbos, Optical and scintillation properties of CsBa2I5:Eu2+, Journal of Luminescence, 145 (2014) 723-728.

[88] P.R. Beck, N.J. Cherepy, S.A. Payne, E.L. Swanberg, K.E. Nelson, P.A. Thelin, S.E. Fisher, S. Hunter, B.M. Wihl, K.S. Shah, R. Hawrami, A. Burger, L.A. Boatner, M. Momayezi, K.T. Stevens, M.H. Randles, D. Solodovnikov, Strontium iodide instrument development for gamma spectroscopy and radioisotope identification, in, 2014, pp. 92130N-92130N-92139.
[89] A.C. Lindsey, M. Zhuravleva, Y. Wu, L. Stand, M. Loyd, S. Gokhale, M. Koschan, C.L. Melcher, Effects of increasing size and changing europium activator concentration in KCaI3 scintillator crystals, Journal of Crystal Growth, 449 (2016) 96-103.
[90] L. Stand, M. Zhuravleva, A. Lindsey, C.L. Melcher, Potassium strontium iodide: A new high light yield scintillator with 2.4% energy resolution, in: 2013 IEEE Nuclear Science Symposium and Medical Imaging Conference (2013 NSS/MIC), 2013, pp. 1-3.
[91] L. Stand, M. Zhuravleva, J. Johnson, M. Koschan, Y. Wu, S. Donnald, K. Vaigneur, E. Lukosi, C.L. Melcher, Exploring Growth Conditions and Eu2+ Concentration Effects for KSr2I5:Eu Scintillator Crystals II: Ø 25 mm Crystals, Journal of Crystal Growth, (2017).
[92] M. Bertolaccini, S. Cova, C. Bussolati, A technique for absolute measurement of the effective photoelectron per keV yield in scintillation counters, Nuclear electronics. Comptes rendus du Colloque international sur le l'e'lectronique nucle'aire., (1968).
[93] J.T.M.d. Haas, P. Dorenbos, Advances in Yield Calibration of Scintillators, IEEE Transactions on Nuclear Science, 55 (2008) 1086-1092.
[94] M.S. Alekhin, J.T.M.d. Haas, K.W. Kramer, P. Dorenbos, Scintillation Properties of and Self Absorption in SrI2:Eu2+, IEEE Transactions on Nuclear Science, 58 (2011) 2519-2527.
[95] B.W. Sturm, N.J. Cherepy, O.B. Drury, P.A. Thelin, S.E. Fisher, A.F. Magyar, S.A. Payne, A. Burger, L.A. Boatner, J.O. Ramey, K.S. Shah, R. Hawrami, Evaluation of large volume SrI2(Eu) scintillator detectors, in: IEEE Nuclear Science Symposuim & Medical Imaging Conference, 2010, pp. 1607-1611.
[96] H. Tan, W.K. Warburton, Modeling scintillation light absorption and re-emission in SrI2(Eu) scintillators, Nuclear Instruments and Methods in Physics Research Section A: Accelerators, Spectrometers, Detectors and Associated Equipment, 652 (2011) 221-225.
[97] L. Soundara-Pandian, R. Hawrami, J. Glodo, E. Ariesanti, E.V.v. Loef, K. Shah, Lithium Alkaline Halides—Next Generation of Dual Mode Scintillators, IEEE Transactions on Nuclear Science, 63 (2016) 490-496.

[98] K. Kamada, T. Yanagida, J. Pejchal, M. Nikl, T. Endo, K. Tsutumi, Y. Fujimoto, A. Fukabori, A. Yoshikawa, Scintillator-oriented combinatorial search in Ce-doped (Y,Gd) 3 (Ga,Al) 5 O 12 multicomponent garnet compounds, Journal of Physics D: Applied Physics, 44 (2011) 505104.
[99] K. Kamada, T. Endo, K. Tsutumi, T. Yanagida, Y. Fujimoto, A. Fukabori, A. Yoshikawa, J. Pejchal, M. Nikl, Composition Engineering in Cerium-Doped (Lu,Gd)3(Ga,Al)5O12 Single-Crystal Scintillators, Crystal Growth & Design, 11 (2011) 4484-4490.
[100] G. Gundiah, G. Bizarri, S.M. Hanrahan, M.J. Weber, E.D. Bourret-Courchesne, S.E. Derenzo, Structure and scintillation of Eu2+-activated solid solutions in the BaBr2–BaI2 system, Nuclear Instruments and Methods in Physics Research Section A: Accelerators, Spectrometers, Detectors and Associated Equipment, 652 (2011) 234-237.
[101] B. Han-Bo, Q. Lai-Shun, D. Yan-Guo, L. Zheng-Guo, S. Hong-Sheng, S. Kang-Ying, Growth and Scintillation Properties of La(Cl 0.05 Br 0.95) 3 :Ce Crystal, Chinese Physics Letters, 30 (2013) 088101.
[102] M.D. Birowosuto, P. Dorenbos, K.W. Krämer, H.U. Güdel, Ce3+ activated LaBr3−xIx: High-light-yield and fast-response mixed halide scintillators, Journal of Applied Physics, 103 (2008) 103517.
[103] A. Lindsey, W. McAlexander, L. Stand, Y. Wu, M. Zhuravleva, C.L. Melcher, Crystal growth and spectroscopic performance of large crystalline boules of CsCaI3:Eu scintillator, Journal of Crystal Growth, 427 (2015) 42-47.
[104] A.V. Gektin, A.N. Belsky, A.N. Vasil'ev, Scintillation Efficiency Improvement by Mixed Crystal Use, IEEE Transactions on Nuclear Science, 61 (2014) 262-270.
[105] J.D. Valentine, W.W. Moses, S.E. Derenzo, D.K. Wehe, G.F. Knoll, Temperature dependence of CsI(Tl) gamma-ray excited scintillation characteristics, Nuclear Instruments and Methods in Physics Research Section A: Accelerators, Spectrometers, Detectors and Associated Equipment, 325 (1993) 147-157.
[106] K. Yang, M. Zhuravleva, C.L. Melcher, Scintillation kinetics and thermoluminescence of SrI_2:Eu^{2+} single crystals, Journal of Luminescence, 132 (2012) 1824-1829.
[107] C.-K. Duan, M.F. Reid, Local field effects on the radiative lifetimes of Ce3+ in different hosts, Current Applied Physics, 6 (2006) 348-350.
[108] A.N. Vasil'ev, A.V. Gektin, Multiscale Approach to Estimation of Scintillation Characteristics, IEEE Transactions on Nuclear Science, 61 (2014) 235-245.

[109] I.V. Khodyuk, J.T.M.d. Haas, P. Dorenbos, Nonproportional Response Between 0.1-100 keV Energy by Means of Highly Monochromatic Synchrotron X-Rays, IEEE Transactions on Nuclear Science, 57 (2010) 1175-1181.
[110] W.S. Choong, G. Hull, W.W. Moses, K.M. Vetter, S.A. Payne, N.J. Cherepy, J.D. Valentine, Performance of a Facility for Measuring Scintillator Non-Proportionality, IEEE Transactions on Nuclear Science, 55 (2008) 1073-1078.
[111] W.S. Choong, K.M. Vetter, W.W. Moses, G. Hull, S.A. Payne, N.J. Cherepy, J.D. Valentine, Design of a Facility for Measuring Scintillator Non-Proportionality, Nuclear Science, IEEE Transactions on, 55 (2008) 1753-1758.
[112] S.A. Payne, N.J. Cherepy, G. Hull, J.D. Valentine, W.W. Moses, C. Woon-Seng, Nonproportionality of Scintillator Detectors: Theory and Experiment, Nuclear Science, IEEE Transactions on, 56 (2009) 2506-2512.
[113] S.A. Payne, W.W. Moses, S. Sheets, L. Ahle, N.J. Cherepy, B. Sturm, S. Dazeley, G. Bizarri, C. Woon-Seng, Nonproportionality of Scintillator Detectors: Theory and Experiment. II, Nuclear Science, IEEE Transactions on, 58 (2011) 3392-3402.
[114] M.S. Alekhin, J.T.M. de Haas, I.V. Khodyuk, K.W. Krämer, P.R. Menge, V. Ouspenski, P. Dorenbos, Improvement of γ-ray energy resolution of LaBr3:Ce3+ scintillation detectors by Sr2+ and Ca2+ co-doping, Applied Physics Letters, 102 (2013) -.
[115] R.H.P. Awater, K.W. Krämer, P. Dorenbos, Effects of Na+, Mg2+, Ca2+, Sr2+and Ba2+ Doping on the Scintillation Properties of CeBr3, IEEE Transactions on Nuclear Science, 62 (2015) 2343-2348.
[116] P.R. Beck, S.A. Payne, S. Hunter, L. Ahle, N.J. Cherepy, E.L. Swanberg, Nonproportionality of Scintillator Detectors. V. Comparing the Gamma and Electron Response, IEEE Transactions on Nuclear Science, 62 (2015) 1429-1436.
[117] A. Syntfeld-Kazuch, L. Swiderski, W. Czarnacki, M. Gierlik, W. Klamra, M. Moszynski, P. Schotanus, Non-Proportionality and Energy Resolution of CsI(Tl), IEEE Transactions on Nuclear Science, 54 (2007) 1836-1841.
[118] F. Zhou, B. Sadigh, P. Erhart, D. Åberg, Ab initio prediction of fast non-equilibrium transport of nascent polarons in SrI2: a key to high-performance scintillation, 2 (2016) 16022.
[119] D. Åberg, B. Sadigh, A. Schleife, P. Erhart, Origin of resolution enhancement by co-doping of scintillators: Insight from electronic structure calculations, Applied Physics Letters, 104 (2014) 211908.
[120] L. Stand, M. Zhuravleva, J. Johnson, M. Koschan, Y. Wu, S. Donnal, K. Vaigneur, E. Lukosi, C.L. Melcher, Exploring Growth Conditions and Eu2+

Concentration Effects for KSr2I5:Eu Scintillator Crystals II: Ø 25 mm Crystals, Journal of Crystal Growth.
[121] B.D. Rooney, J.D. Valentine, Scintillator light yield nonproportionality: calculating photon response using measured electron response, Nuclear Science, IEEE Transactions on, 44 (1997) 509-516.

Appendix

A. Single Crystal x-ray diffraction of KSr_2I_5 and KSr_2Br_5

(This section complements chapters 2 and 3. This work is part of an ongoing collaboration with Dr. Bryan Chakoumakos)

A.1 Experimental

Crystallographic studies utilized ~ 0.001 mm^3 crystal fragments isolated from boules grown in this study and suspended in paratone oil and each mounted on a plastic loop attached to copper pin/goniometer. Single-crystal diffraction data were collected at ~250K using a Rigaku XtaLAB PRO diffractometer with MoKα radiation (**λ** = 0.71073 Å) equipped with a Dectris Pilatus 200K detector and an Oxford N-HeliX cryocooler. Peak indexing and integration was done using d*trek in the CrystalClear package [51]. A numerical absorption correction was applied using ABSCOR [52]. The SIR-2011 in WinGX and SHELXL-2013 software packages were used for data processing and structure solution and refinement [53]. Crystal structure projections were made with VESTA [54].

KSr_2I_5 and KSr_2Br_5 are new compounds with the $TlPb_2Cl_5$ structure-type, which is known for at least 13 different compositions already reported in the Inorganic Crystal Structure Database. The $TlPb_2Cl_5$ structure-type is densely packed despite having ions with large coordination numbers. All polyhedra share corners, edges and faces, with no open channels. There are two types of BX_n polyhedra, a $Sr1X_8$ distorted square antiprism and a $Sr2X_7$ distorted monocapped trigonal prism. The KX_8 is the largest polyhedron and is also a distorted square antiprism. Table 1 summarize the structural parameters and refinement details. The structure drawings for KSr_2I_5 and KSr_2Br_5 are shown in Figure 83 and Figure 84. The fractional atomic coordinates and equivalent isotropic atomic displacement parameters are shown in Table 22 and Table 23, respectively.

Table 21. Crystal structure data and single-crystal X-ray diffraction refinement results for KSr_2I_5 and KSr_2Br_5.

Formula	*KSr_2I_5*	*KSr_2Br_5*
fw (g)	844.64	613.89
T (K)	250	260
Crystal system	monoclinic	monoclinic
Space group	*$P2_1/c$*	*$P2_1/c$*
a (Å)	9.9602(2)	9.3047(2)
b (Å)	8.98024(17)	8.2945(2)
c (Å)	14.2811(3)	13.2852(3)
α (°)	90	90
β (°)	90.021(2)	90.095(2)
γ (°)	90	90
V (Å^3)	1277.37(4)	1025.32(4)
Z	6	4
D_{calc} (g/cm^3)	4.414	3.977
R_F	0.0250	0.0226
R_{wF}	0.0641	0.0593
Goodness of Fit	1.035	1.1013

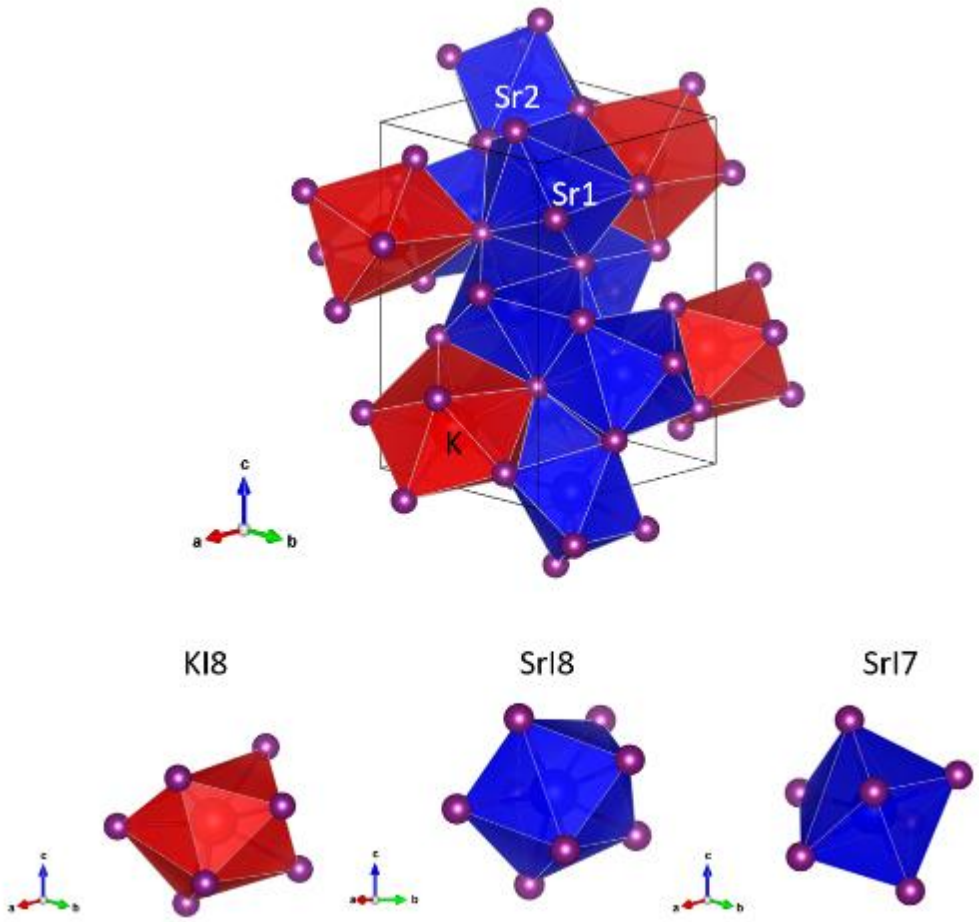

Figure 83. Crystal structure of KSr_2I_5 at 250K showing the KI_8, $Sr1I_7$ and $Sr2I_8$ polyhedra. Anisotropic atomic displacement ellipsoids are plotted at 99% probability.

Table 22. Fractional atomic coordinates and equivalent isotropic atomic displacement parameters for KSr_2I_5 (space group $P2_1/c$)*at 250K.

Atom	*x*	*y*	*Z*	*Ueq (Å2)*
K	*0.0061(2)*	*0.5457(2)*	*0.82961(18)*	*0.038(5)*
Sr1	*0.24839(6)*	*0.07259(6)*	*0.99417(4)*	*0.01480(12)*
Sr2	*0.49755(7)*	*0.02498(7)*	*0.67908(5)*	*0.01643(14)*
I1	*0.54064(4)*	*0.16209(5)*	*0.90172(3)*	*0.01520(10)*
I2	*0.73450(5)*	*-0.19075(5)*	*0.78241(3)*	*0.01757(10)*
I3	*0.72093(4)*	*0.54095(5)*	*0.00207(3)*	*0.01757(10)*
I4	*0.96078(5)*	*0.17507(5)*	*0.91163(4)*	*0.02469(13)*
I5	*0.72291(5)*	*0.16707(5)*	*0.18308(3)*	*0.02049(11)*

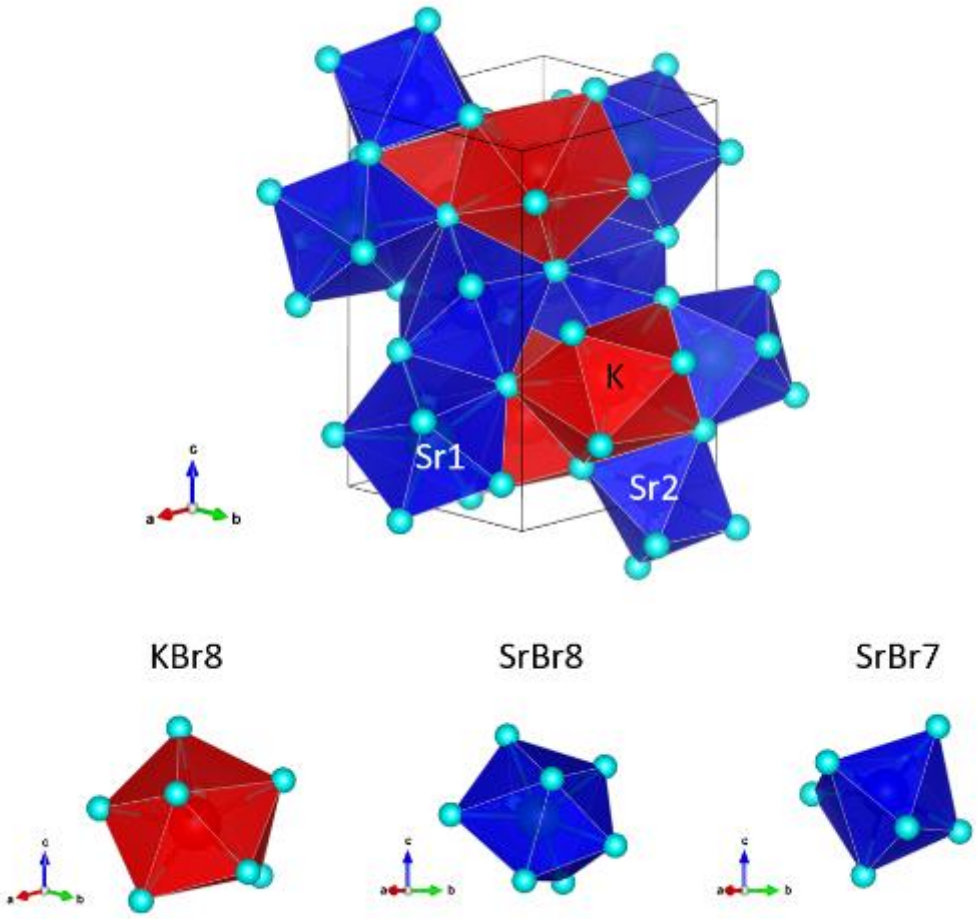

Figure 84. Crystal structure of KSr_2Br_5 at 260K showing the KI_8, $Sr1Br_7$ and $Sr2Br_8$ polyhedra. Anisotropic atomic displacement ellipsoids are plotted at 99% probability.

Table 23. Fractional atomic coordinates and equivalent isotropic atomic displacement parameters for KSr_2Br_5 (space group $P2_1/c$)*at 250K.

Atom	*x*	*y*	*Z*	U_{eq} (Å^2)
K	0.49188(12)	0.54531(14)	0.83102(9)	0.0326(3)
Sr1	0.00143(4)	0.02371(4)	0.67770(3)	0.01302(10)
Sr2	0.25151(4)	0.06947(4)	0.99351(3)	0.01275(9)
Br1	0.03928(4)	0.16112(5)	0.90095(3)	0.01633(10)
Br2	0.23288(4)	0.30742(5)	0.71735(3)	0.01773(10)
Br3	0.21974(5)	0.45623(5)	0.99786(3)	0.01768(11)
Br4	0.21999(5)	0.33112(5)	0.68409(3)	0.02042(11)
Br5	0.53785(5)	0.17394(5)	0.91175(4)	0.02544(12)

B. Photon and Electron Response of K-Based Scintillators

(This work is part of an ongoing collaboration with Drs. S. A. Payne, N. J. Cherepy, and S. Hunter, from Lawrence Livermore National Laboratory, Livermore, CA)

B.1 Abstract

In this work the scintillation the thermoluminescence and non-proportional response of the following K-based scintillators were investigated. Scintillator such as KSr_2I_5:Eu and KBa_2I_5:Eu show light yields higher than 90,000 ph/MeV and energy resolutions as low as 2.4% at 662 keV. These energy resolutions are accompanied by excellent proportional responses to gamma-ray excitation. To more thoroughly understand the scintillation mechanism of these new scintillators, we are investigated the electron response and thermoluminescence to determine whether charge traps affect the proportionality and scintillation kinetics. In this work we compare the thermoluminescence, the photon response, and the electron response (measured at LLNL with Scintillator Light Yield Non- proportionality Characterization Instrument - SLYNCI) of the following K-based scintillators: KSr_2I_5:Eu, KSr_2BrI_4:Eu, KSr_2Br_5:Eu, KBa_2I_5:Eu, and K_2BaI_4:Eu.

B.2 Experimental

The pulse height spectra of a variety of sealed radioactive sources were collected using a super bialkali Hamamatsu R6231 - 100 PMT connected to a Canberra 2006 pre-amplifier, an Ortec 672 amplifier (10 μs shaping time), and a Tukan 8K multi-channel analyzer. Several layers of Teflon and a hemispherical dome of Spectralon were used as reflectors. The energy resolution and the non-proportionality (nPR) or gamma response of the crystals were measured using the R6231-100 PMT with a standard set of γ-ray sources (^{137}Cs, ^{22}Na, ^{133}Ba, ^{57}Co and ^{241}Am). The energy resolution was defined as the Full Width Half Maximum over the centroid of the photopeak of energy E (R=ΔE(FWHM)/E). The nPR or relative

light yield was defined as the ratio between centroid position of a photopeak of energy E and centroid position at 662 keV.

The scintillation decay time was measured under irradiation from a ^{137}Cs sealed source with the time-correlated single photon counting technique.

For the thermoluminescence measurements, a 0.125 cm^3 crystal was bonded to a copper sample holder using a two-part thermal epoxy (Epotek - H20E). The sample holder was attached to the cold finger from a DE202AE cryostat (Advance Research System, inc.) and placed under vacuum. While under 20 mTorr vacuum, the crystal was heated to 550 K to release the previously stored luminescence and then cooled down to 10 K, where the irradiation took place. The crystal was irradiated with X-rays (35 kV, 0.1 mA) for 15 min. The sample was heated at a rate of 0.15 K/s from 10 K to 550 K using a Lakeshore 331 temperature controller. The luminescence emitted from the crystal was collected using a R2059 PMT. The current signal from the PMT was transformed into a voltage signal using standard NIM electronics. A National Instruments 6002-E data acquisition card was used to digitize the signal and a LabVIEW-based program developed in-house was used to collect the desired curves. The luminescence signal arises from electrons that thermally escape from traps and migrate to luminescence centers. Peaks in the spectrum provide evidence of discrete trapping levels.

The SLYNCI facility at LLNL was used to measure the electron response of the same samples; a description of the set up can be found in W. S Choong et al. [110].

B.3 Results

Figure 83 shows the gamma response of the crystals studied for this work. When compared to NaI:Tl and $LaBr_3$:Ce, the K-based scintillators showed a more proportional photon response. Note that the K-based scintillators had a slight “halide hump” that deviated from 1 to 4% from the ideal response. In general, the Ba-based crystals had better gamma response than the Sr-based crystals. Also,

we observed that replacing iodide for bromine in KSr_2I_5:Eu has negative effect on the gamma response.

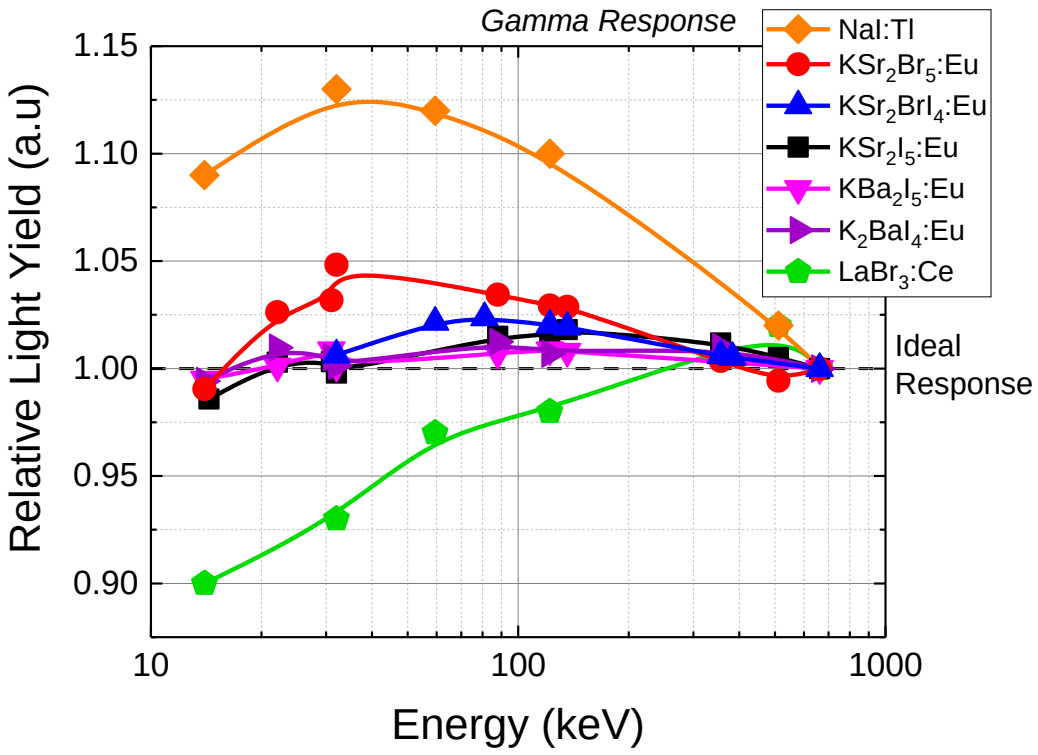

Figure 85. Photon response of KSr_2Br_5:Eu, KSr_2BrI_4:Eu, KSr_2I_5:Eu, KBa_2I_5:Eu, and K_2BaI_4:Eu compared to $LaBr_3$:Ce and NaI:Tl

Figure 86 shows the electron response of the K-based scintillators. As expected the “halide hump” was present on all the scintillators tested. However, the electron response showed a larger deviation of 2 to 9% from the ideal response compared to the 1 to 4% deviation observed for the gamma response. These results are under further investigation.

Figure 87 shows the thermoluminescence glow curve and the integrated radioluminescence intensity of KBa_2I_5:Eu, KSr_2I_5:Eu, KSr_2BrI_4:Eu and KSr_2Br_5:Eu measured between 10 K and 600 K. It is known that there is strong correlation between the shallow traps that participate in the scintillation process and the non-proportionality of scintillators. At this stage would be inaccurate to draw any conclusion by making comparisons KBa_2I_5:Eu, KSr_2I_5:Eu and KSr_2Br_5:Eu, however a clear trend can be observed between the presence of shallow traps in KSr_2I_5:Eu, KSr_2BrI_4:Eu and KSr_2Br_5:Eu and their non-proportionality. At room temperature, the shallows traps in KSr_2I_5:Eu caused delay emission, which is not observed on KSr_2BrI_4:Eu nor KSr_2Br_5:Eu. Thus is likely that KSr_2I_5:Eu would yield higher theoretical energy resolution accompanied with a better non-proportionality compare to $KSr_2Br_xI_{5-x}$:Eu.

The gamma response and thermoluminescence glow curve of KSr_2I_5 with varying Eu^{2+} concentration was measured, as shown in Figure 89 and Figure 88. The addition of europium introduced new shallow traps (shaded in orange in Figure 88) when compared to undoped KSr_2I_5, but once the Eu^{2+} was incorporated in the matrix nor further changes to the trap structure were observed as the Eu^{2+} concentration increased. Similarly, the only significant change in the gamma response was observed upon the addition of Eu^{2+} in KSr_2I_5. Thus, the reduction in the energy resolution with decreasing Eu is related to statistical limitations (R_{stat}), and exciton and carrier losses due the reduced number of luminescence centers in the matrix.

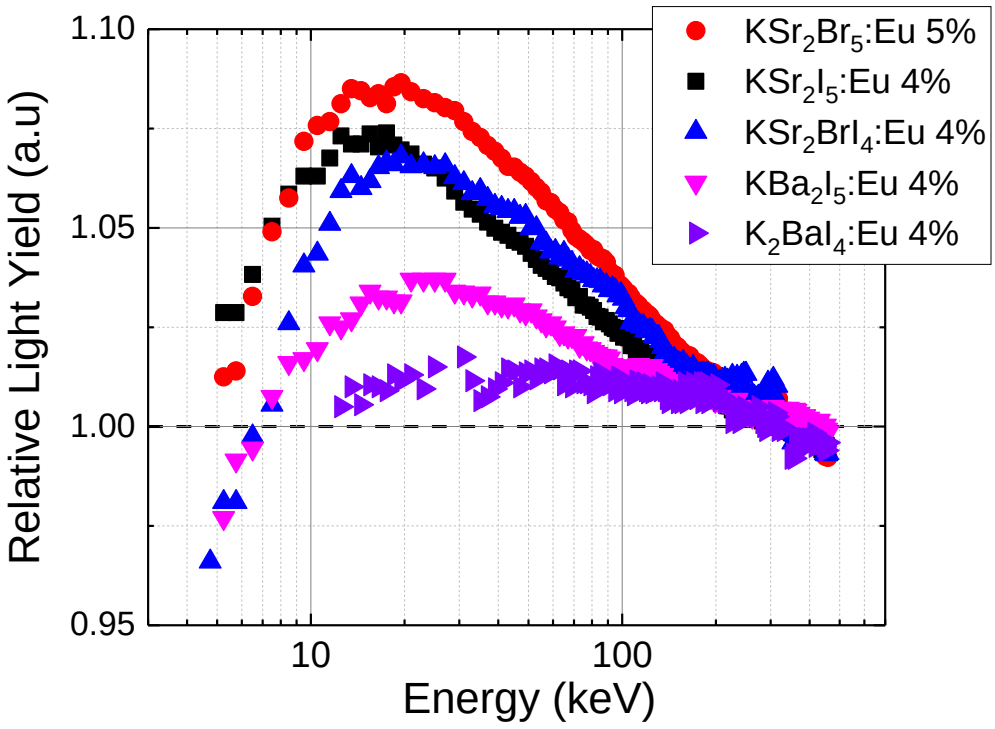

Figure 86. The electron response of KSr_2Br_5:Eu, KSr_2BrI_4:Eu, KSr_2I_5:Eu, KBa_2I_5:Eu, and K_2BaI_4:Eu was measured with the SLYNCI at LLNL

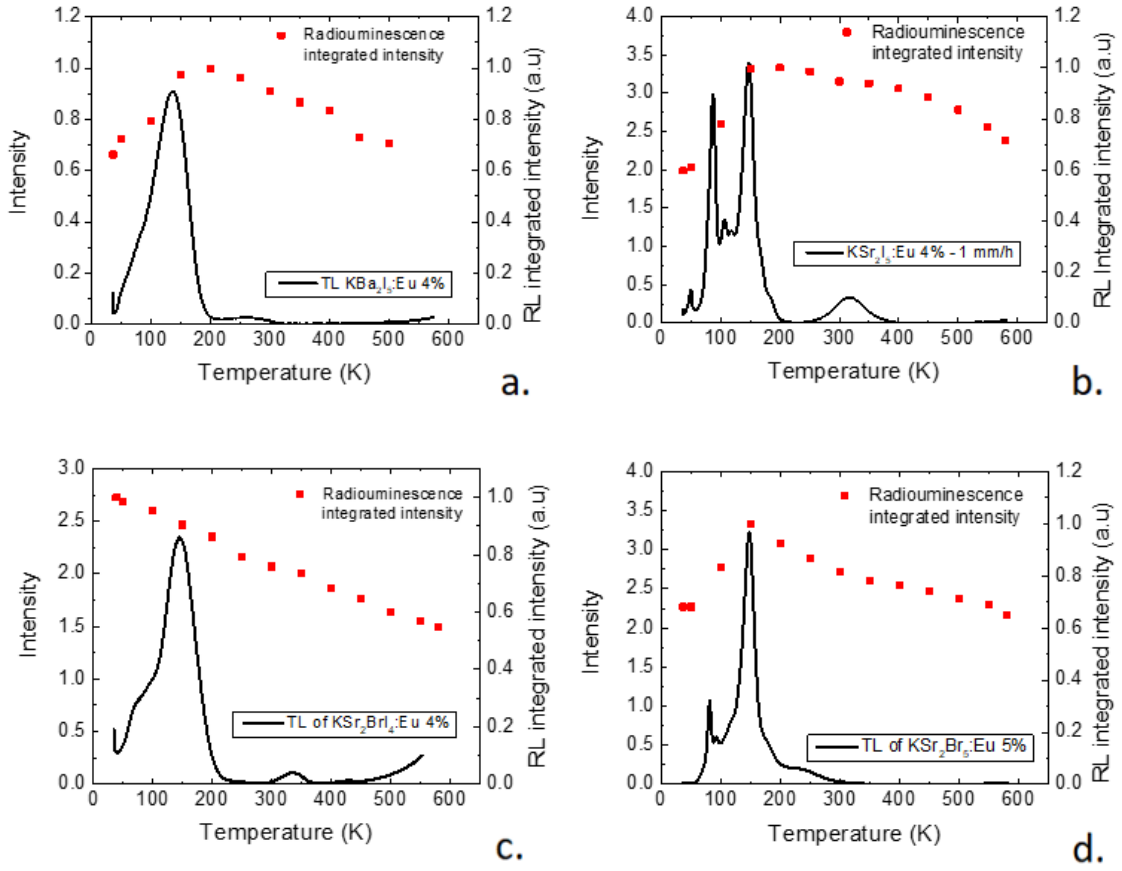

Figure 87. Thermoluminescence of KBa_2I_5:Eu, KSr_2I_5:Eu, KSr_2BrI_4:Eu and KSr_2Br_5:Eu.

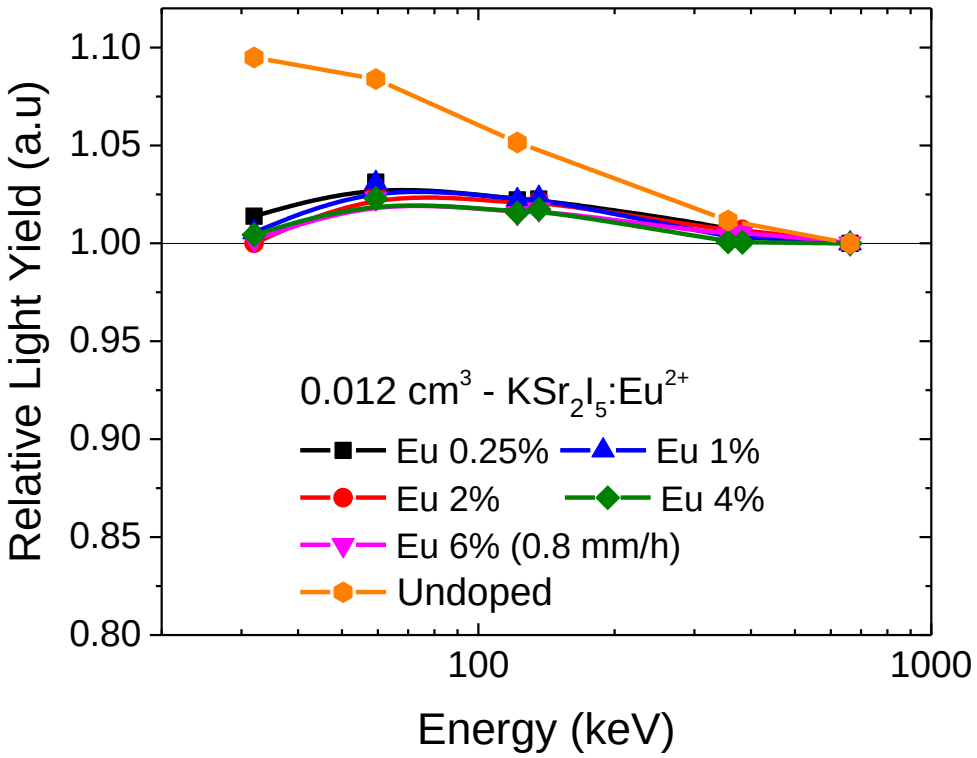

Figure 88. Gamma response of KSr_2I_5 with varying Eu^{2+} concentration.

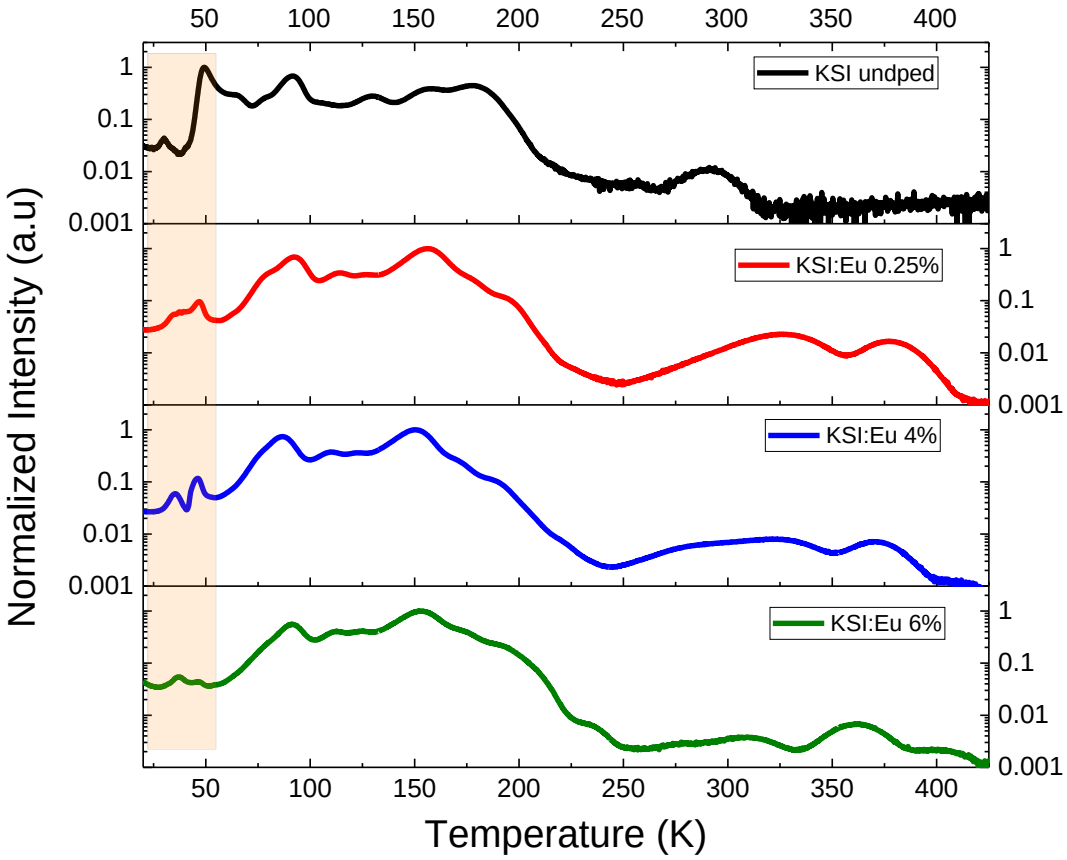

Figure 89. Thermoluminescence glow curves of KSr_2I_5 with varying Eu^{2+} concentrations

Vita

Ecuador born, Luis Manuel Stand, began his journey 14 years ago with a desire to play collegiate tennis at a U.S institution. A year later he was awarded a tennis scholarship to attend Bethel College. There he played tennis for three years receiving multiple sport and academic awards. and graduated with a bachelor in business administration. After a brief hiatus from his studies, he continued his educations at the University of Tennessee, earning a second bachelor in Nuclear Engineering and a master in Material Science and Engineering. During this period, he married Paula. Together they are happy parents of baby boy, Matthew Alexander Stand, and two ugly dogs, Pia and Teig. To this day Luis enjoys playing tennis and doing research in difference areas. Into the future, Luis looks forward to pass along his knowledge to his baby boy and hopes to play tennis with him someday.